Cranfield UNIVERSITY

An analysis of the Flight Dynamics of a Second Generation SST Aircraft

Interim Report

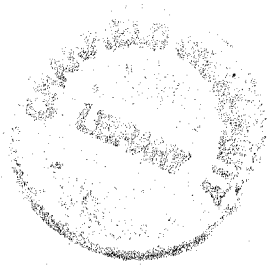

A J Steer

COA report No.9914
October 1999

College of Aeronautics
Cranfield University
Cranfield
Bedford MK43 0AL
England

College of Aeronautics Report No.9914
October 1999

AN ANALYSIS OF THE FLIGHT DYNAMICS OF A SECOND GENERATION SST AIRCRAFT

INTERIM REPORT

A J Steer
Flight Test and Dynamics Group
College of Aeronautics
Cranfield University
Cranfield
Bedford MK43 0AL

MV Cook
Academic Supervisor

October 1999

ISBN 1 86194 046 7

ACKNOWLEDGEMENTS

The work presented within this report has been carried out, under the active supervision of M V Cook, by A J Steer during a part time PhD study. Financial support has been provided by FMC Dept, DERA Bedford.

In addition, technical support has been provided by the future projects team, BAe Airbus in the form of aerodynamic and performance data as part of the European supersonic research programme (ESRP).

NOTATION

Abbreviations

AC	aerodynamic centre
ATC	air traffic control
BAC	British aircraft corporation
C^*	C star
CG	centre of gravity
CP	centre of pressure
CSAS	command and stability augmentation system
DoF	degree of freedom
EVS	enhanced vision system
FBW	fly-by-wire
FCS	flight control system
FMS	flight management system
HST	high speed transport
IAS	indicated airspeed
ICR	instantaneous centre of rotation
MAC	mean aerodynamic chord
MP	manoeuvre point
NDI	non-linear dynamic inversion
NP	neutral point
PIO	pilot involved oscillation
PR	pilot rating
SCT	supersonic commercial transport
SST	supersonic transport
SVS	synthetic vision system
UC	undercarriage

NOTATION

Symbols - Greek

α	angle of attack
β	sideslip angle
$\partial C_m / \partial_\alpha$	pitch moment due to incidence (AoA)
γ	flight path angle
ϕ, θ, ψ	roll, pitch and yaw angles (attitudes)
p, q, r	roll, pitch and yaw rates
ξ, η, ζ	aileron (differential elevon), elevator (symmetrical elevon) and rudder
τ_p	roll mode time constant
$\zeta_p, \zeta_s, \zeta_d$	damping ratio – phugoid, short period and dutch roll
$\omega_p, \omega_s, \omega_d$	frequency – phugoid, short period and dutch roll

Symbols

C_L, C_{Di}	coefficients of lift and induced drag
h_n	neutral point
I_x, I_y, I_z	moments of inertia - roll, pitch and yaw
L_p	roll damping derivative
L_v	roll moment due to sideslip
M_q	pitch damping derivative
M_w	pitch moment due to normal velocity
N_v	yaw moment due to sideslip
S	laplace operator
T	time constant
U_e	equilibrium airspeed
$V_{min,\ emd,\ ref}$	minimum airspeed, minimum drag speed, reference airspeed
Z_w	normal force due to normal velocity

1 INTRODUCTION

1.1 Background

It could be argued that Concorde has been a great success after more than 20 years in operational service without a major incident. More than 180,000 flight hours have been accumulated by only 14 in-service aircraft, at cruising speeds of Mach 2.0, carrying more than 2 million passengers. In addition, aircrews have been impressed by the predictability of its flying qualities exhibited throughout its expanded flight envelope [1].

Concorde may have been a great technical achievement, however it has to operate within its own set of rules and procedures, requiring special air corridors and dispensation to operate from a limited number of airports. This situation may be acceptable with so few examples in operational service, however to be a commercial success a second generation aircraft would need to be both economically viable and environmentally acceptable.

To be economically viable, a second generation aircraft would need to carry significantly more passengers than Concorde, together with their accompanying baggage, over a far greater range. Hence the aircraft would be much larger and heavier with the accompanying increased inertias and control requirements. In addition, it would have to be produced in far greater numbers than was Concorde, in the region of 500 to 1000 aircraft, if it is to remain affordable.

To be environmentally acceptable, a new supersonic transport (SST) aircraft, known hereon as a supersonic commercial transport (SCT), would have to comply with the same international regulations for airport noise as the contemporary subsonic fleets. Improved engine design would therefore be essential in order to meet the regulations and additionally the overall aircraft design would be strongly influenced by the need to reduce noise. Therefore good low speed flying qualities, which are in conflict with those for supersonic cruise, would be necessary for take-off and landing. Some further reduction in noise could be expected from the adoption of specific flight procedures, such as thrust modulation, effected with a modern flight management system (FMS). Additionally, a reduction in induced drag via a reduced approach attitude would decrease the thrust required.

In addition, a second generation SCT would have to be compatible with current subsonic aircraft traffic operations. This could mean a landing speed no greater than 155 kts, the speed being that specified for the new A3XX family of large capacity subsonic civil transport aircraft. An SCT would also be subject to a maximum speed of 250 kts below 10,000 ft as required by ATC.

A further consideration is that due to the high approach attitudes required to generate sufficient lift at low speeds, Concorde required a variable position drooping nose in order to provide adequate forward vision. This has proved a workable solution, however the weight, complexity and increased drag of such a mechanism is a significant performance penalty. A future SCT aircraft would be required to have adequate forward vision for landing in all conditions possibly by adopting a significantly reduced approach attitude

combined with the aid of a fully integrated enhanced and, or, synthetic vision system (EVS, SVS) overlaid on a head up display (HUD).

To summarise, the main features required of a possible second generation aircraft are compared to Concorde's in table 1.1.

	SCT	Concorde
Maximum Take-off weight	340t	185t
Range	5500nm	3340nm
Span	42m	25.6m
Length	89m	61.66m
Passengers	250+	100
Supersonic cruise	Mach 2.0	2.0

Table 1.1 Aircraft specifications

1.2 Flight control and handling qualities

Since Concorde entered service, control of both military and civil transport aircraft by fly-by-wire (FBW) has become fully accepted by both manufacturers and public alike. The increasing use of FBW technology on civil commercial transport aircraft is driven principally by the need to reduce aircrew cross-type training by designing a fleet of aircraft with similar flying qualities. Additional benefits include reduced weight, approximately 270 kgs on the Boeing 777 [2], through removal of the mechanical system and improved aerodynamic efficiency resulting from a reduction in trim drag leading to increased fuel economy and range.

There are still a large number of commercial transport aircraft controlled through mechanical links to the hydraulic control surface actuators, whilst smaller aircraft almost exclusively employ mechanical flight control systems. However, the latest '*large*' subsonic transport aircraft (Boeing 777, Airbus A320, A330 and A340) have been designed from the outset with full authority FCS coupled to manoeuvre command type control functions, whilst retaining only limited mechanical back-up for emergencies [2].

Currently there is no standard command type as each manufacturer develops their own design resulting in variations in functionality and handling qualities. However, evidence suggests that the major civil aircraft manufacturers, both Airbus and Boeing, are now opting for some form of C* command and stability augmentation system [3]. This linear combination of normal acceleration and pitch rate command seems to give the desired handling qualities at low-speed, when combined with some form of restored speed stability, and has become accepted by airlines and aircrew alike. In addition, research has been ongoing into the direct control of flightpath through a combination of command law and a HUD for improved feedback of the controlled parameter to the pilot [4].

To enable the design and validation of these command and stability augmentation systems (CSAS) a comprehensive set of flying qualities and performance criteria have also been developed, the majority for application to military aircraft [5].

"*The importance of flying qualities is inversely proportional to altitude*" - commander of the 4th shuttle flight [6]. Most previous studies into the flying qualities of commercial transport aircraft have identified the approach and landing phase of flight as being the most demanding. It is within this flight region, at the lower boundary of its safe flight envelope where control power is at a minimum, that the pilot is required to fly a narrowly defined path using tight manoeuvre control. Any misjudgement by the pilot can result in, at best a heavy landing, and worst a major accident. It can therefore be inferred that the area of principal concern relating to handling qualities requirements for an SCT is the same as that for a subsonic aircraft, i.e. the low speed region, typically low-speed cruise, approach and landing.

1.3 Aims of study

The first generation of supersonic commercial transport aircraft exhibited handling qualities, which were a natural function of the aerodynamics derived from the inherent aircraft design [6-10].

Concorde's performance and flying qualities, especially at low-speed during the approach and landing, are generally accepted as adequate when the aircraft operates within a pre-defined flight envelope and is flown in a procedural manner. However, as has already been highlighted a second generation SCT would need to integrate with current and future subsonic air traffic. This requirement, when combined with its increased mass and inertias over Concorde's, could result in unsatisfactory flying qualities due to insufficient control power at low-speed and the associated reduction in safety margins. Indeed, studies during and subsequent to Concorde's entry into service addressed the requirement for additional pitch control power to alleviate some of the perceived handling deficiencies at low-speed [11-14]

Modern commercial transport aircraft are mainly '*control configured vehicles*' with their handling qualities principally defined by the control law design. Therefore, it should be possible for a second generation SCT to exhibit similar low-speed handling qualities as conventional, large subsonic transport aircraft through careful command control law selection and implementation, when designed within the framework of relevant flying qualities criteria. The success of this operation is obviously dependent on there being sufficient degrees of freedom within the fundamental aircraft design. Advantages of this commonality with subsonic aircraft would be: reduced aircrew conversion training and increased safety, extended understanding of what constitutes desirable handling qualities, faster design and simplified airworthiness certification.

It follows that the aims of the research are to:

1. Provide an overview of existing SCT aircraft performance characteristics.
2. Quantify and establish a second generation aircraft's unaugmented low-speed static and dynamic stability. Principally, to identify SCT specific issues that may adversely affect the performance, handling qualities and associated safety margins.
3. Investigate current flying qualities criteria and assess their suitability for SCT specific control law design and subsequent evaluation.

4. Design and implement advanced control law techniques incorporating selected command response types.
5. Ensure aircraft augmented response satisfies handling qualities criteria using both off-line analysis and piloted simulation.

1.4 Research programme

This interim report covers an initial overview of delta-wing aircraft static, dynamic and control characteristics, collated from publications within the public domain and the authors related research [15-18]. This is to give the reader an overall understanding how a delta-winged supersonic transport aircraft's characteristics differ to those of a conventional civil transport aircraft.

This is followed by identifying the aircraft's static and dynamic stability, with the effect of speed and CG location on the aircraft dynamic modes specifically addressed. Following this, a comprehensive investigation and analysis of the open loop response of a SCT baseline aircraft, in both low-speed cruise and approach and landing conditions, has been carried out. Both time and frequency domain techniques have been utilised. Finally, conclusions are made based on the results of the work presented.

The PhD study will continue with an investigation of existing flying qualities criteria which may be applicable to this type of aircraft. This will be addressed principally through a comprehensive literature survey combined with information collected through related studies as stated previously. Analytical performance criteria specifying the desirable dynamic response of the aircraft are to be found in the American 'Military Specification for the Flying Qualities of Piloted Airplanes', MIL-STD-1797A [5]. This publication provides some analytical specifications that are required of U.S. military aircraft and now contains additional information on criteria applicable to augmented command response types. These military specifications define classes of aircraft, flight phases, and levels of flying qualities in order to specify different modes for the various combinations. An SCT, with a maximum take-off weight (MTOW) of 340 tonnes, is classified as a class III (large, heavy, low-to-medium manoeuvrability) aircraft.

A set of values for the dynamic response parameters will be identified then selected which, when combined with desirable command response types operating within a command and stability augmentation system (CSAS), should imbue the aircraft with level 1 handling qualities. The CSAS will be implemented using both conventional 'state feedback' and non-linear dynamic inversion (NDI), an advanced control law prototyping and analysis technique. NDI, as its name suggests, inverts the dynamics of the aircraft system before adding additional loops to provide the desired bandwidth of response [19-22].

It is planned that the research will finish with a comprehensive piloted simulation assessment to verify the results obtained during the 'off-line' assessment of the implemented CSAS flight control laws.

2 SST AIRCRAFT CHARACTERISTICS

One of the major differences, when compared with conventional civil transport aircraft, is the wide variation in the moments of inertia. The low aspect ratio slender delta planform results in a mass concentrated towards the fuselage centreline. This means that the ratios of roll, pitch and yaw moments of inertia are different compared with those for a conventional layout subsonic aircraft, see table 2.1. The large yaw/roll inertia ratio will result in a tendency for the unaugmented aircraft to roll about the longitudinal axis and not the velocity vector.

	Conventional subsonic transport	Concorde	SCT
Roll	1	1	1
Pitch	3.5	7	6
Yaw	4.5	8	7

Table 2.1 Moments of inertia

In addition, the pitch inertia is greater than that of a conventional sub-sonic aircraft, hence it could have a significant effect on the pitch response to a control input.

2.1 Longitudinal aerodynamics

The principal characteristic of the slender-delta design is the low aspect ratio wing resulting in a low lift-curve slope compared with a conventional sub-sonic aircraft. Indeed, the best achievable lift to drag (L/D) ratio, at low-speed, for an SCT is approximately half of that for a conventional subsonic aircraft. However, this is offset to some extent by the low wing loading due to the large surface area.

Another important property of the slender delta wing is that it does not stall in the accepted sense at any normal operating attitude. This is due to the generation of vortices of increasing magnitude from the leading edge apex of the wing, which start to separate at approximately 7° incidence on Concorde, and for example, continue to increase in magnitude as incidence increases further. These vortices contribute directly to lift generation, and at a given incidence the effect of the leading edge vortex is to increase the lift above the value that would occur due to attached flow alone. The low lift curve slope, and lack of trailing edge flaps to augment low-speed lift, requires that the aircraft is flown at large pitch attitudes on the approach. A consequence of this flight attitude is the high induced drag which causes the aircraft to fly considerably below its minimum drag speed, resulting in speed instability.

2.2 Longitudinal stability

An SCT is characterised by relatively low stability due to a small static margin at low speed, which is required to reduce trim as the aircraft accelerates. As the Mach number is increased beyond Mach 1.0 there is a significant rearward shift of the aerodynamic centre (AC) which can result in unacceptably high trim drag due to the consequent large control surface deflection required to trim. Concorde provides aerodynamic trimming with a cambered wing which is most effective at the lower incidence associated with higher

speeds. However, if the CG remains stationary throughout the transition from subsonic to supersonic flight then, the trim requirements become exceptionally large. Hence, the trim required from the controls is reduced further, to within ±2.5° at all Mach numbers, by shifting the CG rearwards through fuel transfer as the airspeed increases.

2.3 Ground effect

When operating in ground effect, the large pitch attitude during landing, together with the large area of wing located behind the aircraft CG, can amplify the basic lift by as much as 30%, greatly reducing the rate of descent and hence cushioning the landing together with the addition of large nose down pitching moments. However, the amount of additional lift will be reduced, by up to a third, due to the pilot being required to continuously pull back on the column to maintain landing attitude and oppose the increased pitch down moment.

The large nose down pitching moments will, in addition, oppose pitch up rotation for take-off. Therefore, as the aircraft climbs rapidly out of ground effect the pilot may experience abrupt and substantial pitch up characteristics, which must be opposed by continuous control inputs.

2.4 Lateral-directional aerodynamics and stability

The lateral motion is characterised by low roll inertia, I_x, due to the concentration of mass along the aircraft centreline, low roll damping, L_p, due to the low aspect ratio wing, and a high value of roll due to sideslip, L_v, due to the large wing sweepback angle. The low roll inertia relative to the yaw, results in a tendency to roll about the longitudinal body axis rather than the velocity vector. This results in the conversion of incidence to sideslip in rolling motion which can be significant for a slender delta aircraft that flies at relatively large angles of incidence at low speed.

As incidence increases the flow field around the fin deteriorates due to asymmetric vortex shedding from the fuselage and wing. The vortices produce negative sidewash at the vertical tail, which results in directional instability at certain flight conditions. This was overcome on Concorde by fitting forward fuselage strakes, sometimes known as a *moustache*, which generate vortices and retain streamwise flow over the fin thereby improving its aerodynamic effectiveness.

2.5 Control requirements

Pitch and roll control of a tail-less delta is effected by moving surfaces at the trailing edge of the wing called *elevons*. Elevons are independently actuated and function as conventional elevators when deflected symmetrically and as ailerons when deflected differentially. When Concorde performs a roll manoeuvre, because of the marked fuselage and fin interference effects of the displacement of the inner elevons coupling into yaw, their travel is restricted compared with the middle and outer surfaces.

Control about the directional axis is through a conventional fin mounted rudder. Rudder effectiveness is near constant for increasing incidence, this is due to the high level of downwash at the empennage which means there are no low energy wakes from the fuselage or wing to embrace the vertical fin.

Subsonic aircraft have wings sized for cruise resulting in a small wing area. This means that for a low stall speed, and hence satisfactory low speed landing, high lift devices are required. The leading and trailing edge flaps used generate large pitching moments, which require trimming out by the tailplane. A tail-less delta configuration can either, opt for the necessarily high take-off speeds and use the high lift at high incidence qualities of the slender delta on landing to give the essential lower landing speeds as with Concorde, or, as with the Russian Tu-144, a foreplane can be used to trim out the nose down pitching moments generated by the elevons which are off-set to act as trailing edge flaps during landing.

Low actuator rate limits, in the region of 20 to 30°/s for elevon control, result in effective time delays of 0.2 to 0.4 seconds in the pitch and roll responses to pilot inputs, thus degrading the aircraft handling qualities and leading to possible pilot involved oscillations (PIO). PIOs manifest themselves as coupled pilot-aircraft motion significantly out-of-phase with pilot input. They can be initiated by pilot-in-the-loop phase lag exceeding 180°, through greater than required control inputs, for a sluggish or delayed aircraft manoeuvre response.

2.6 Aeroelastic effects

For minimum supersonic drag, a SST should have a small diameter/length ratio fuselage and a highly swept wing with a small thickness/chord ratio hence aeroelastic distortion can result from a lack of stiffness and the internal volume is small for the required fuel load. A delta wing can go some way to solving these two problems, its large root chord allows considerable depth whilst remaining aerodynamically thin, this minimises drag and provides space for the fuel and undercarriage. The relative stiffness of the delta planform minimises aeroelastic distortions. A second generation SCT will be structurally lighter and more flexible than Concorde and equivalent military supersonic aircraft due to it being stressed for lower 'g' manoeuvres, similar to that of current civil transport aircraft (+2.5 g and -1 g), and the need to reduce weight. Such a flexible aircraft may exhibit considerable motion at its longitudinal extremes, due either as a result of aircraft commanded manoeuvres or the aircraft's passage through turbulent air. This type of motion can result in a reduction in the structural life of the airframe together with degraded ride quality for aircrew and passengers.

2.7 Pilot station and motion cues

As supersonic transport aircraft are long, and the pilot maybe located far forward of the instantaneous centre of rotation (ICR), he may then be subject to relatively large translational as well as rotational accelerations. Velocity vector manoeuvres can also exacerbate the problem by adding to the lateral acceleration sensed by the pilot. However, due to the use of elevons for pitch control, and their corresponding short moment arm about the CG, the ICR is located a significant distance ahead of the aircraft CG so reducing the magnitude of these effects. Additionally, the pilot can have difficulty in judging the position of the main-wheels during landing, hence adding to the workload and resulting in large variations in the quality of touchdown.

3 AIRCRAFT STABILITY

It is envisaged that increasing levels of longitudinal static instability may be utilised in order to improve aerodynamic efficiency. In addition, Gibson [23] states that *"The idea of further improving efficiency by relaxing the static stability requirements is now becoming accepted. It is believed that the USA's proposed supersonic high speed transport (HST) will feature substantial static instability, presumably in the subsonic region, so that the stability in supersonic cruise can be optimised"*. Therefore, in order to minimise trim drag, reduce control power requirements and hence optimise the aircraft's aerodynamic efficiency, the CG should be located at the aircraft's aerodynamic centre (AC), equating to the neutral stability point (NP).

It is therefore required to establish the aircraft's low speed NP. In addition, the position of the manoeuvre point (MP) is required to ensure that the CG position does not transgress beyond it and result in an uncontrollable aircraft.

3.1 Mathematical model description

A complete 6 DoF mathematical model of a second generation SCT aircraft, know as the European SCT (ESCT) baseline configuration, has been coded in FORTRAN and embedded within MATLAB/SIMULINK. This dynamic simulation and analysis environment provides the numerical integration of model states plus monitoring facilities during development of the model and flight control laws. The model has three elevon control surfaces, located inboard, mid and outboard of the engine exhaust nozzles on the trailing edge of both wings, operating as independent port and starboard units. The elevons operate as both a conventional elevator when deflected symmetrically to control pitch about the lateral axis, and as ailerons when deflected differentially to provide lateral control about the longitudinal axis. The rudder provides directional control through yaw moment generation in the usual way. A second control surface, either tailplane or foreplane, can be added to provide additional pitching moments.

Aerodynamic moments and forces are generated by linear interpolation of aerodynamic data tables located within the model. BAe Airbus generated the aerodynamic data from both wind tunnel tests and software packages. The rigid body equations of motion and the inertial moments and forces are provided by a set of standard routines known as a *System of Equations for the Simulation of Aircraft in a Modular Environment* (SESAME) [24].

SESAME is a collection of subroutines, which contain all the equations for the simulation of an aircraft rigid-body motion in real time. This includes the basic equations of motion, axis transformations and the generation of inertial moments and forces acting on the aircraft. The SESAME package also contains an atmospheric model and simulations of wind, both with and without turbulence. The model developer is required to create a small group of additional routines to describe his particular vehicle.

The equations of motion use a conventional right-hand axis system whose origin is at the CG. The body fixed axes are orientated with the positive x-axis pointing forward along the body, the positive y-axis along the starboard wing and the positive z-axis down.

3.2 Static stability

The longitudinal static stability determines whether the aircraft tends to return to, or depart from its trimmed airspeed. Whilst the manoeuvre stability is defined by the aircraft's return, or otherwise, to the trim load factor after release of the control column following an input.

The longitudinal handling qualities involve motion in pitch about the lateral axis where a disturbance results in an effective change in the angle of attack. Stability will result in an opposing pitching moment to any disturbance, which will tend to restore the aircraft to its original angle of attack. As both α and M are positive nose up, $\partial M/\partial \alpha$ will be negative for a stable aircraft.

The lateral/directional stability requirements are very much inter-linked. To satisfy positive lateral stability, requires that the aircraft is able to maintain its wings level in flight. To satisfy the directional static stability requirements requires that the aircraft can maintain heading.

3.2.1 Longitudinal static stability

When the aircraft is in steady trimmed flight the moments are balanced and the elevator angle is the elevator to trim. If the airspeed is reduced by increasing the angle of attack through negative elevator input, then this is the new elevator to trim position for a change in angle of attack. The implication is that stability is indicated by a negative trend to the curve of control angle to trim plotted against angle of attack, known as the trim curve.

To calculate the baseline aircraft's NP for low speed, low altitude, flight the non-linear mathematical model was flown at different speeds equating to different lift coefficients, C_L, and the corresponding elevator position to trim measured. The elevator position to trim curves were then plotted against C_L and the process repeated for different CG positions, see figure 3.1.

The NP, h_n, is a function of C_L as indicated by the trim curve, a C_L of 0.6 approximating to an approach speed of 155 to 160 kts was selected and the slopes for different CG positions measured. The slopes were then plotted against CG position, , the points connected and extended in order to determine the controls fixed NP, h_n, see figure 3.2.

In order to illustrate the dynamic response of configurations possessing positive and neutral longitudinal static stability a time response simulation was performed exciting the longitudinal dynamics. The aircraft was initialised at 250 kts and an altitude of 1000 ft in straight and level flight trim conditions. An elevator pulse input of -1° was applied at 1 second for 0.5 seconds and then returned to its trim position of –1.67°, see figure 3.3. During the duration of the elevator input the aircraft is out of trim due to the additional pitching moment, this results in a positive pitch rate and hence corresponding increase in aircraft attitude. On removal of the input the rate of pitch reverses and returns to zero at 6 seconds (trim conditions).

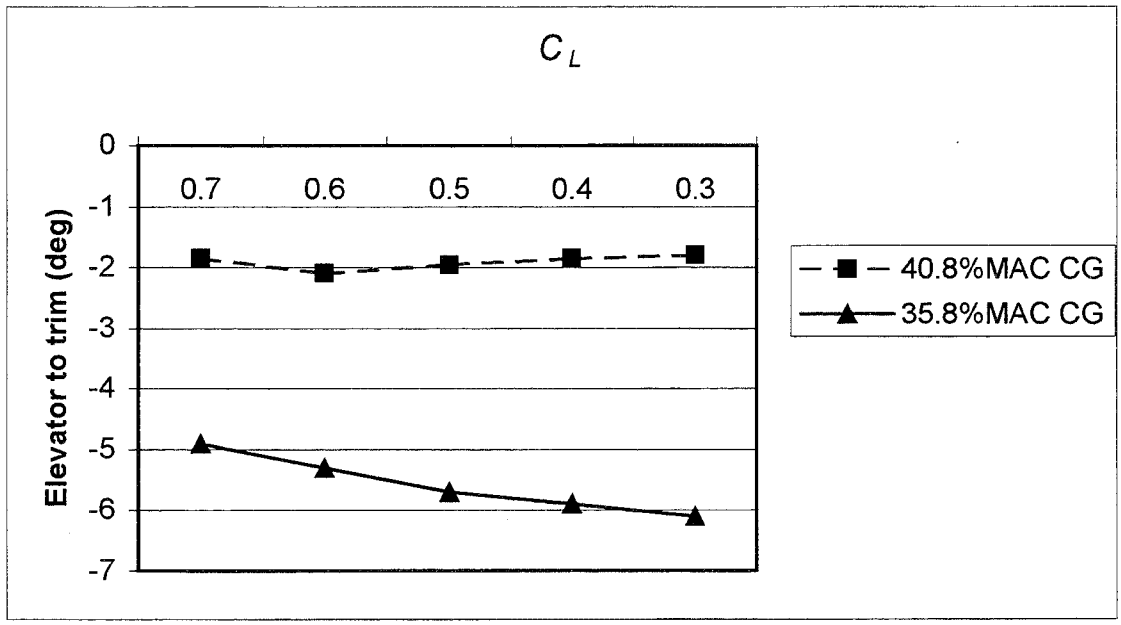

Figure 3.1 Longitudinal trim curves

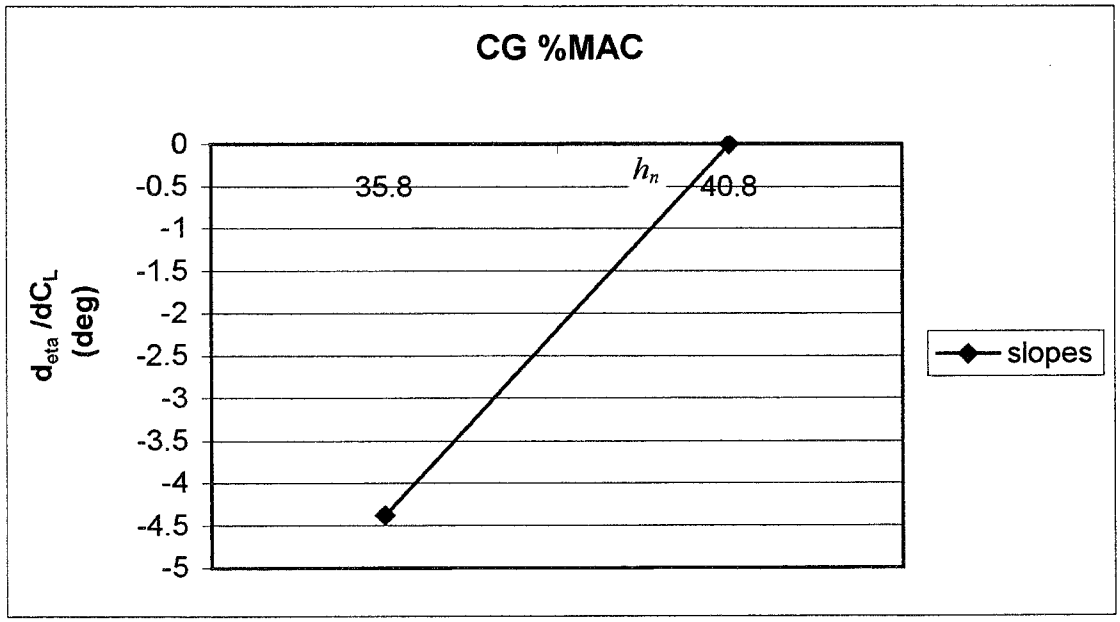

Figure 3.2 NP at a C_L of 0.6

A secondary effect of the '*up*' elevator at 1 second is an effective loss of lift from the large aerodynamic control surface and hence an opposite sense normal acceleration, N_z, at the CG which returns to a steady state of 1g as the wing angle of attack (AoA) and hence total lift increase. However, on removal of the input at 1.5 seconds there is an effective momentary increase in control surface direct lift, resulting in a positive normal acceleration which again returns to a steady state condition of 1g after 7 seconds.

The statically stable configuration's pitch response slowly returns to its trim condition after removal of the control input, whereas the neutrally stable aircraft maintains the

'*disturbed*' attitude of 7.6° after removal of the input. This is due to the change in pitching moment due to AoA, $\partial Cm/\partial\alpha$, equalling zero, hence illustrating how a neutrally stable vehicle will remain in a disturbed condition after removal of the disturbance.

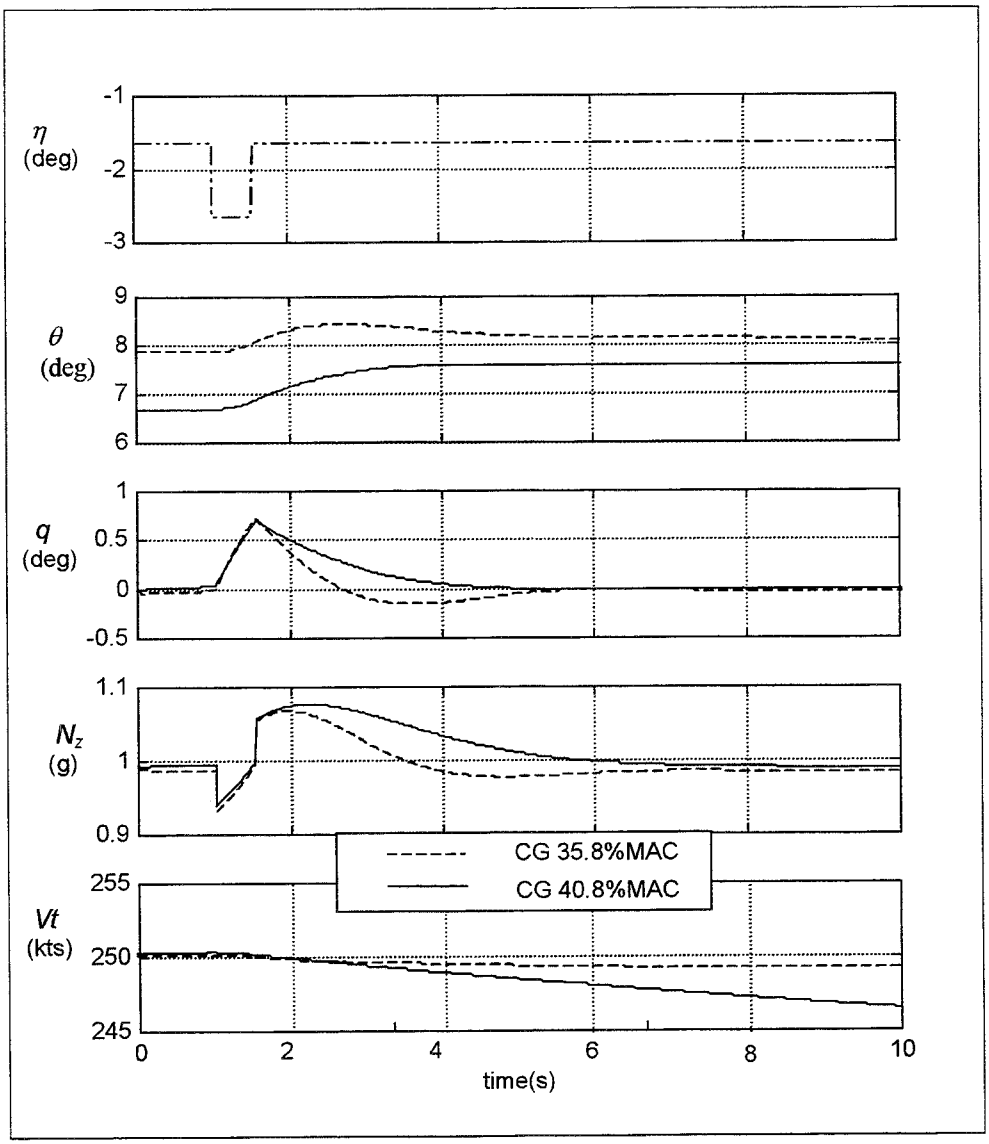

Figure 3.3 Time response to pulse elevator input

3.2.2 Longitudinal manoeuvre stability

In the longitudinal axis a manoeuvre is characterised by a rate of change, q, in pitch attitude, θ. The manoeuvre characteristics are CG dependent due to the change in pitching moment with CG position. The relationship between pilot input, in terms of the control input and force, and the resultant manoeuvre determines the stick travel per g and the stick force per g: referred to as the controls fixed and controls free manoeuvre margins respectively. As the CG is moved rearwards there will be a point reached where both the stick travel per g and stick force per g will each become zero, this is known as the manoeuvre point. The distance to the CG called the manoeuvre margin, which indicates the tendency of the aircraft to return to the original manoeuvre state after a

disturbance. The manoeuvre points (controls fixed and free) will be aft of the neutral points by an amount, which is a function of the pitch damping, M_q, of the aircraft.

The stick force per g is a very important handling characteristic of the aircraft with transport aircraft stressed to relatively low levels of g, typically 2.5, as they do not need to manoeuvre aggressively. However, for aircraft with modern FCSs, and certainly for those utilising sidesticks for pilot input, the stick force per g has to be set artificially through dynamic feel, *'q feel'*.

The aircraft was initialised in trim conditions equating to straight and level flight at 250 kts and at an altitude of 1000 ft. The CG was located at the aircraft's approach NP of 40.8%MAC.

The aircraft was flown at these conditions equating to 1g and the control position measured and noted. The 'g' force was then increased by manoeuvring the aircraft, in this case through carrying out a bank and then pitch manoeuvre, and the control position measured. This process was repeated for several values of g up to approximately 2g and then repeated for 3 CG positions, see table 3.1.

Airspeed (kts)	AoA (deg)	Normal load (g)	Elevator (deg)	CG (%MAC)
250	6.67	0.995	-1.667	40.8
250	8.55	1.3	-2.667	40.8
250	10.87	1.72	-3.667	40.8
250	13.22	2.19	-4.667	40.8
250	7.441	0.995	-4.319	35.8
250	8.646	1.173	-5.319	35.8
250	11.6847	1.6276	-7.319	35.8
250	14.5252	2.0684	-9.319	35.8
250	7.893	0.995	-5.876	30.8
250	8.9007	1.1365	-6.876	30.8
250	9.9047	1.2915	-7.876	30.8
250	12.449	1.6073	-9.876	30.8
250	15.6032	1.999	-12.876	30.8

Table 3.1 Elevator control position per 'g'

The elevator position was then plotted against the corresponding normal load and the points joined. This was repeated using the data at the 3 CG positions, 40.8, 35.8 and 30.8%MAC, see figure 3.4. The slopes of the lines were then calculated and tabulated, see table 3.2.

CG (%MAC)	Slope ($\partial\eta/\partial g$) (deg/g)
30.8	-6.8946
35.8	-4.5986
40.8	-2.4752

Table 3.2

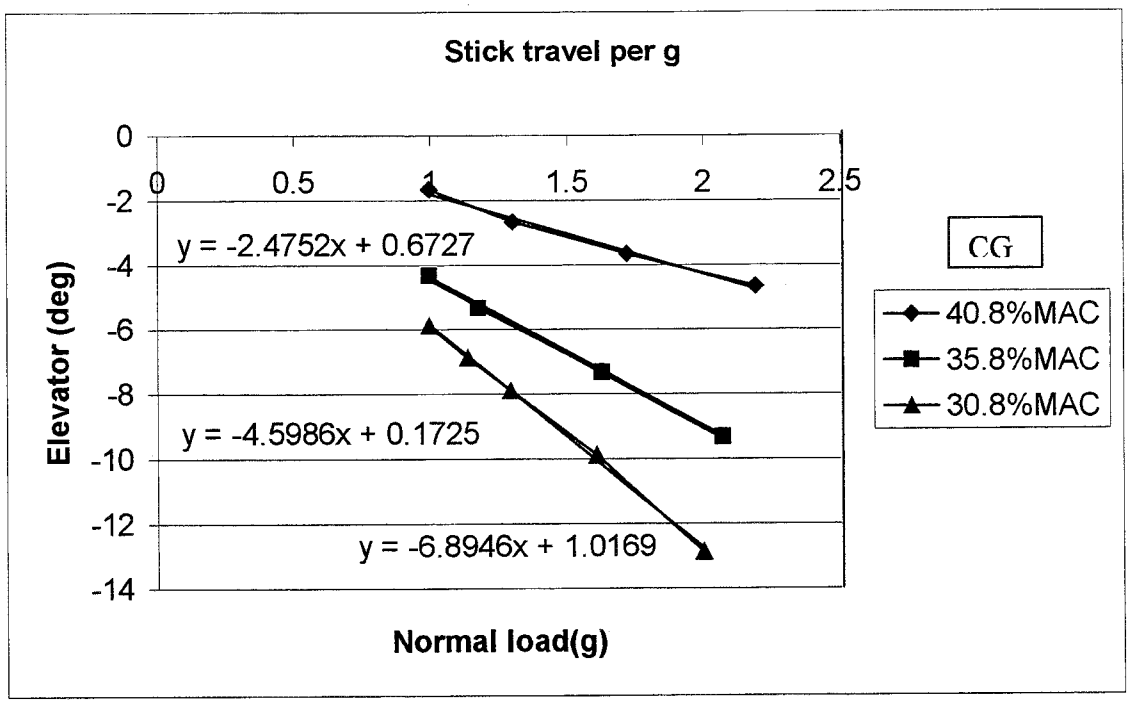

Figure 3.4 Calculation of CG dependent slopes

The slopes were then plotted against their respective CG positions, the points joined and the line extended to intercept the zero gradient axis to indicate the manoeuvre point, see figure 3.5. From the equation of the line, $y = 0.4419x - 20.478$, the point of interception and hence the manoeuvre point can be calculated.

As when

$$y = 0.4419x - 20.478 = 0 \tag{3-1}$$

and rearranging

$$x = \frac{20.478}{0.4419} = 46.34 \tag{3-2}$$

giving a manoeuvre point of 46.34%MAC and a manoeuvre margin with the CG located at the NP of 5.5%MAC.

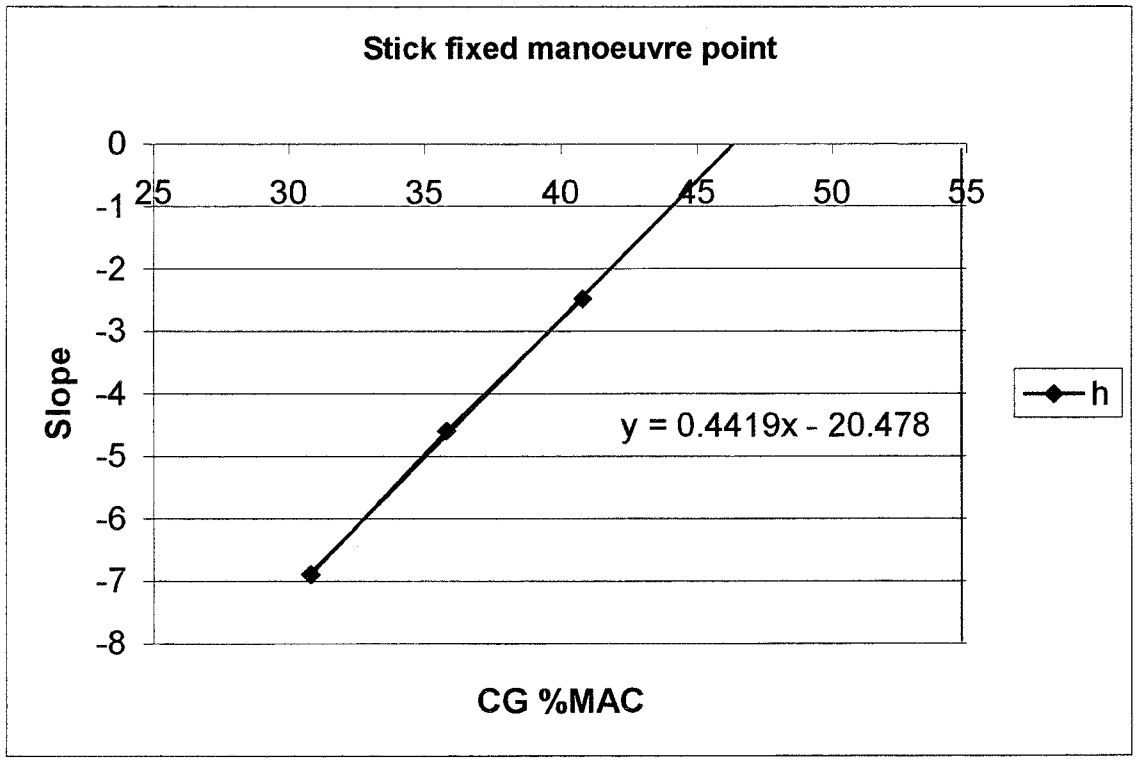

Figure 3.5 Estimation of manoeuvre point

The time response over 10 seconds to a step elevator demand at 1 second has been simulated for 4 CG locations: 35.8%, 40.8% (NP), 43.3%, and 46.8%MAC equating to a negative manoeuvre margin. The aircraft was initialised at 250 kts and an altitude of 1000 ft in straight and level flight.

With the CG located forward of the MP the aircraft longitudinal responses settle at a steady state condition after the initial demand. Reducing the manoeuvre margin reduces the stick/control travel per g. With the CG at 35.8%MAC equating to a positive manoeuvre margin of 10.5%MAC, 9° of elevator deflection is required to generate a 2g manoeuvre. With the CG located at the NP (40.8%) only 4.5° of elevator is required to generate a similar load and this is reduced further to 2.5° with the CG located behind the NP at 43.3%MAC. However, reducing the manoeuvre margin and hence control moment arm slows the speed of response of the aircraft in pitch and hence AoA and normal acceleration.

If the CG is moved behind the MP, there is a steadily increasing exponential rise in pitch rate and AoA coupled with a near linear rise in normal acceleration for only a 0.5° elevator input. Thus illustrating that if the CG is located behind the MP then a control input will result in a manoeuvre with an increasing rate of pitch, i.e. it is divergent.

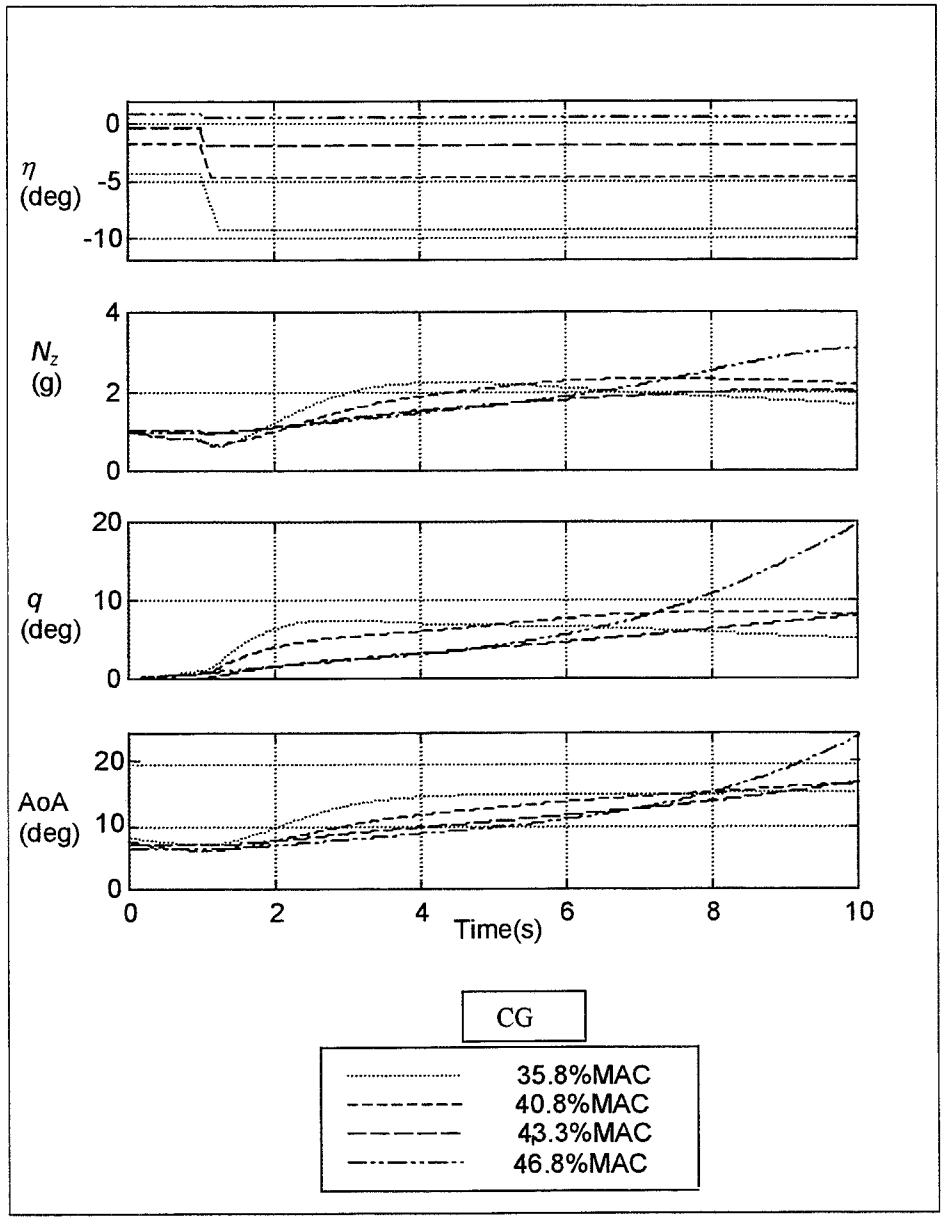

Figure 3.6 Longitudinal manoeuvre response

3.2.3 Lateral/directional static stability

Ailerons and the rudder can be used to provide trim curves which will indicate if the aircraft exhibits static stability with respect to a lateral/directional disturbance in sideslip, β. The trim curves indicate the magnitude of the restoring moment generated by the aircraft when it is forced into an out-of-trim condition by a control input.

The lateral stability comes mainly from the dihedral angle of the wings for a conventional aircraft, for a delta-wing planform, sweepback is the main contributor. A laterally stable aircraft will generate a rolling moment due to sideslip, L_v, when sideslipping, which will tend to restore the aircraft to wings level flight.

The directional stability is derived almost entirely from the fin with the other parts of the aircraft directionally de-stabilising. When held in a sideslip the aircraft will generate

yawing moment due to sideslip, N_v, which will tend to restore the aircraft to symmetric flight, known as 'weathercock' stability.

Measurement of lateral/directional static stability commences by forcing the aircraft into a sideslip using aileron and rudder input. To maintain the sideslip the aileron control must be used to overcome the stabilising moment and hence can be used as a measure of the magnitude of the stabilising roll moment. Likewise the rudder must be used to overcome the stabilising yawing moment, N_v, hence the rudder deflection can be used as a measure of the magnitude of stability.

A number of sideslip angles were flown and the aileron control deflection, ξ, and rudder control deflection, ζ, measured, see table 3.3.

Sideslip angle ($\beta°$)	Aileron ($\xi°$)	Rudder ($\zeta°$)
8	-8.21	17.19
4	-4.09	7.08
2	-2.04	3.2
1	-1.02	1.62
0	0	0
-1	1.02	-1.62
-2	2.04	-3.2
-4	4.09	-7.08
-8	8.21	-17.19

Table 3.3

The control positions were then plotted against sideslip angle, figures 3.7 and 3.8.

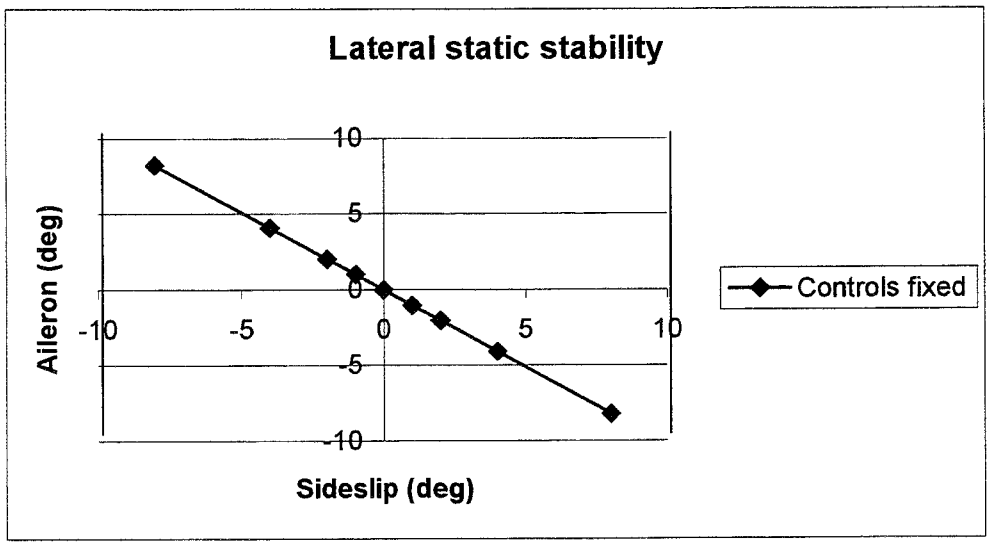

Figure 3.7 Lateral stability curve

The slope of aileron to sideslip angle, figure 3.7, is negative indicating that the aircraft is laterally stable under normal sign convention. Hence, negative aileron is required to maintain the sideslip angle against the restoring roll due to sideslip moment, L_v, i.e. L_v

will be negative if the aircraft is statically stable. The magnitude of the slope indicates the level of lateral stability, a steeper slope equating to a larger restoring moment, hence, increased static stability.

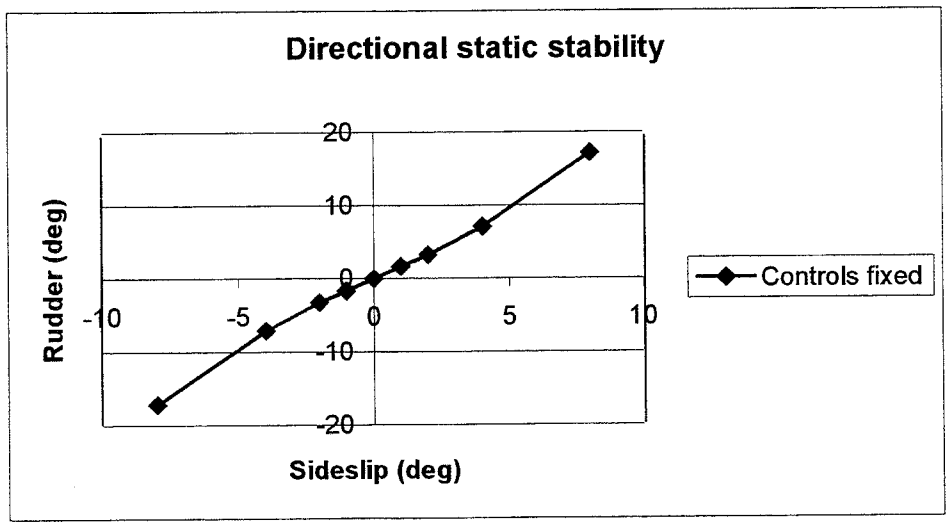

Figure 3.8 Directional stability curve

The positive slope indicates that the aircraft is directionally stable. A positive rudder deflection is required to maintain a positive angle of sideslip against the restoring moment, N_v. Hence, N_v will be negative for a directionally stable aircraft. Once again the magnitude of the slope indicates the amount of stability.

3.3 Longitudinal dynamic stability

The longitudinal characteristic equation is 4th order and for a statically stable airframe usually factorises into two pairs of complex roots, equation 3-3.

$$(s^2 + 2\zeta_p\omega_p s + \omega_p^2)(s^2 + 2\zeta_s\omega_s s + \omega_s^2) \tag{3-3}$$

These second order characteristics describe the phugoid and short period modes respectively and are excited whenever the aircraft is disturbed from its equilibrium trim state. The disturbance can take many forms such as control inputs, airframe configuration changes and external atmospheric influences.

However, a statically unstable aircraft configuration and those with marginal stability in certain flight conditions may possess unconventional dynamic stability modes. It is well known that a third oscillatory mode can exist for an unstable configuration which possesses short period like damping combined with a phugoid like frequency. Additionally, an unstable real root may also exist resulting in divergent aircraft response characteristics. Therefore, the roots may be either real or complex, stable or unstable increasing the difficulty of analysing their effect on aircraft behaviour.

3.3.1 Dynamic stability mode approximation

To gain an insight into the important aerodynamic derivatives affecting the longitudinal dynamics, approximations for the short period and phugoid modes can be formulated, see ref 25.

The short period pitching oscillation mode can be calculated from the dominant concise derivatives taken directly from the 'A' matrix of the longitudinal state equation, 3-5, as

$$\dot{\mathbf{x}} = \mathbf{A}\mathbf{x} + \mathbf{B}\mathbf{u} \tag{3-4}$$

$$\begin{bmatrix} \dot{u} \\ \dot{w} \\ \dot{q} \\ \dot{\theta} \end{bmatrix} = \begin{bmatrix} x_u & x_w & x_q & x_\theta \\ z_u & z_w & z_q & z_\theta \\ m_u & m_w & m_q & m_\theta \\ 0 & 0 & 1 & 0 \end{bmatrix} \begin{bmatrix} u \\ w \\ q \\ \theta \end{bmatrix} + \begin{bmatrix} x_\eta \\ z_\eta \\ m_\eta \\ 0 \end{bmatrix} [\eta] \tag{3-5}$$

The SPPO is a damped oscillation in pitch with a frequency of approximately 1 to 2 rad/s for a large civil transport aircraft. The principal variables are incidence α, pitch rate q and attitude θ with the speed U_e remaining largely constant.

solving equation 3-5 to obtain the determinant, $(sI - A)$:

$$s^2 - (m_q + z_w)s + (m_q z_w - m_w U_e) = s^2 + 2\zeta_s \omega_s s + \omega_s{}^2 = 0 \tag{3-6}$$

therefore

$$2\zeta_s \omega_s \approx -(m_q + z_w) \tag{3-7}$$

and

$$\omega_s \approx \sqrt{m_q z_w - m_w U_e} \tag{3-8}$$

giving good approximations to the short period damping and frequency, equations 3-7 and 3-8.

The concise derivatives describing longitudinal motion are composed of the dimensional derivatives, which are generated by the aircraft's configuration. Those defining the approximations above are:

$$m_q = \frac{M_q}{Iy} + \frac{(Z_q + mU_e)M_{\dot{w}}}{I_y(m - Z_{\dot{w}})} \tag{3-9}$$

and

$$m_w = \frac{M_w}{I_y} + \frac{Z_w M_{\dot{w}}}{I_y (m - Z_{\dot{w}})} \tag{3-10}$$

and

$$z_w = \frac{Z_w}{(m - Z_{\dot{w}})} \tag{3-11}$$

defining the pitch damping, pitching moment and normal force due to normal velocity respectively.

For a conventional aircraft, $M_{\dot{w}}$, the pitching moment due to normal acceleration is generated by the tailplane operating in the wing down-wash field and though measurable is usually quite small, therefore approximately:

$$m_q = \frac{M_q}{I_y} \tag{3-12}$$

and

$$m_w = \frac{M_w}{I_y} \tag{3-13}$$

For a slender delta aircraft, M_q is assumed to arise predominantly from the moment of the wing trailing edge (*TE*) lift about the CG. M_q is negative for positive static stability.

The pitching moment due to normal velocity, M_w, is a very important longitudinal derivative in that it plays a fundamental part in determining the frequency of the short period pitching oscillation, the pitch stiffness, and is always negative for a statically stable aircraft, see equations 3-6 and 3-13.

Z_w is principally dependent on the lift/curve slope, $\partial C_L / \partial_\alpha$ as can be seen in equation 3-14 and is always negative for a statically stable aircraft. Due to conventional sign convention, with normal force positive down, Z_w is always negative.

$$Z_w = -0.5 \rho V_e S \left(\frac{\partial C_L}{\partial \alpha} + C_D \right) \tag{3-14}$$

In terms of the dimensional derivatives, taking into consideration their relative magnitudes

$$2\zeta_s\omega_s = -\frac{M_q}{I_y} \tag{3-15}$$

and

$$\omega_s = \sqrt{\frac{-M_w U_e}{I_y}} \tag{3-16}$$

and

$$\zeta_s = -\frac{M_q}{2\omega_s I_y} \tag{3-17}$$

The phugoid mode is a low frequency oscillation in speed, which couples into pitch attitude and height. It is very lightly damped and hence many cycles of the motion will be visible before it eventually disappears. The undamped natural frequency of the motion for a large civil transport aircraft is typically in the range of 0.05 to 0.1 rad/s equating to a period of oscillation of 125 to 63 seconds.

$$\omega_p = \sqrt{\frac{\rho g S C_L}{m}}, \quad = \frac{g\sqrt{2}}{V_o} \tag{3-18}$$

The phugoid frequency, ω_p, is inversely proportional to speed due to the V_o term in the denominator, 3-18. A simplification of the approximation shows the damping as zero.

However

$$\zeta_p \approx \frac{1}{\sqrt{2}}\left(\frac{C_D}{C_L}\right) \tag{3-19}$$

and as aircraft are designed for a large lift to drag ratio the phugoid damping is correspondingly low.

3.3.2 Airspeed effects

The CG was positioned at 35.8%MAC, 5% forward of the NP, resulting in a statically stable aircraft. The aircraft trim conditions were obtained from 250 kts to the approach/landing speed of 155 kts and at spot points between. Linear models were then generated at these trim conditions. From these linear models the longitudinal dynamic modes were calculated and their damping ratios and frequencies tabulated in table 3.4. The important concise aerodynamic derivatives, m_w, m_q and z_w, which describe the longitudinal stability modes have also been taken from the state matrices.

Airspeed (kts)	ζ_s	$\omega_{s(rad/s)}$	ζ_p	$\omega_{p(rad/s)}$	m_w	m_q	z_w
250	0.6055	1.2219	0.0432	0.0940	-0.0082	-0.6568	-0.8108
225	0.7025	0.9925	0.0384	0.0969	-0.0049	-0.5855	-0.7919
215	0.7019	0.9508	0.0412	0.1011	-0.0047	-0.5579	-0.7585
200	0.7581	0.8238	0.0744	0.1003	-0.0033	-0.5163	-0.7170
190	0.7617	0.7891	0.0217	0.1066	-0.0032	-0.4886	-0.6837
175	0.7710	0.7827	0.0253	0.1079	-0.0034	-0.4475	-0.7192
155	0.7734	0.7094	0.0099	0.1200	-0.0032	-0.3944	-0.6474

Table 3.4 Airspeed effects

On initial inspection it can be seen that all of the concise derivatives, m_w, m_q and z_w, are negative indicating a longitudinally stable airframe.

With the aircraft at 250 kts the short period frequency and damping are 1.2219 rad/s and 0.6055 respectively, as the speed decays to 155 kts the short period frequency, ω_s, decreases to 0.7094 rad/s and the damping increases to 0.7734. The reduction in frequency is due to the forward velocity term, U_e, in the numerator equation 3-16.

The short period damping, ζ_s, increases as the airspeed reduces due to the decrease in the short period frequency in the denominator term, equation 3-17, being greater than the decrease in the pitch rate damping term, m_q in the numerator. It is to be expected that the '*viscous paddle*' generated pitch damping will reduce with airspeed as the dynamic pressure decreases.

The frequency of the phugoid mode, ω_p increases as speed decreases due to the V_o term in the denominator, equation 3-18. No clear trend can be seen in the phugoid damping term, although it does generally reduce with the airspeed.

To aid visualisation of how the SPPO mode characteristics change with airspeed, the roots have been plotted on the s-plane, figure 3.9. The SPPO roots migrate towards the origin as airspeed decreases, thus reducing in frequency. In addition, damping increases as the roots approach the real axis. However, the behaviour of the phugoid mode is difficult due to the scaling of the diagram for the '*fast*' mode.

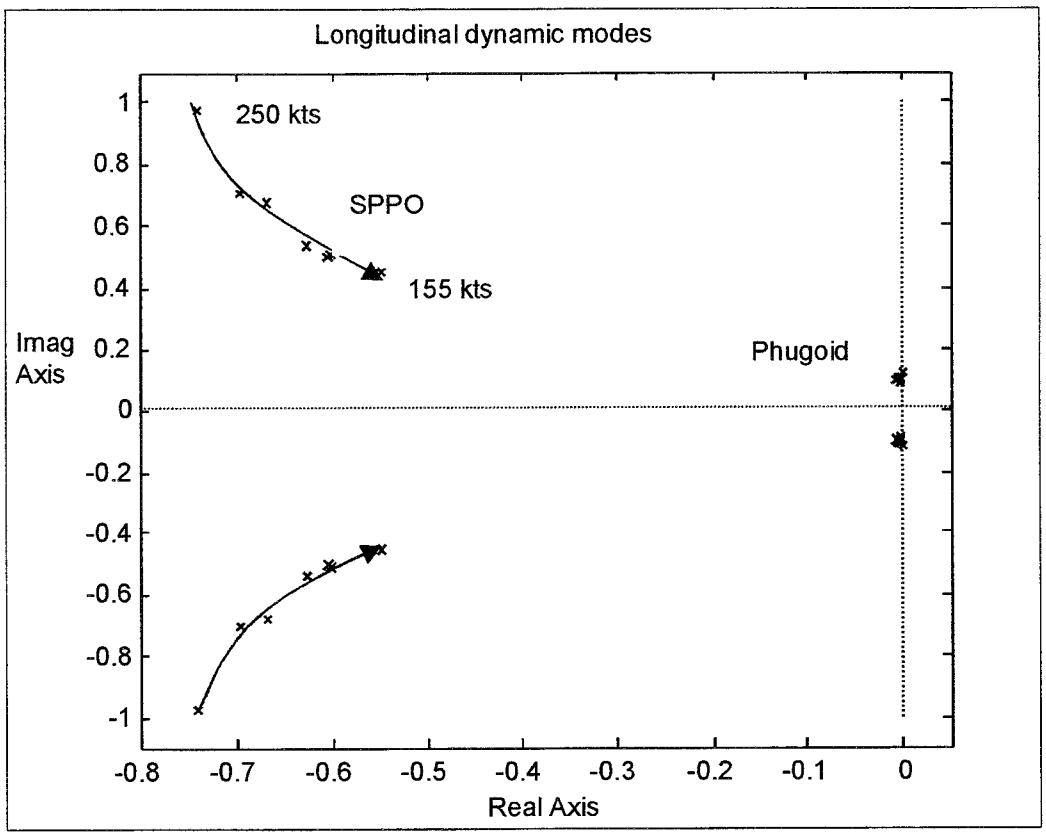

Figure 3.9 Migration of SPPO mode

3.3.3 CG position

The aircraft was initialised at 250 kts and an altitude of 1000 ft. The CG was positioned ahead of the NP, at 35.8%MAC resulting in a 5%MAC positive static margin. It was then progressively shifted rearwards, relaxing the static stability until reaching a final CG position at 45.8%MAC equating to a 5%MAC negative static margin.

The longitudinal dynamic modes were obtained and the data tabulated in table 3.5. The concise aerodynamic derivatives, m_w and m_q, have also been tabulated. Relaxing the static stability is seen to reduce the short period frequency, which when combined with the increase in damping, would manifest itself as a sluggish aircraft pitch response.

Figure 3.10 shows how the short period roots move towards the real axis as the static stability reduces eventually becoming negative as the CG moves behind the NP. The complex pair join the real axis with the CG located significantly behind the NP, after 43%MAC, whereupon they migrate rapidly in opposite directions, the root moving towards the positive part of the s-plane intercepts the real, frequency increasing '*phugoid root*' moving left. When they join, after 43.3%MAC, they become a complex pair and form a '*3rd oscillatory mode*' having the characteristics of a phugoid frequency combined with a short period damping. The frequency and damping of this third mode increases rapidly with the increasing level of instability, see figure 3.11.

CG (%MAC)	Roots	ζ_s	$\omega_{s(rad/s)}$	ζ_p	$\omega_{p(rad/s)}$	m_w	m_q
35.8	complex	0.6055	1.2219	0.0432	0.0940	-0.0082	-0.6568
38.3	complex	0.6713	1.0731	0.0486	0.0895	-0.0055	-0.6190
40.8	complex	0.7806	0.9001	0.0334	0.0811	-0.0029	-0.5811
41.8	complex	0.8429	0.8129	0.1612	0.0754	-0.0018	-0.5659
42.8	complex	0.9367	0.6745	0.8084	0.0715	-0.0007	-0.5508
43.0	SPPO + 2 real	0.9707	0.6320	-0.0554 -0.0937		-0.0005	-0.5477
43.3	4 real	-0.7678	-0.3316	-0.2447	-0.0273	-0.0002	-0.5432
		σ	ζ	ω	σ		
44.0	complex 3rd + 2 real	-0.9470	0.6305	0.3201	-0.0095	-0.0003	-0.5326
45.8	complex 3rd + 2 real	0.1877	0.9657	0.752	0.0013	-0.0004	-0.5052

Table 3.5 Effect of CG position on longitudinal dynamic parameters at 250 kts

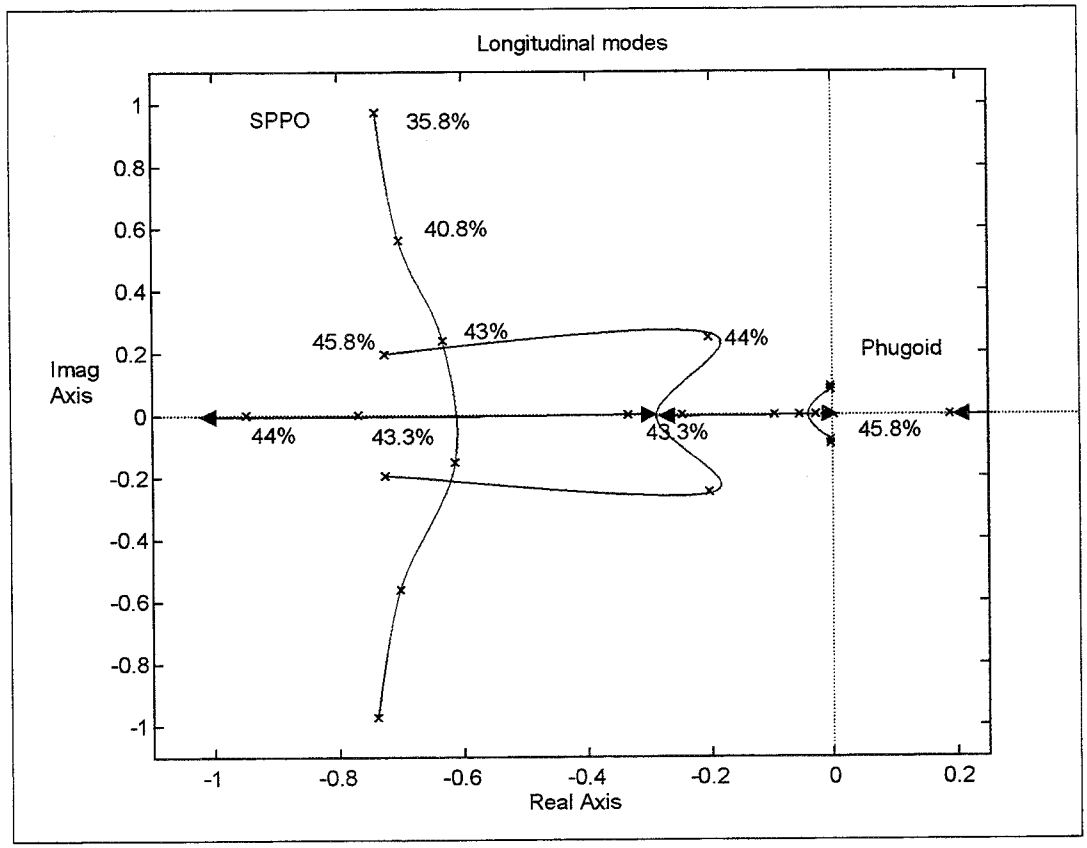

Figure 3.10 Effect of CG position on longitudinal modes

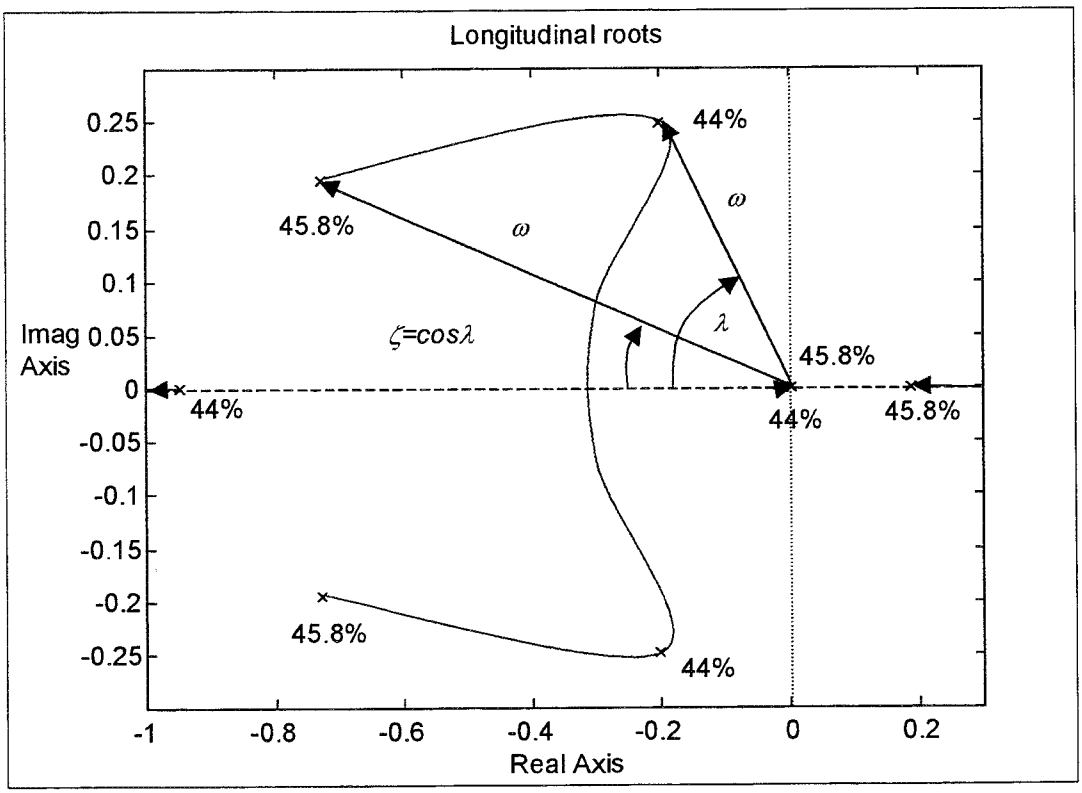

Figure 3.11 3rd oscillatory mode + 2 real roots

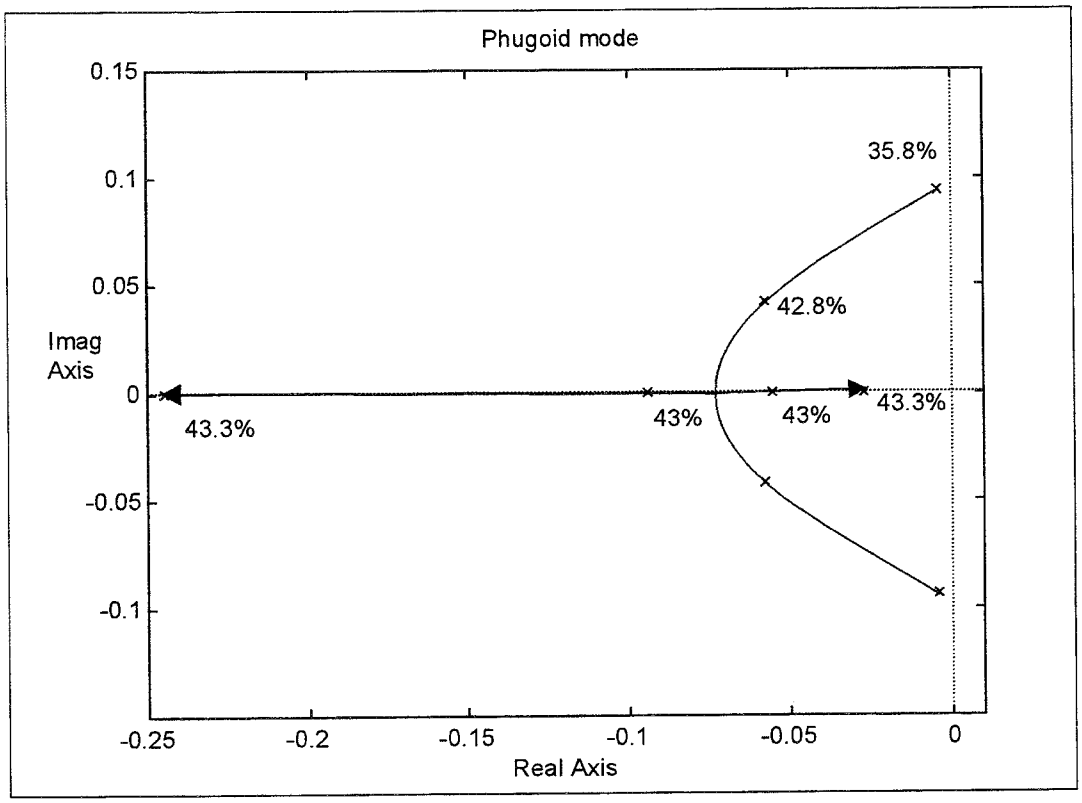

Figure 3.12 Migration of phugoid mode

Figure 3.12 shows how the phugoid roots migrate in an arc towards the real axis as the CG is moved progressively rearwards. The damping increases rapidly with the CG located behind the NP and becomes critical (unity damping ratio) at approximately 42.9%MAC when the roots become real. They then rapidly move in opposite directions along the real axis, both becoming positive unstable roots when the CG reaches 45.8%MAC.

To aid visualisation of the migration of the roots as the CG is moved rearwards figure 3.13 has been generated. Complex conjugate pairs are represented by solid lines and real roots as dashed lines. Four real roots can be seen to exist at a CG position of 43.3%MAC. Two real roots join to form the 3rd oscillatory mode while the other two migrate into the right-half plane to become unstable.

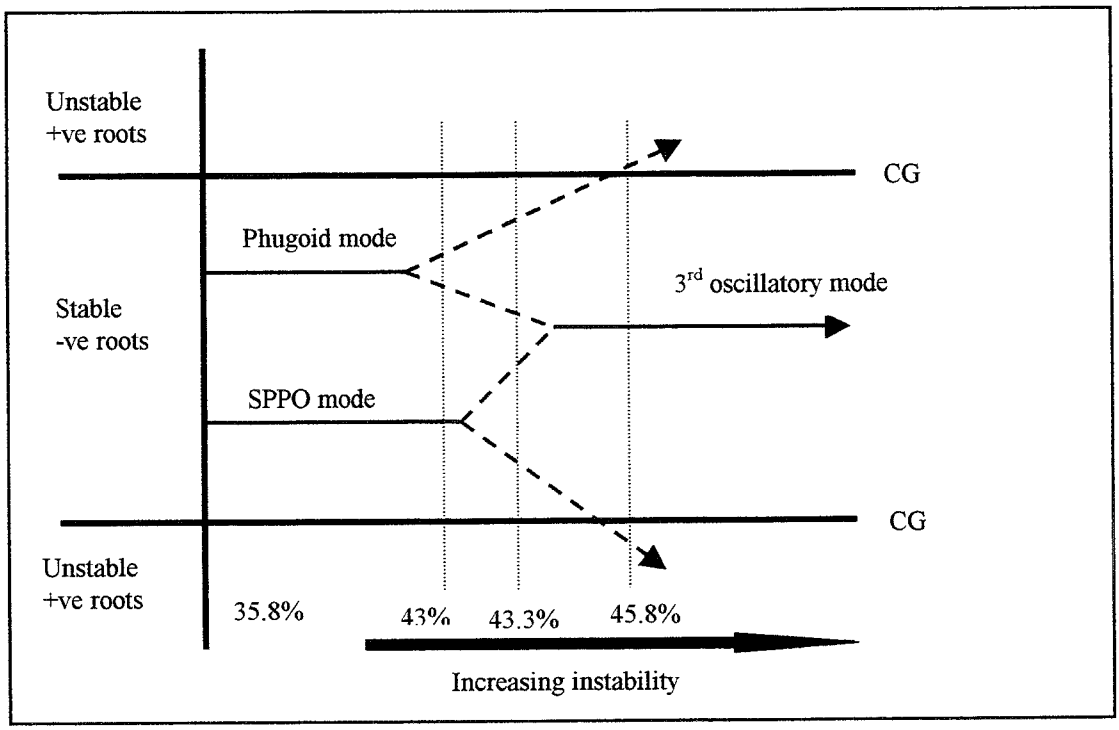

Figure 3.13 Migration of dynamic modes with increasing instability

3.3.4 Approach conditions

The CG was positioned at the aircraft's approximate NP of 40.8%MAC on the final approach.

An approach flightpath was generated based on Concorde's, starting at an altitude of 1000 ft and an airspeed of 190 kts, on a glideslope of -3°. The aircraft trim conditions were obtained from 190 kts down to ESCT's final approach speed of 155 kts in increments of 5 kts. The trim states were then used to initialise the non-linear model in order to generate the longitudinal linear models. The longitudinal dynamic modes were calculated for each flight condition and the data entered in table 3.6. The important concise aerodynamic derivatives, m_w and m_q which describe the longitudinal stability modes have also been tabulated.

From the table it can be seen that m_w is positive, indicating a loss of pitch stiffness, signifying a slow divergence in pitch to an external disturbance. The pitch damping derivative, m_q, is negative and decreases with airspeed, as expected.

Throughout the deceleration a third oscillatory mode is again in evidence which, retains the same general characteristics of a slow '*phugoid like*' frequency and '*short period like*' damping ratio. The other two roots are real and located either side of the imaginary axis, one '*slow*' and unstable the other '*fast*' and stable.

Speed (kts)	Altitude (ft)	Complex roots	σ	ζ_{3rd}	ω_{3rd} *(rad/s)*	σ	m_w	m_q
190	1000	-0.1271 ±0.0959i	0.0427	0.7981	0.1592	-0.9433	0.0014	-0.4382
185	928.5	-0.1343 ±0.0523i	0.0624	0.9319	0.1441	-0.9240	0.0013	-0.4207
180	857.1	-0.1345 ±0.0578i	0.0623	0.9187	0.1464	-0.8990	0.0013	-0.4094
175	785.7	-0.1342 ±0.0702i	0.0675	0.8860	0.1515	-0.8798	0.0012	-0.3979
170	714.2	-0.1349 ±0.0473i	0.0650	0.9437	0.1429	-0.9350	0.0014	-0.3874
165	642.8	-0.1356 ±0.0627i	0.0724	0.9077	0.1494	-0.9135	0.0013	-0.3755
160	571.4	-0.1363 ±0.0682i	0.0718	0.8945	0.1524	-0.8875	0.0012	-0.3651
155	500.0	-0.1383 ±0.0810i	0.0746	0.8629	0.1602	-0.8607	0.0012	-0.3541

Table 3.6 Decelerating approach

3.3.5 Unconventional mode analysis

To gain a greater understanding of the effect the mode contents have in each of the motion variables an eigenvector analysis can be performed. As ESCT's final approach airspeed will be 155 kts, the eigenvalue matrix representing the longitudinal modes has been generated at this speed, see equation 3-20.

$$\begin{array}{c} \text{real - ve mode} \qquad \text{3rd oscillatory mode} \qquad \text{real + ve mode} \\ \Lambda = \begin{bmatrix} -0.8607 & 0 & 0 & 0 \\ 0 & -0.1383+0.0810i & 0 & 0 \\ 0 & 0 & -0.1383-0.0810i & 0 \\ 0 & 0 & 0 & 0.0746 \end{bmatrix} \end{array} \quad (3\text{-}20)$$

The mode content in each of the motion variables are represented by the eigenvectors, see equation 3-21

$$\mathbf{V}=\begin{array}{c} \begin{matrix} \text{real-ve mode} & \text{3rd oscillatory mode} & & \text{real+ve mode} \end{matrix} \\ \begin{bmatrix} -0.1702 & -0.3905-0.2800i & -0.3905+0.2800i & -0.9525 \\ -0.9854 & 0.8733-0.0801i & 0.8733+0.0801i & -0.3043 \\ 0.0029 & 0.0010-0.0007i & 0.0010+0.0007i & 0.0006 \\ -0.0034 & -0.0076+0.0006i & -0.0076-0.0006i & 0.0077 \end{bmatrix} \end{array} \begin{matrix} :u \\ :w \\ :q \\ :\theta \end{matrix} \quad (3\text{-}21)$$

and their magnitudes are represented by equation 3-22

$$|\mathbf{V}|=\begin{bmatrix} 0.1702 & 0.4805 & 0.4805 & 0.9525 \\ 0.9854 & 0.877 & 0.877 & 0.3043 \\ 0.0029 & 0.00122 & 0.00122 & 0.0006 \\ 0.0034 & 0.00762 & 0.00762 & 0.0077 \end{bmatrix} \begin{matrix} :u \\ :w \\ :q \\ :\theta \end{matrix} \quad (3\text{-}22)$$

An analysis of the eigenvector magnitudes, equation 3-22, show that in row one, representing forward velocity, the positive real root at 0.9525 is dominant, indicating an unstable speed subsidence mode. However, this will be modified to some extent by the oscillatory mode resulting in an exponentially increasing speed divergence.

The fast and stable real root dominates in normal velocity, row two, which can be interpreted as the '*heave mode*'. However, again the third mode will have a large influence on the vertical motion resulting in a well damped, long period oscillation in height.

Row three, representing pitch rate, shows the stable real root in the first column as the dominant mode. The '*other*' modes have very little influence on the pitch response. In the fourth row, both the oscillatory mode and unstable root have equal influence, which would result in an exponentially increasing oscillation in pitch attitude response.

The final mode positions have been plotted on the s-plane, see figure 3.14.

3.4 Speed instability

As has been stated previously, to generate sufficient lift at low-speed a slender-delta winged aircraft requires a large approach attitude of approximately 14°, equating to a C_L of 0.6. These large incidence angles generate correspondingly large amounts of lift-induced drag, C_{Di}, resulting in the familiar '*back-side*' operation, see figure 3.15. SCT's approach airspeed, V_{ref}, is significantly below its minimum drag speed (V_{emd}) and this speed instability will adversely affect the aircraft's flightpath response.

The aircraft's CG has been positioned at 35.8%MAC equating to a 5%MAC positive stability margin on the approach. At this flight condition the aircraft's longitudinal dynamic modes are the conventional short period and phugoid as follows

short period frequency $\omega_s = 0.71$ rad/s

damping ratio $\zeta_s = 0.773$

phugoid frequency $\omega_p = 0.12$ rad/s

$Tp = 52$ s

damping ratio $\zeta_p = 0.0099$

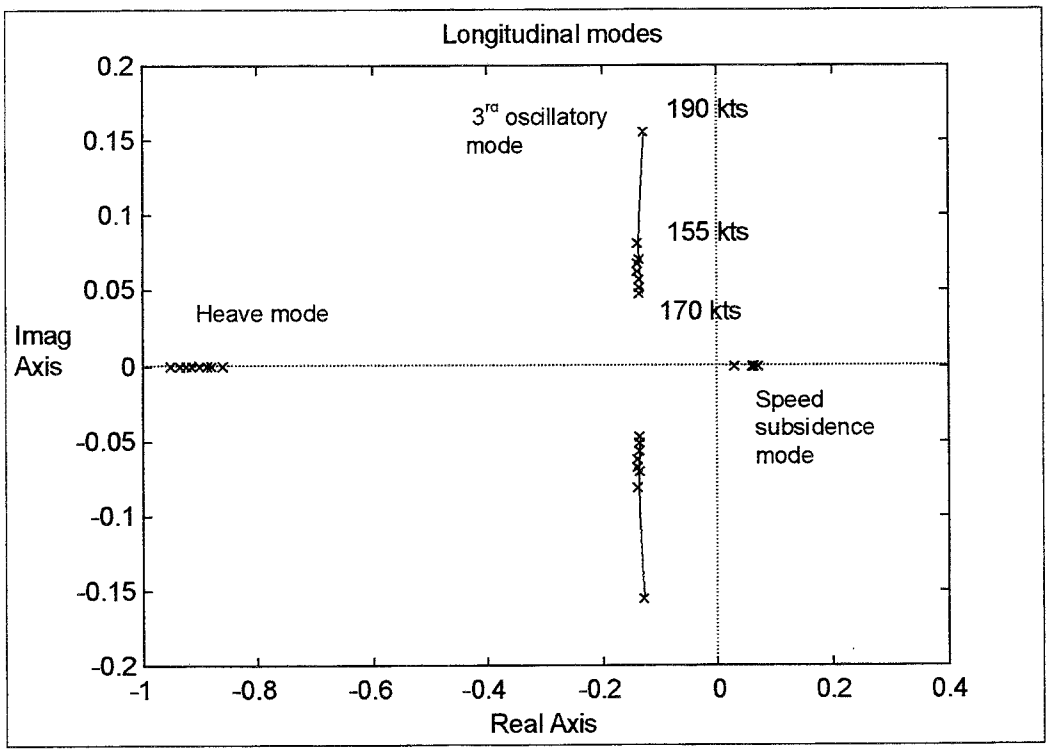

Figure 3.14 Decelerating approach, CG at approximate NP

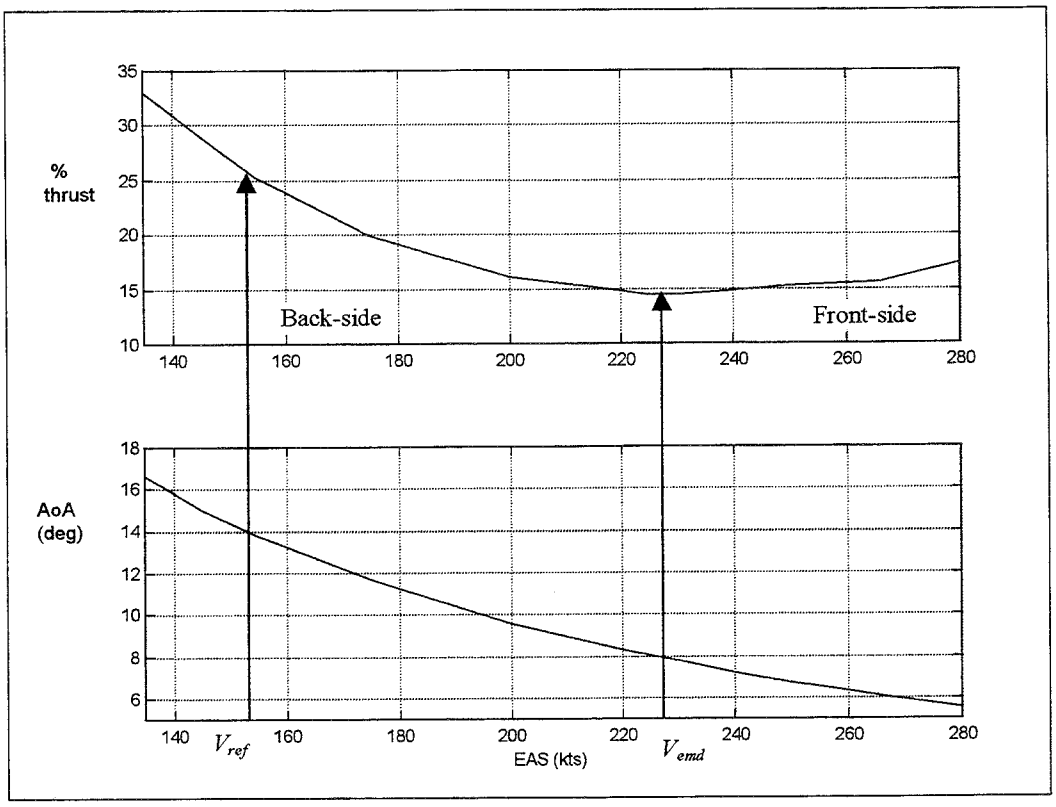

Figure 3.15 Drag (thrust) polar – approach

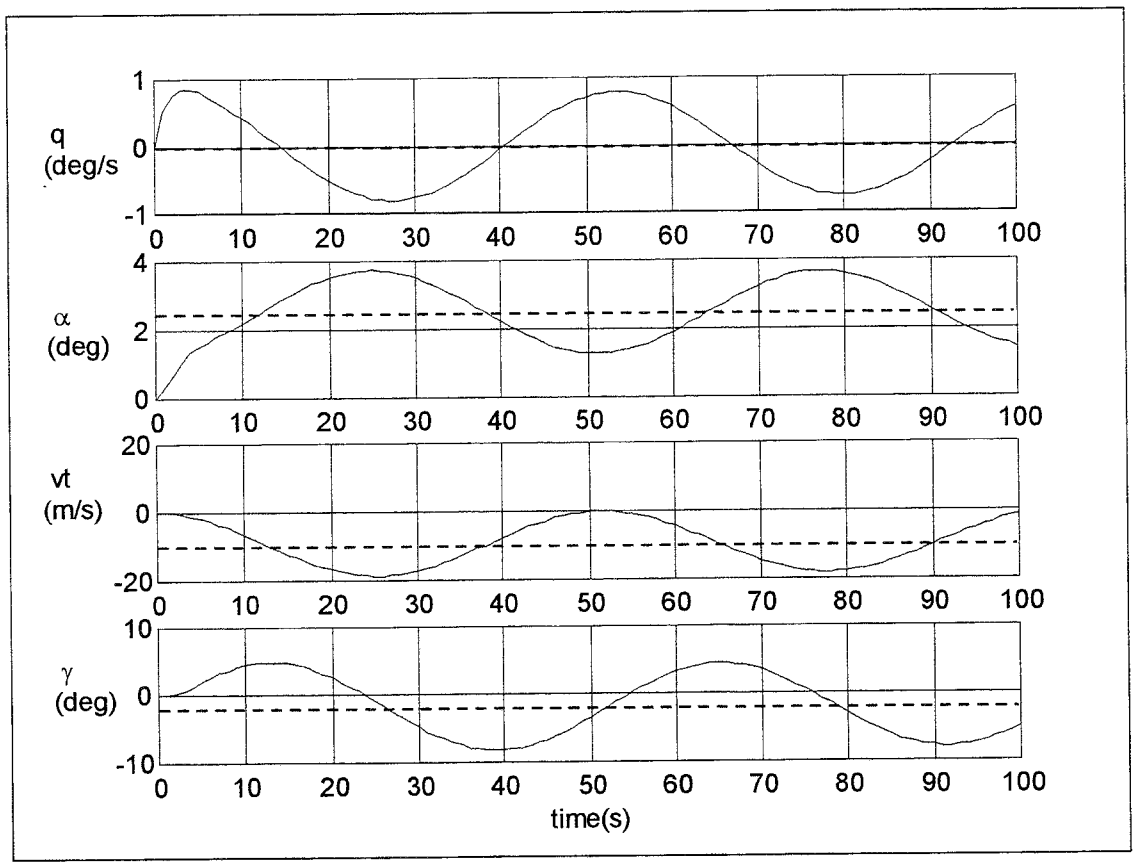

Figure 3.16 Long term longitudinal response

Figure 3.16 shows the aircraft's response, over 100 seconds, to a positive flightpath angle command when flying on the backside of the drag curve. The very low phugoid damping results in a highly oscillatory long term response, however it is the steady state response, shown in dashed line that is of significance.

The positive stick input generates an increase in AoA, lift and hence initial positive flightpath response as required. However, aircraft speed drops quickly resulting in a large increase in total drag due to C_{Di}, ultimately resulting in a long-term flightpath response opposite to that commanded. An increase in thrust, controlled either manually via the throttle levers or automatically through an autothrottle, would be required to maintain a positive flightpath response.

4 LOW SPEED CRUISE

4.1 Introduction

To enable a comprehensive analysis of the low-speed flight dynamics of the aircraft the 6 DoF non-linear mathematical model was initialised as per table 4.1 and the linear state space representations generated.

Low speed cruise	α°	θ°	γ°	Airspeed (kts)	Height (ft)	U/C	CG	η°
	6.67	6.67	0	250	1000	up	40.8%MAC	-1.67

Table 4.1 Initial trim conditions

The 9 state linear model was then split into de-coupled longitudinal and lateral/directional models.

4.2 Longitudinal mathematical model

The state, 4-1 and output equations, 4-2 in terms of the concise aerodynamic derivatives describing longitudinal motion are shown below.

$$\begin{bmatrix} \dot{u} \\ \dot{w} \\ \dot{q} \\ \dot{\theta} \end{bmatrix} = \begin{bmatrix} -0.0193 & -0.0516 & 0.0000 & -16.4543 \\ -0.1443 & -0.8102 & -11.5737 & -104.2678 \\ 0.0002 & -0.0029 & -0.5811 & -0.3672 \\ 0.0 & 0.0 & 1.0000 & 0.0 \end{bmatrix} \begin{bmatrix} u \\ w \\ q \\ \theta \end{bmatrix} + \begin{bmatrix} -0.0442 \\ -0.5304 \\ -0.0258 \\ 0.0000 \end{bmatrix} [\eta] \qquad (4\text{-}1)$$

$$\begin{bmatrix} q \\ \theta \\ \alpha \\ vt \\ n_{zcg} \\ n_{zp} \\ \gamma \end{bmatrix} = \begin{bmatrix} 0.0 & 0.0 & 57.2958 & 0.0 \\ 0.0 & 0.0 & 0.0 & 57.2958 \\ 0.0 & 0.4452 & 0.0 & 57.2958 \\ 1.0001 & 0.0005 & 0.0 & 0.0 \\ -0.0148 & -0.0826 & -1.1817 & -10.6295 \\ -0.0156 & -0.0702 & 1.3968 & -9.0201 \\ 0.0000 & -0.4452 & 0.0 & 0.0 \end{bmatrix} \begin{bmatrix} u \\ w \\ q \\ \theta \end{bmatrix} + \begin{bmatrix} 0.0 \\ 0.0 \\ 0.0 \\ 0.0 \\ -0.0542 \\ 0.0594 \\ 0.0 \end{bmatrix} [\eta] \qquad (4\text{-}2)$$

The relative magnitudes and signs of the concise pitching moment aerodynamic derivatives, m_u, m_w, m_q and m_θ are important to the stability and dynamic properties of the aircraft, shown as the third row, equation 4-1. The first value represents the speed derivative term, m_u, and is positive due to the thrust centre-line being located below the vertical location of the CG. Too large a value of m_u can cause large trim changes and aircraft response to gust disturbances however, it is nearly zero (0.0002) indicating that for this particular aircraft configuration, at this flight condition, it has little effect on

stability. The other three derivatives, m_w, m_q, and m_θ respectively are all negative and hence stabilising.

The output equation, 4-2, shows the conversion from radians to degrees of the first three variables while the other outputs are composed of elements of the model states. The accelerations, n_{zcg} and n_{zp} have the addition of components in the D matrix indicating direct lift effects from the elevator control, η.

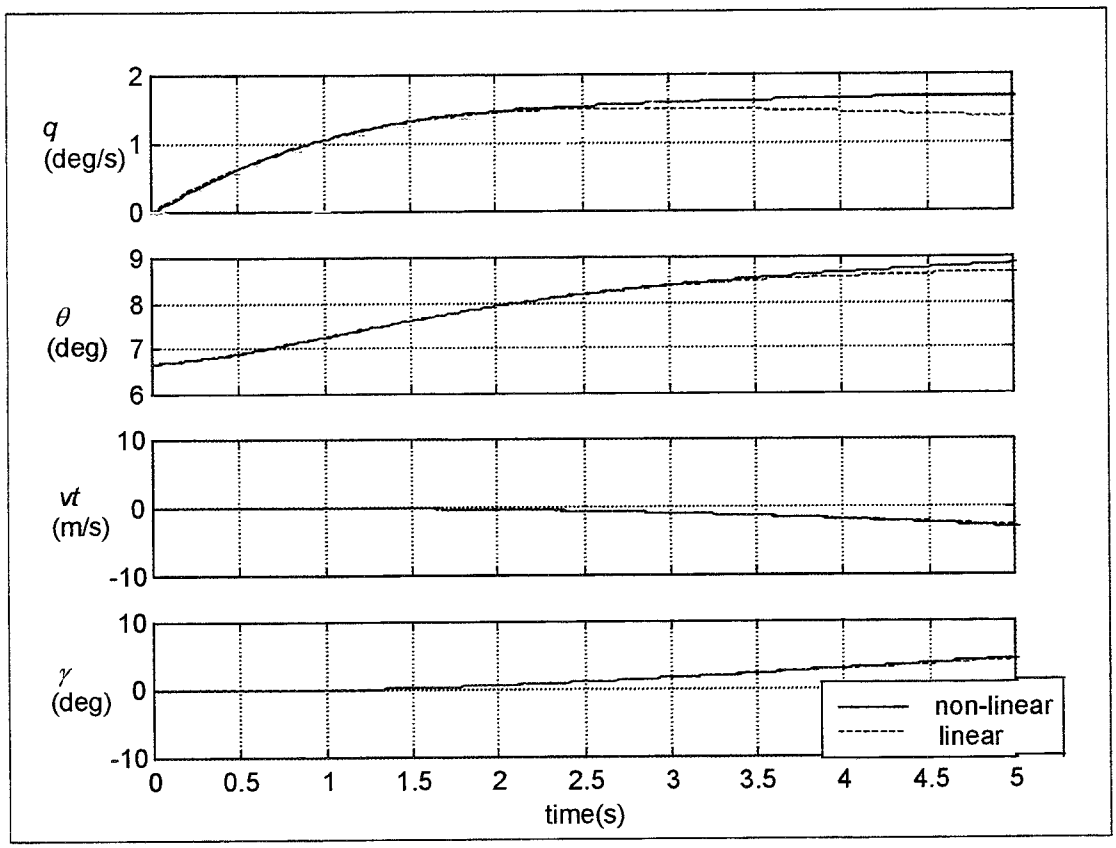

Figure 4.1 Model comparison

The validity of the longitudinal linear model was checked by comparing the response of a selection of longitudinal response parameters to a step control input with those generated by the non-linear model at the same flight conditions, see figure 4.1. The responses show a good match over the first 5 seconds of the simulation, hence confirming its validity for small perturbation analysis.

4.3 Longitudinal dynamic modes

The longitudinal dynamic modes are excited whenever the aircraft is disturbed from its equilibrium state. The denominator of the transfer function describes the characteristic polynomial, which in turn describes the longitudinal stability characteristics of the aircraft.

The characteristic equation is fourth order and at this particular flight condition factorises into two pairs of complex roots, equation 4-3

$$(s^2 + 0.00549s + 0.006593)(s^2 + 1.4051s + 0.81) \quad (4\text{-}3)$$

The second order characteristics in the above equation describe the phugoid and SPPO modes respectively, equation 4-4

$$(s^2 + 2\zeta_p\omega_p s + \omega_p{}^2)(s^2 + 2\zeta_s\omega_s s + \omega_s{}^2) \quad (4\text{-}4)$$

The roots describing the phugoid and SPPO modes have been plotted on the s-plane, figure 4.2. The complex pair of phugoid roots lie close to the origin showing them to be very slow, while their low damping is indicated by their close proximity to the imaginary axis. The short period roots are much faster coupled with characteristically increased damping, ζ_s, over the phugoid. The airframe can be seen to be aerodynamically stable due to all the roots possessing negative real parts.

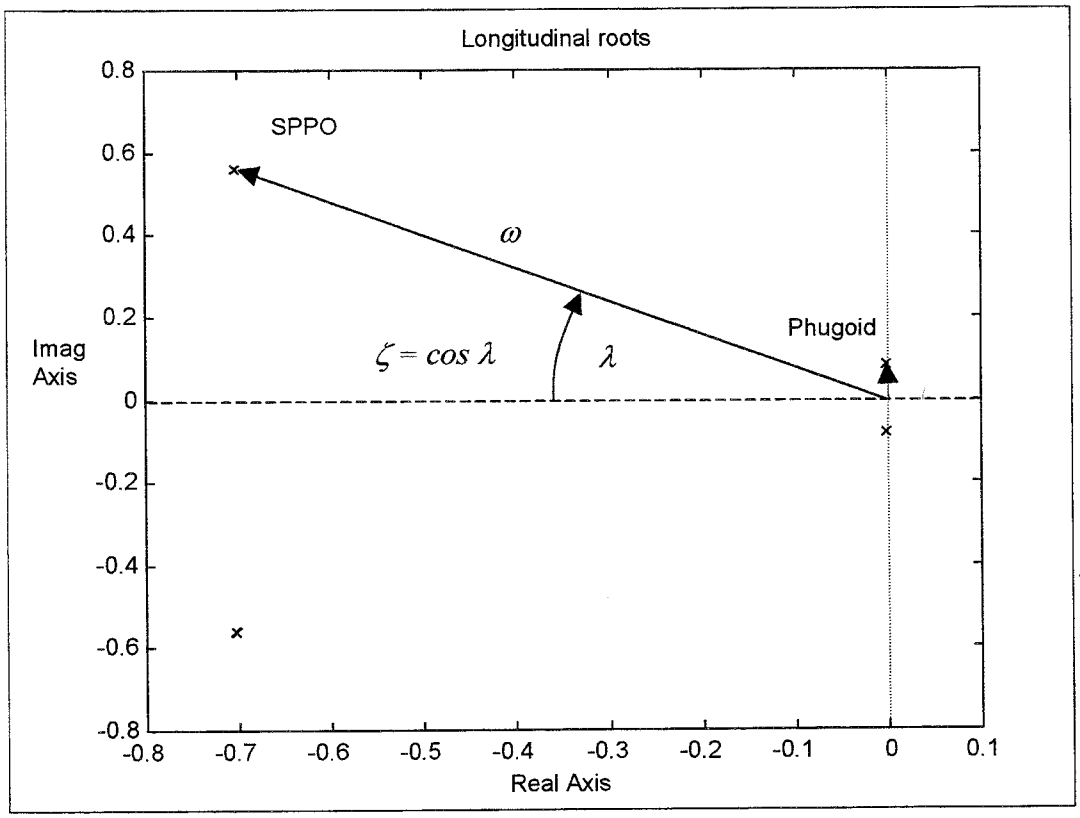

Figure 4.2 Longitudinal roots on the s-plane

4.3.1 Phugoid mode

The first pair of complex roots describing the phugoid mode are characterised by a very low frequency and damping ratio as shown below.

damping ratio $\zeta_p = 0.0338$

undamped natural frequency $\omega_p = 0.0812$ rad/s

period $T_p = 2\pi/\omega = 77.4$s

In order to excite the airframes longitudinal dynamic modes a 1 second pulse has been input to the elevator at 5 seconds, see figure 4.3. The phugoid mode can clearly be seen as long period oscillation in airspeed and flight-path, with minimal visibility of pitch rate and incidence. From the airspeed and flight-path response a time period for the phugoid mode, T_p, of approximately 65-70s can be measured, this compares very favourably with the time period calculated from the linear state model.

4.3.2 SPPO mode

The second pair of complex roots describes the SPPO, with damping ratio, frequency and time period characteristics

$$\text{damping ratio } \zeta_s = 0.7806$$

$$\text{undamped natural frequency } \omega_s = 0.9 \text{ rad/s}$$

$$\text{period } T_s = 2\pi/\omega = 6.98\text{s}$$

The SPPO mode has also been excited by the control input, figure 4.3, and can be observed within the first few seconds principally as perturbations in pitch rate and incidence. There is very little effect of this fast acting mode on the flight-path and speed responses, however due to the low phugoid damping some residual elements are still visible.

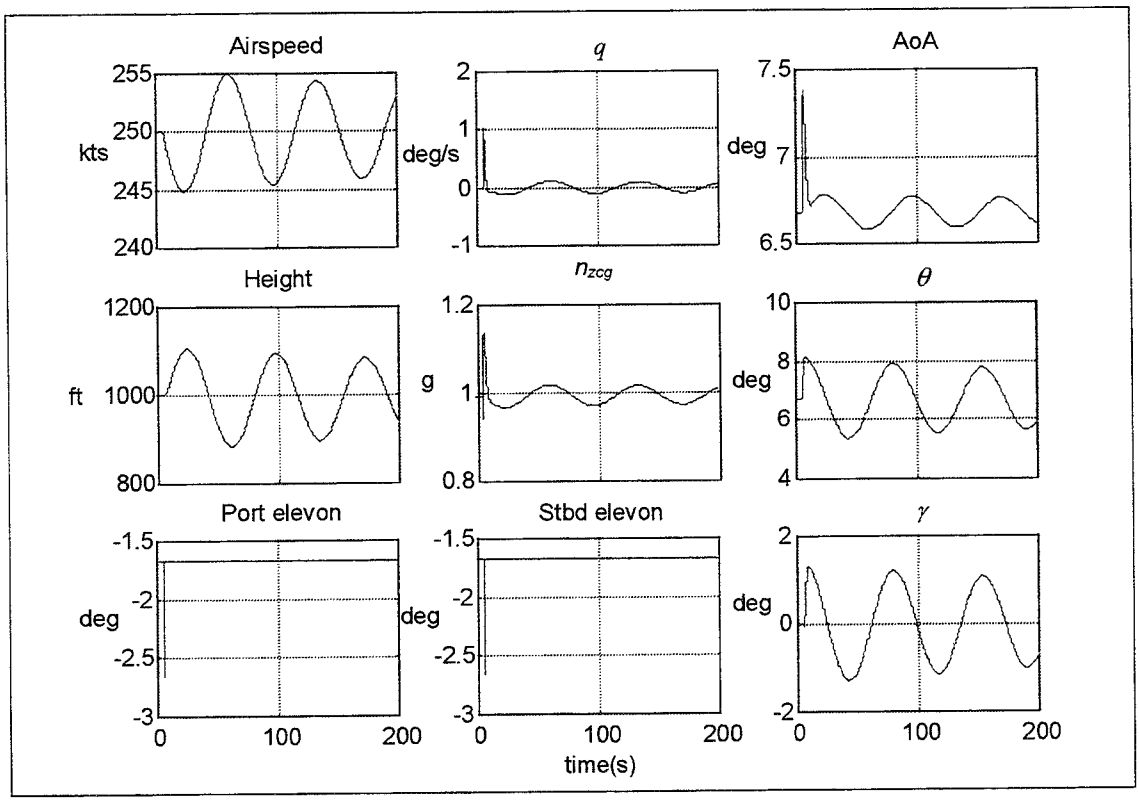

Figure 4.3 Excitation of longitudinal dynamic modes

4.3.3 Flying quality requirements

The parameters describing the longitudinal dynamic modes have been compared with the performance and flying qualities criteria for classical aircraft specified in MIL-STD-1797A [5]. Low speed cruise can be interpreted as either flight phase category B or C.

Acceptable limits on the stability of the SPPO mode are quantified in terms of the maximum and minimum values of the damping ratio as a function of the flight phase category and level of flying qualities, see table 4.2.

	Level 1		Level 2		Level 3
Flight phase	ζ_s min	ζ_s max	ζ_s min	ζ_s max	ζ_s min
Cat B	0.3	2.0	0.2	2.0	-
Cat C	0.35	1.3	0.25	2.0	0.15

Table 4.2 SPPO damping requirements

The low-speed SPPO damping ratio of 0.7806 equates to level 1 flying qualities as it is greater than the stated minimum requirement for both flight phase categories.

Level	Minimum ζ_p
1	0.04
2	0
3	Unstable, period $T_p > 55$s

Table 4.3 Phugoid damping requirements

The aircraft's phugoid damping ratio of 0.034 equates to level 2 flying qualities. It has been stated that *"generally, the phugoid dynamics are acceptable if they are stable and the values tabulated in table 4.3 are adhered to"*.

In addition, if the separation between the short period and phugoid frequencies is small,

$$\text{i.e. } \omega_p/\omega_s < 0.1$$

handling qualities difficulties may arise. For the current flight condition

$$\omega_p/\omega_s = 0.0812/0.9 = 0.0902$$

which is slightly lower than the minimum suggested.

4.4 Longitudinal response transfer function analysis

The response of the longitudinal variables to a control input is dominated by the denominator parameters, namely the time constants, damping ratios and natural frequencies. Additionally, the differences between the individual responses are determined by their respective numerators. The pitch rate transfer function differs from that of attitude through the addition of a pure integrator in the numerator, therefore only the attitude transfer function has been analysed.

To support the following transfer function analysis, the time response of selected longitudinal response parameters to a step elevator input at $t = 0$ have been plotted and some important relationships identified, see figure 4.4.

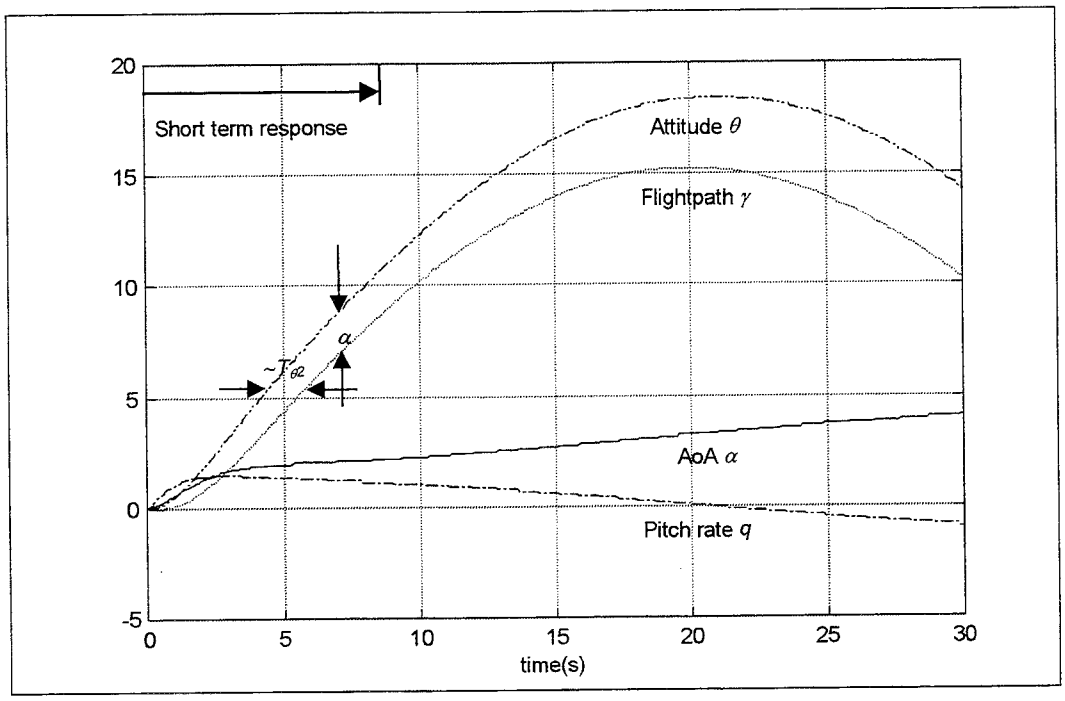

Figure 4.4 Longitudinal response to a step elevator input

4.4.1 Aircraft bandwidth

The limiting frequency at which the response commences to rapidly diminish is referred to as the *bandwidth* of the aircraft with respect to the output variable of interest. This is due to the mass and inertia properties of the aircraft constraining its response to command inputs, hence is the range of frequencies over which the response will follow the stick. Therefore it is a measure of the speed of response achievable in a given aircraft, the greater the bandwidth the faster response.

The aircraft is acting as a low pass system with resonant frequencies at the phugoid and short period modes and their magnitudes dependent on their respective damping ratios.

4.4.2 Pitch attitude to elevator

$$\frac{\theta}{\eta}(s) = \frac{(s+0.0102)(s+0.7609)}{(s+0.00275\pm 0.0812i)(s+0.703\pm 0.563i)} \text{deg/deg} \tag{4-5}$$

where

$$\frac{\theta}{\eta}(s) = \frac{(s+1/T_{\theta 1})(s+1/T_{\theta 2})}{(s^2+2\zeta_p\omega_p s+\omega_p{}^2)(s^2+2\zeta_s\omega_s s+\omega_s{}^2)} \tag{4-6}$$

hence $T_{\theta 1}$ = 1/0.0102 = 98 s and $T_{\theta 2}$ = 1/0.7609 = 1.3142 s

$T_{\theta 1}$ refers to the effective lag in the airframe airspeed response and is predominantly dependent upon drag.

$T_{\theta 2}$ provides lead and overshoot in the initial pitch rate response compared to that of incidence and defines the lag, known as *'incidence lag'*, between the pitch attitude and flightpath responses, see figure 4.4. The negative term in the numerator of the response transfer function is a result of the control input sign convention and manifests itself as a positive aircraft response in pitch for a negative elevator input. It can also be seen in the bode plot as -180° of phase shift at low frequencies, see figure 4.5.

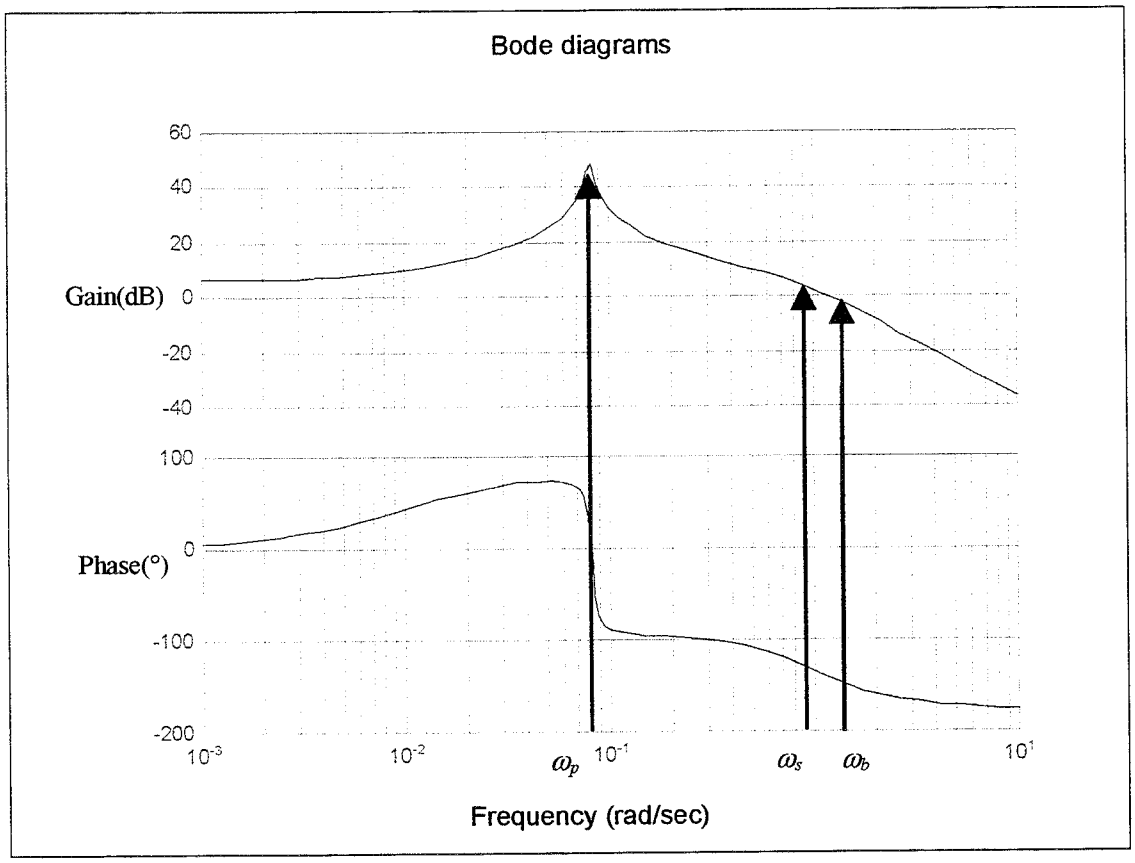

Figure 4.5 Pitch attitude response to elevator

The bode diagrams, figure 4.5, show a *'classical'* pitch attitude frequency response. There is little gain, only 6.0 dB equating to a doubling of the input, below a frequency of 0.01 rad/s indicating that the pitch response follows the input linearly. As the frequency of the input is increased, both gain and phase increase, reaching maximum values at the phugoid frequency, ω_p, of 50dB and 90° respectively. After this point the gain steadily drops off and the phase decreases rapidly settling at -90° of lag until reaching the short period frequency.

At frequencies greater than the short period frequency, ω_s of 0.9 rad/s, the gain drops off rapidly due to the increased damping attenuating the aircraft's pitch response. The bandwidth, ω_b, defined here as the frequency at which the gain first drops to –3dB below the zero frequency, or steady state gain, is approximately 1.5 rad/s.

4.4.3 Incidence (AoA) to elevator

$$\frac{\alpha}{\eta}(s) = \frac{(s+6.2736)(s^2+0.0166s+0.0112)}{(s+0.00275\pm 0.0812i)(s+0.703\pm 0.563i)} \text{deg/deg} \tag{4-7}$$

where

$$\frac{\alpha}{\eta}(s) = \frac{(s+1/T_\alpha)(s^2+2\zeta_\alpha\omega_\alpha s+\omega_\alpha^2)}{(s^2+2\zeta_p\omega_p s+\omega_p{}^2)(s^2+2\zeta_s\omega_s s+\omega_s{}^2)} \tag{4-8}$$

hence $\omega_\alpha = 0.106$ rad/s, $\zeta_\alpha = 0.0784$, and $T = 2\pi/\omega_\alpha = 59.3$ s and $T_\alpha = 0.159$ s

T_α is the incidence zero due to the instantaneous centre of rotation being forward of the CG. In addition, it's time constant of 0.159 seconds shows it to be fast acting.

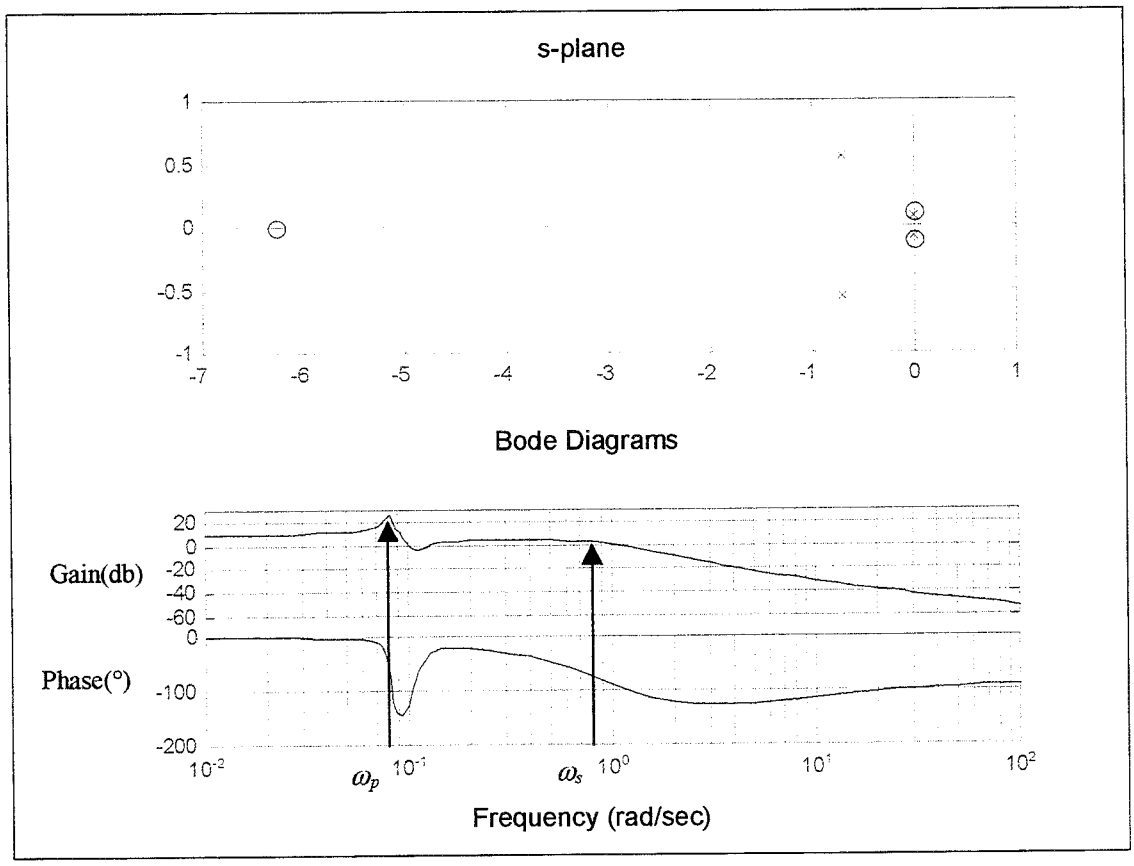

Figure 4.6 Incidence (AoA) response to elevator

As can be observed in both the transfer function and the s-plane diagram, figure 4.6, the long-term oscillatory incidence zeros effectively cancel out the phugoid poles, resulting in minimal visibility of the phugoid mode in the AoA response.

From the bode gain plot, the long-term response to a 1° elevator deflection is an incidence of 8.8 dB or 3.12°. As the frequency increases there is a larger peak gain than usual at the phugoid frequency, due to their inexact cancellation by the numerator zeros, which have an effect at a slightly higher frequency by adding 180° of phase.

At frequencies greater than ω_p the gain is more or less constant until after the short period frequency, ω_s, resulting in the aircraft incidence response following the control input with 90° of phase lag. After this point the gain rapidly decreases and the aircraft will no longer be seen to respond in incidence.

4.4.4 Flightpath to elevator

$$\frac{\gamma}{\eta}(s) = \frac{(s-0.0046)(s-2.1568)(s+2.1863)}{(s+0.00275 \pm 0.0812i)(s+0.703 \pm 0.563i)} \text{deg/deg} \tag{4-9}$$

where

$$\frac{\gamma}{\eta}(s) = \frac{(s+1/T_{\gamma 1})(s+1/T_{\gamma 2})(s+1/T_{\gamma 3})}{(s^2+2\zeta_p\omega_p s+\omega_p{}^2)(s^2+2\zeta_s\omega_s s+\omega_s{}^2)} \tag{4-10}$$

hence $T_{\gamma 1} = 217.4$ s, $T_{\gamma 2} = 0.463$ s, $T_{\gamma 3} = 0.457$ s

$T_{\gamma 1}$ is a very slow flightpath zero, in this case an unstable positive mode, indicating the expected back side of the drag curve operation. $T_{\gamma 2}$ and $T_{\gamma 3}$ are of similar magnitude and located either side of the imaginary axis, their location determines the degree of non-minimum phase behaviour in the aircraft response.

Non-minimum phase behaviour, characterised by an initial opposite sense aircraft response to that demanded, is mathematically represented by transfer functions zeros in the right half of the s-plane, i.e. positive. This type of system must have two or more forward paths from input to output so that at some complex frequency a cancellation of the signals passing down these paths may occur. It should be noted that a minimum phase system is defined in *that 'the system transfer function has no poles or zeros in the right half s-plane'*. This behaviour can also be observed in the normal acceleration responses, as well as coupling into forward velocity.

From the bode diagram, figure 4.7, it can be seen that there is quite a peak in gain at the phugoid frequency, ω_p, this is to be expected as the phugoid is very lightly damped so describing large oscillatory flight path deviations. The useable bandwidth extends up to approximately 1 rad/s or the short period frequency, ω_s. At this frequency the response will follow the input in both gain and phase, as there is a gain of 1 and 360° of phase shift.

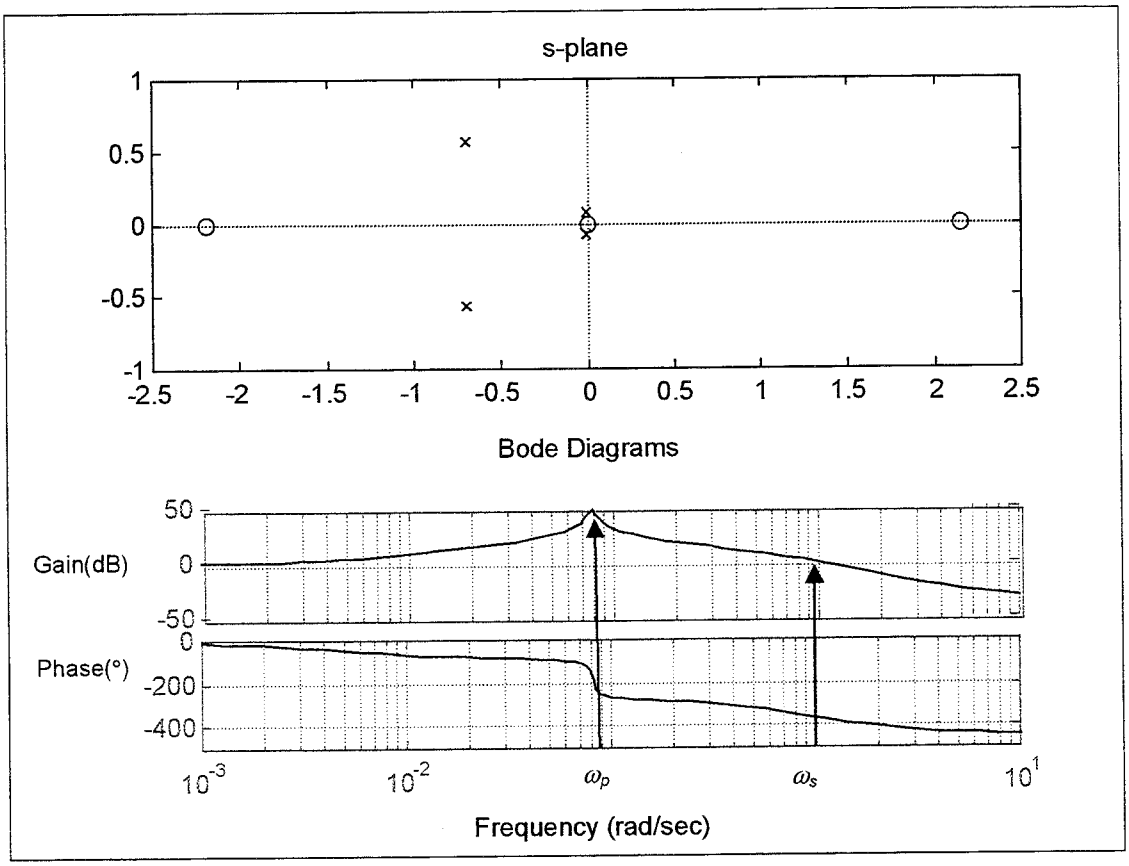

Figure 4.7 Flightpath response to elevator

4.4.5 Normal acceleration at the CG

$$\frac{a_{zcg}}{\eta}(s) = \frac{(s-0.0127)(s-2.151)(s+0.0077)(s+2.184)}{(s+0.00275\pm 0.0812i)(s+0.703\pm 0.563i)} g/\deg \qquad (4\text{-}11)$$

where

$$\frac{a_{zcg}}{\eta}(s) = \frac{(s+1/T_{a1_{zcg}})(s+1/T_{a2_{zcg}})(s+1/T_{a3_{zcg}})(s+1/T_{a4_{zcg}})}{(s^2+2\zeta_p\omega_p s+\omega_p{}^2)(s^2+2\zeta_s\omega_s s+\omega_s{}^2)} \qquad (4\text{-}12)$$

and T_{a1zcg}= 78.74s, T_{a2zcg} = 0.465s, T_{az3cg} = 129.9s, T_{az4cg}= 0.458s.

The response transfer function numerator is composed of four real roots, two fast and two slow. If the normal acceleration transfer function, equation 4-11, is compared with that of flight path response, equation 4-9, it can be seen that they are quite similar, however normal acceleration has an additional slow acting zero equivalent to a differentiation term. From this observation it can be deduced that normal acceleration at the CG is effectively rate of change of flight path.

From the step input response, figure 4.8, the effect of the fast non-minimum phase zero can be observed as an initial opposite sense acceleration response felt at the CG over the first half a second. The phugoid mode dominates the flightpath response resulting in long term oscillatory motion, which is lightly damped and eventually returning to zero as shown.

The bode diagram shows that the acceleration response is highly attenuated at low frequencies, hence the normal acceleration response will only become noticeable to the pilot between the phugoid and short period frequencies equating to the useable response bandwidth.

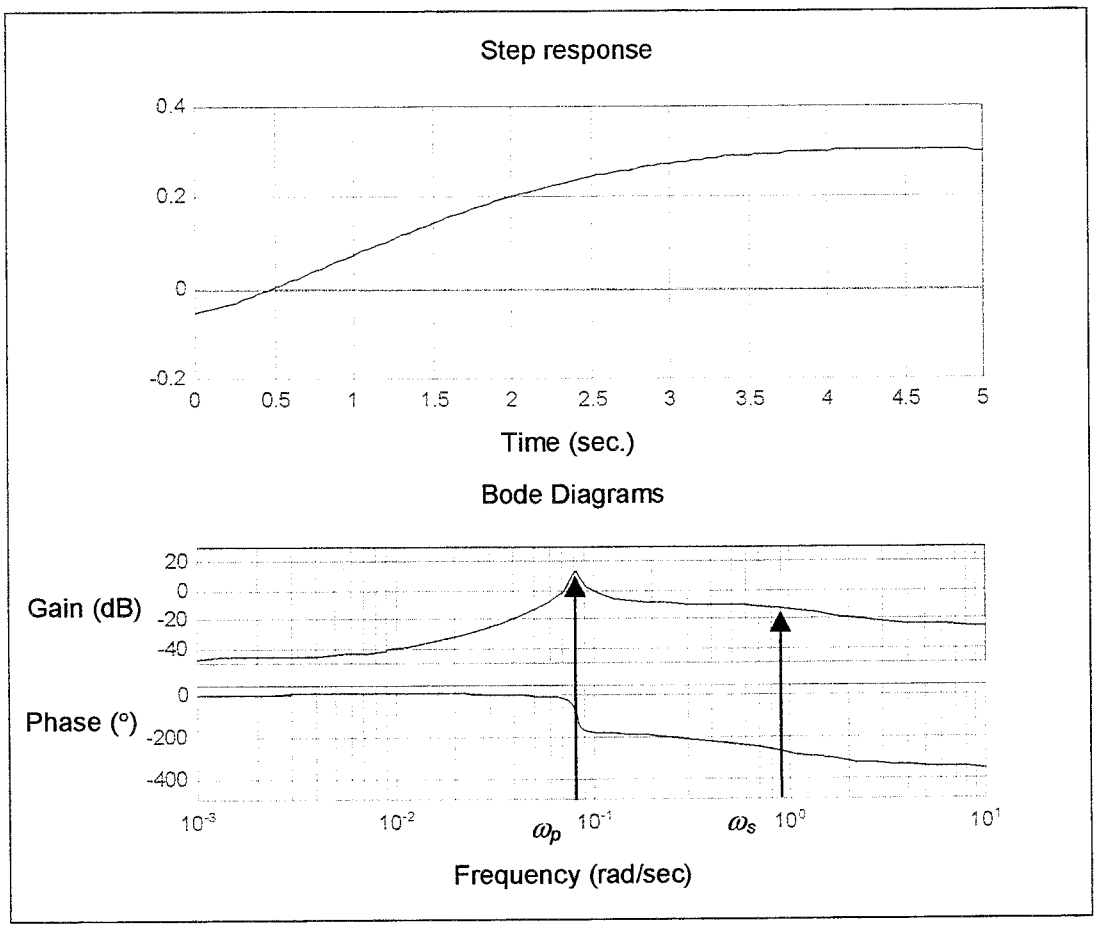

Figure 4.8 n_{zcg} response to elevator

4.4.6 Normal acceleration at the pilot station

$$\frac{a_{zp}}{\eta}(s) = \frac{(s-0.0134)(s+0.077)(s+0.724\pm1.945i)}{(s+0.00275\pm0.0812i)(s+0.703\pm0.563i)} g/\deg \qquad (4\text{-}13)$$

where

$$\frac{a_{zp}}{\eta}(s) = \frac{(s+1/T_{a_{zp1}})(s+1/T_{a_{zp2}})(s^2+2\zeta_{azp}\omega_{azp}+\omega_{azp}{}^2)}{(s^2+2\zeta_p\omega_p s+\omega_p{}^2)(s^2+2\zeta_s\omega_s s+\omega_s{}^2)} \tag{4-14}$$

and T_{azp1} = 74.62s, T_{azp2} = 12.99s, ζ_{azp} = 0.349 and ω_{azp} = 2.08 rad/s.

The numerator differs from that describing the normal acceleration at the CG in having a complex conjugate pair with the above damping and frequency properties instead of two real roots.

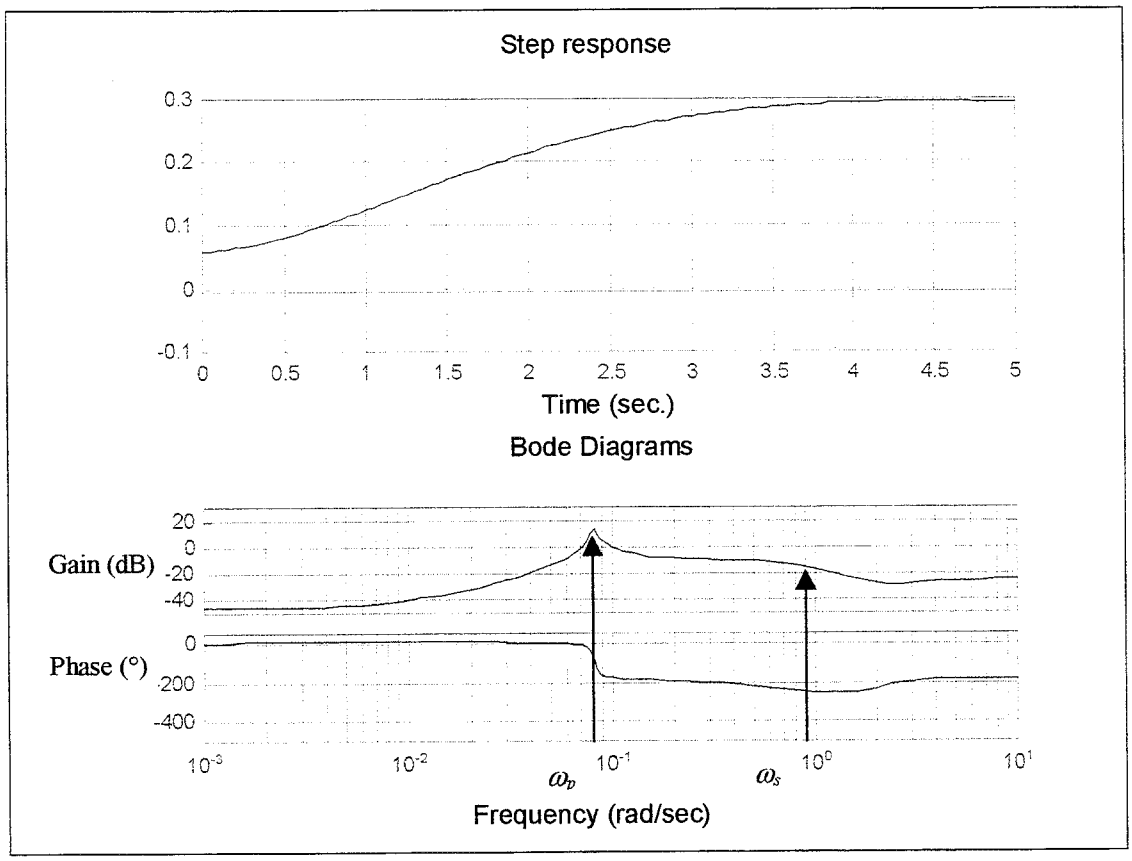

Figure 4.9 n_{zp} response to elevator

The time response, figure 4.9, shows no initial opposite sense motion due to the lack of a fast non-minimum phase zero in the transfer function, however the long-term response is similar to the normal acceleration at the CG.

The bode diagrams show that the gain at low frequencies is highly attenuated until approaching the phugoid frequency where it rises rapidly to a peak due again to the low damping. The gain falls and then stays roughly constant until reaching the short period frequency whereupon it rapidly drops off. The useable frequency range lies once again between the phugoid and short period frequencies.

4.4.7 Airspeed to elevator

$$\frac{vt}{\eta}(s) = \frac{(s-2.8482)(s+0.47933)(s+3.1364)}{(s+0.00275\pm 0.0812i)(s+0.703\pm 0.563i)} ms^{-1}/\deg \qquad (4\text{-}15)$$

where

$$\frac{vt}{\eta}(s) = \frac{(s+1/T_{vt1})(s+1/T_{vt2})(s+1/T_{vt3})}{(s^2+2\zeta_p\omega_p s+\omega_p{}^2)(s^2+2\zeta_s\omega_s s+\omega_s{}^2)} \qquad (4\text{-}16)$$

and $T_{vt1} = 0.351$s, $T_{vt2} = 2.088$s, $T_{vt3} = 0.319$s.

The numerator has factorised into three real roots, one of which is located in the right half of the s-plane.

For a positive step elevator input there is a corresponding decrease in airspeed as the aircraft rotates to a positive attitude resulting in a steady state gain of -35.6 m/s. The step response shows no SPPO visibility, however the phugoid mode is very noticeable as expected. Velocity perturbations at frequencies in the vicinity of the SPPO are usually small.

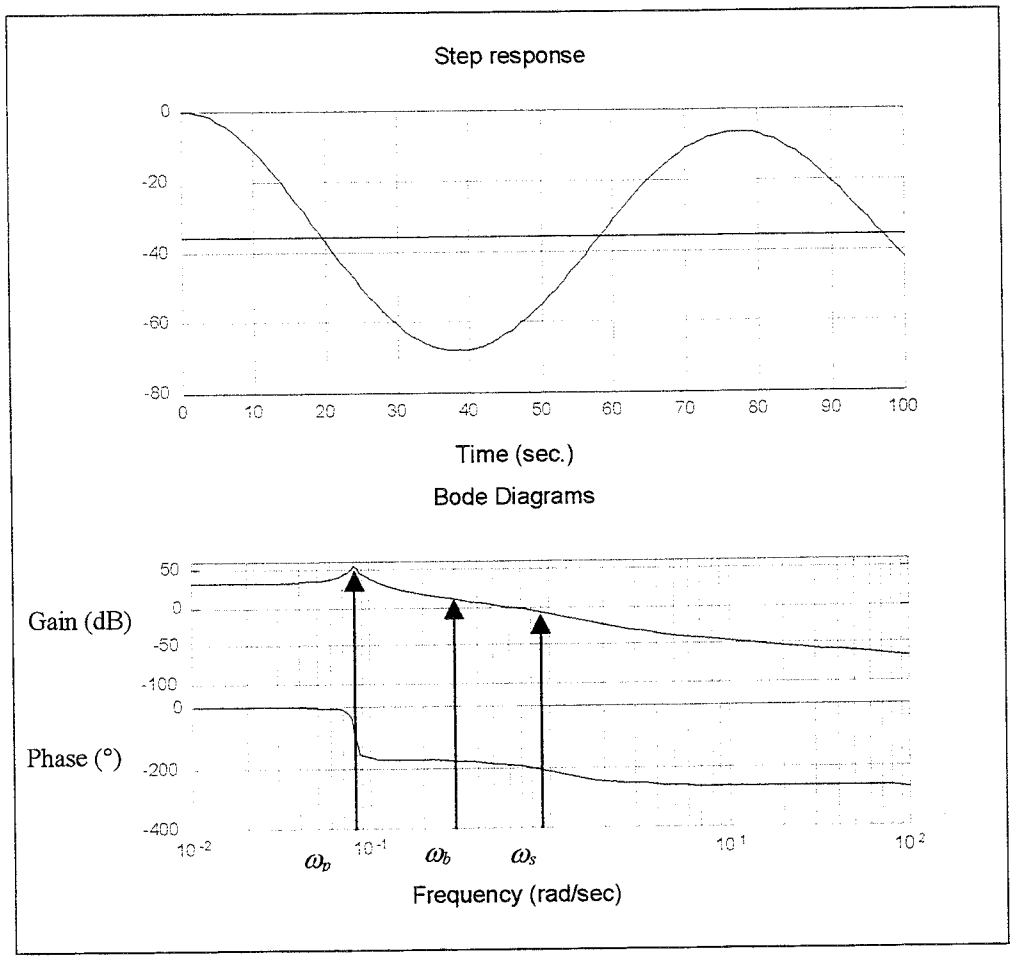

Figure 4.10 Airspeed response to elevator

From the frequency response, figure 4.10, it can be observed that for all practical purposes speed changes demanded by the pilot will follow the stick in the useable frequency range, i.e. up to the bandwidth frequency, ω_b, of approximately 0.3 rad/s. At the phugoid frequency, ω_p, the gain ratio is approximately 55dB illustrating the large speed variation visible in the phugoid mode. While at the short period frequency, ω_s, the pilot input has very little effect on speed as the dc gain is approximately 1.

4.5 Lateral/directional mathematical model

Once again, the aircraft initial flight conditions are as set out in table 4.1.

The state, (4-17) and output equations, (4-18) in terms of the concise aerodynamic derivatives describing lateral/directional motion are shown below.

$$\begin{bmatrix} \dot{v} \\ \dot{p} \\ \dot{r} \\ \dot{\phi} \\ \dot{\psi} \end{bmatrix} = \begin{bmatrix} -0.0893 & 1.2546 & 1.0311 & 8.4045 & 11.4939 \\ -0.0161 & -1.5392 & 0.5677 & -0.2403 & 2.0677 \\ 0.0017 & -0.0654 & -0.1583 & 0.0249 & -0.2143 \\ 0 & 1.0 & 0.117 & 0 & 0 \\ 0 & 0 & 1.0068 & 0 & 0 \end{bmatrix} \begin{bmatrix} v \\ p \\ r \\ \phi \\ \psi \end{bmatrix} + \begin{bmatrix} -0.0601 & 0.0495 \\ 0.0664 & 0.0022 \\ 0.0063 & -0.0044 \\ 0 & 0 \\ 0 & 0 \end{bmatrix} \begin{bmatrix} \xi \\ \zeta \end{bmatrix} \quad (4\text{-}17)$$

$$\begin{bmatrix} p \\ r \\ \beta \\ \phi \\ \psi \\ n_{ycg} \end{bmatrix} = \begin{bmatrix} 0 & 57.2958 & 0 & 0 & 0 \\ 0 & 0 & 57.2958 & 0 & 0 \\ 0.4452 & 0 & 0 & 6.6588 & -57.2958 \\ 0 & 0 & 0 & 57.2958 & 0 \\ 0 & 0 & 0 & 0 & 57.2958 \\ -0.0091 & 0.1279 & 0.1051 & -0.1362 & 1.1720 \end{bmatrix} \begin{bmatrix} v \\ p \\ r \\ \phi \\ \psi \end{bmatrix} + \begin{bmatrix} 0 & 0 \\ 0 & 0 \\ 0 & 0 \\ 0 & 0 \\ 0 & 0 \\ -0.0061 & 0.005 \end{bmatrix} \begin{bmatrix} \xi \\ \zeta \end{bmatrix} \quad (4\text{-}18)$$

where the A and B state matrix equations are composed of the following state variables in concise form

$$\begin{bmatrix} \dot{v} \\ \dot{p} \\ \dot{r} \\ \dot{\phi} \\ \dot{\psi} \end{bmatrix} = \begin{bmatrix} y_v & y_p & y_r & y_\phi & y_\psi \\ l_v & l_p & l_r & l_\phi & l_\psi \\ n_v & n_p & n_r & n_\phi & n_\psi \\ 0 & 1 & 0 & 0 & 0 \\ 0 & 0 & 1 & 0 & 0 \end{bmatrix} \begin{bmatrix} v \\ p \\ r \\ \phi \\ \psi \end{bmatrix} + \begin{bmatrix} y_\xi & y_\zeta \\ l_\xi & l_\zeta \\ r_\xi & r_\zeta \\ \phi_\xi & \phi_\zeta \\ \psi_\xi & \psi_\zeta \end{bmatrix} \begin{bmatrix} \xi \\ \zeta \end{bmatrix} \quad (4\text{-}19)$$

The important derivatives describing motion about the lateral-directional axes are:

l_v, roll moment due to sideslip and known as the dihedral derivative. This is negative due to wing sweepback (dihedral effect) indicating positive roll stiffness.

l_p, roll moment due to roll rate, this is negative, opposes the roll response and hence is known as the roll mode damping derivative. It is important in determining the roll-rate performance of an aircraft.

l_r, roll moment due to yaw rate, this is positive due to wing sweepback and fuselage interference effects.

n_v, yaw moment due to sideslip is known as the yaw stiffness derivative, this is positive due to fin lift effects.

n_p, yaw moment due to roll rate, this is negative due to differential induced drag.

n_r, yaw moment due to yaw rate known as the yaw-damping derivative, this is negative due to fin lift and describes 'weathercock' stability.

The input matrix illustrates the relative effects of the controls on the principal parameters of interest. Aileron, ξ, is seen to affect the side, v, and roll accelerations in equal measure whilst having little influence on yaw. The rudder, ζ, has a principal effect on the side acceleration, however, it does make a contribution to the roll and yaw acceleration responses, p and r.

The output equation 4-18, illustrates the conversion from radians to degrees of the roll and yaw rates, p and r, and the respective attitudes, ϕ and ψ. Sideslip, β, is composed principally of negative heading with additional elements of side velocity, v, and roll attitude, ϕ, due to the aircraft incidence at this flight condition. The side acceleration, n_{ycg}, has elements of all the states combined with direct feed-through components of the control inputs observable in the second matrix.

Figures 4.11 and 4.12 compare the linear and non-linear model lateral-directional state parameter responses of interest to aileron and rudder inputs respectively. It can be clearly observed that over the short term, up to 15 to 20 seconds, they match closely.

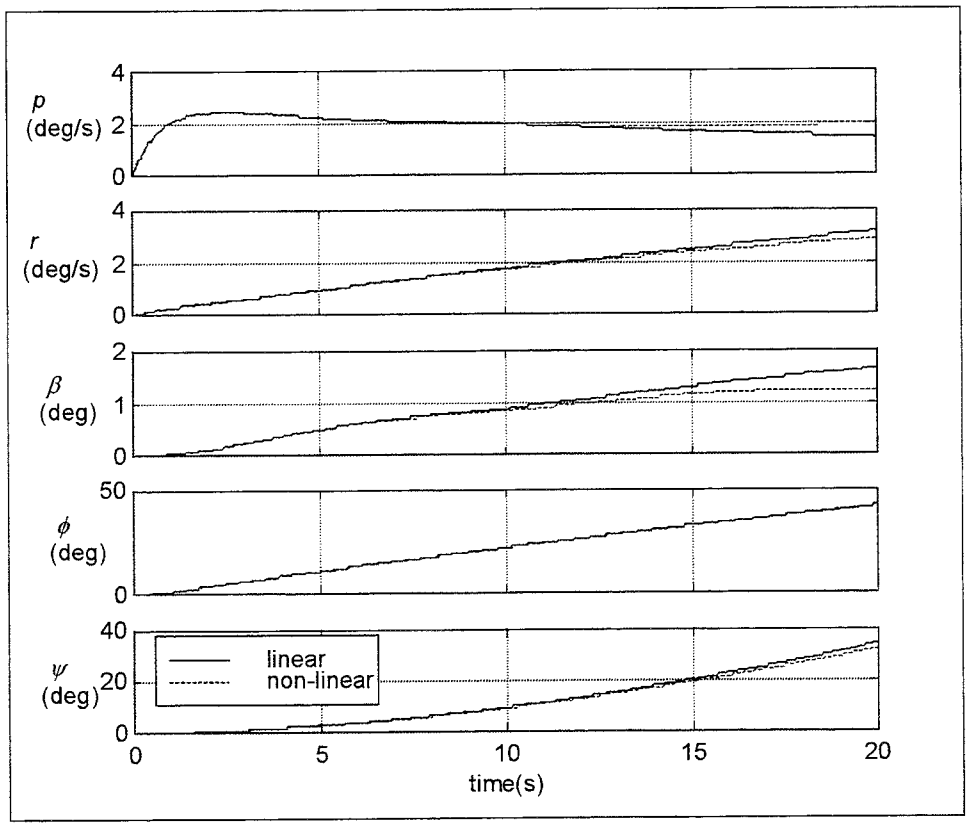

Figure 4.11 Lateral/directional response to an aileron step input

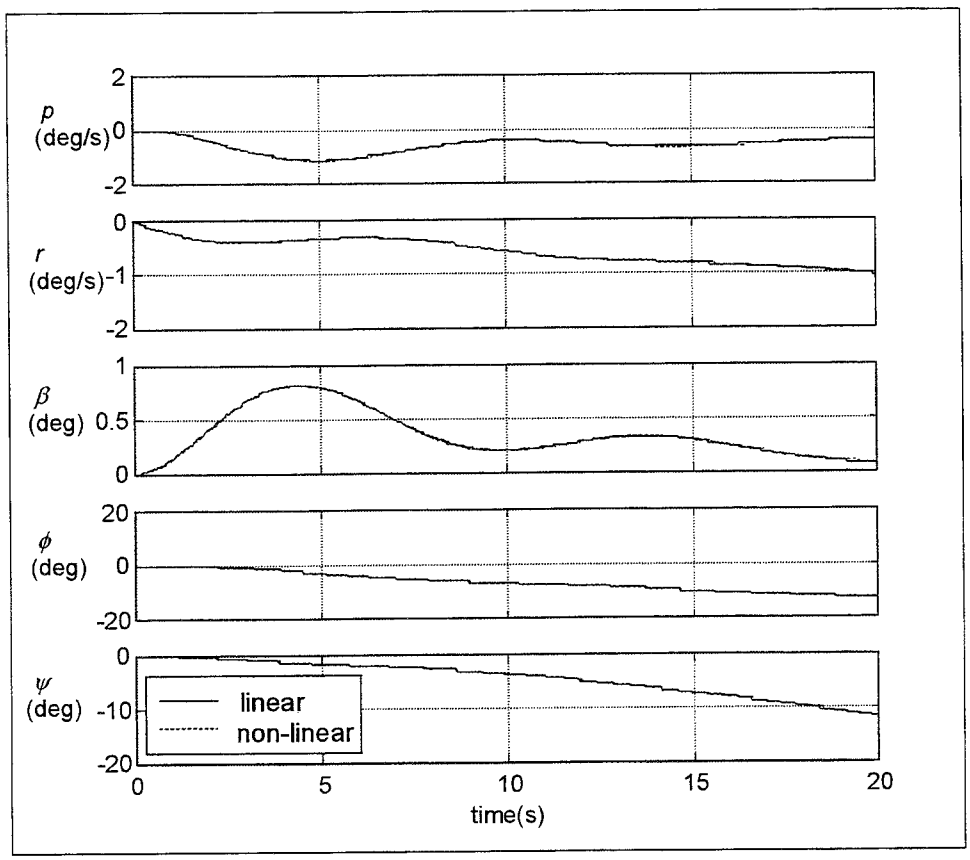

Figure 4.12 Lateral/directional response to a rudder step input

4.6 The lateral/directional dynamic modes

The lateral/directional characteristic equation is fifth order and factorises into a zero root, two real roots and a complex pair, equation 4-20.

$$s(s+1.4755)(s+0.0176)(s^2+0.2937s+0.44) \tag{4-20}$$

The real roots represent the roll subsidence mode and spiral mode respectively and the complex pair describes damped harmonic motion known as the dutch roll mode. The zero root indicates neutral stability in yaw (heading) angle, however, it is of little consequence in the assessment of dynamic stability.

$$s(s+1/T_r)(s+1/T_s)(s^2+2\zeta_d\omega_d s+\omega_d{}^2) \tag{4-21}$$

Equation 4-21 represents the roll subsidence and spiral modes in terms of their respective time constants, T_r and T_s, and the dutch roll mode in terms of its damping ratio, ζ_d, and frequency, ω_d. Their relative magnitudes are

$$T_r = 0.68\text{s}$$

$$T_s = 56.8\text{s}$$

$$\zeta_d = 0.2215$$

$$\omega_d = 0.663 \text{ rad/s.}$$

The dutch roll frequency, ω_d, is relatively low due to the large yaw moment of inertia and rear CG position. The damped natural frequency is

$$\omega = \omega_n\sqrt{1-\zeta^2} \tag{4-22}$$

hence

$$\omega = 0.663\sqrt{1-0.2215^2} = 0.646\ rad/s \tag{4-23}$$

due to the low dutch roll damping the damped natural frequency, ω, is little changed from the natural frequency. The damped natural frequency equates to a time period for one complete cycle of $T = 2\pi/\omega = 9.726$s.

The lateral/directional dynamic modes have been plotted on the s-plane, see figure 4.13.

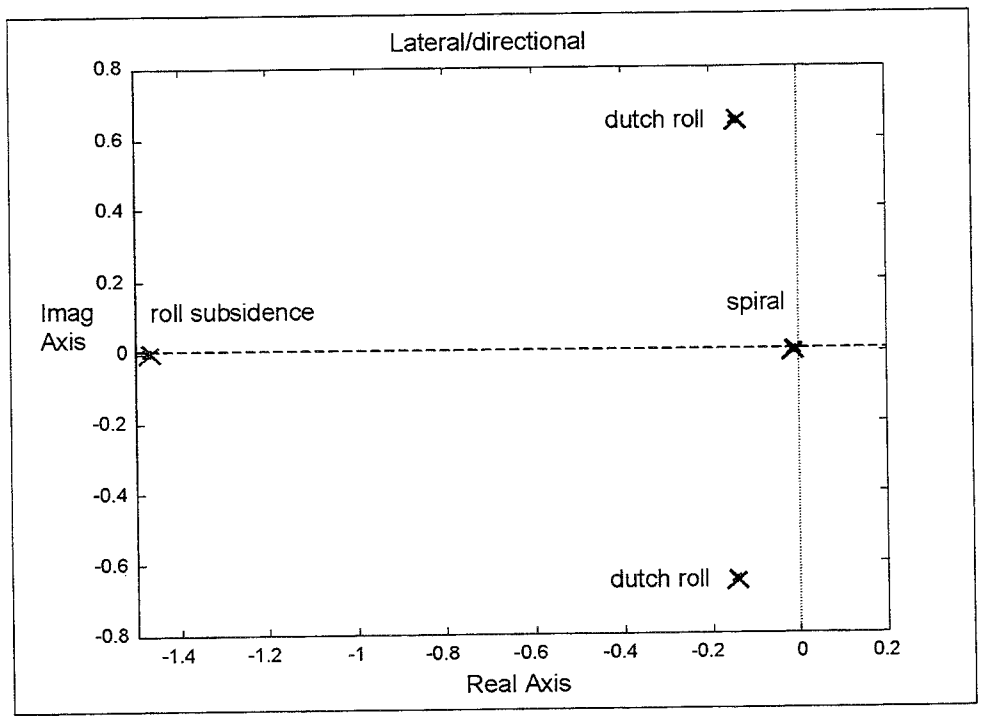

Figure 4.13 Lateral/directional stability modes

4.6.1 Roll subsidence mode

The roll mode can be excited through a step aileron input to the roll rate transfer function. The overshoot in the response, solid line, can be attributed to inexact cancellation of the dutch roll mode together with the effect of a numerator zero in the full order roll rate transfer function. The first order roll subsidence mode response is shown, in dashed line, for comparison, see figure 4.14.

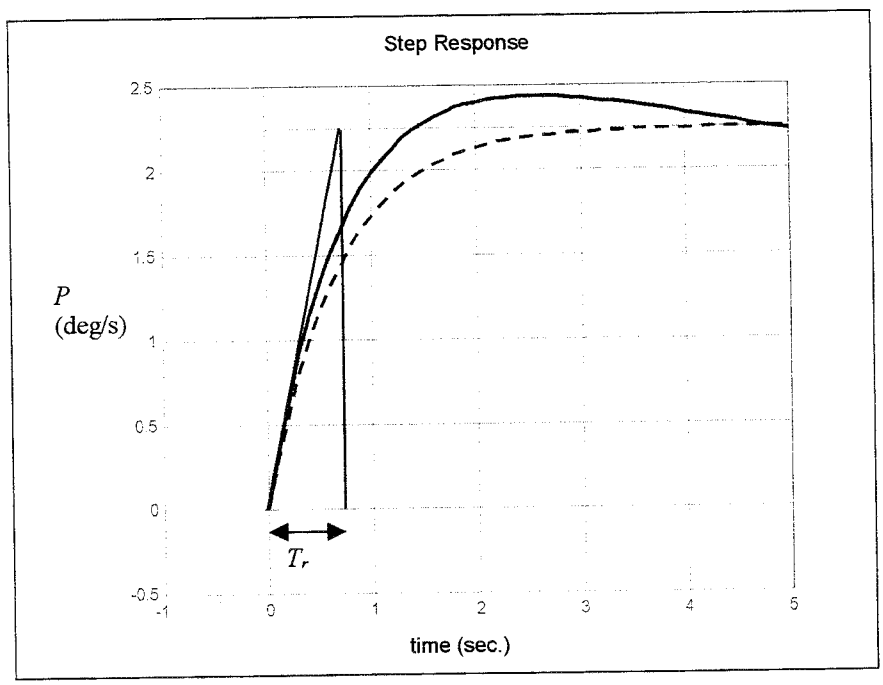

Figure 4.14 Roll response and associated time constant

To explain the aircraft roll response there is an initial acceleration in roll rate until the steady state is attained where roll damping L_p equals the control moment. The negative roll damping, L_p, will retard the response and is a function of roll rate. The exponential rise in roll rate is determined by the mode time constant, T_r, which has been calculated previously as 0.68s, see figure 4.14.

4.6.2 Spiral mode

The spiral mode is excited by a rudder step input. This is the smaller of the two real roots, therefore T_s is larger and requires an extended simulation period in order to be observed. When the spiral mode is stable it is characterised by a convergence in sideslip and angle of bank, see figure 4.15. The initial positive sideslip generated by the rudder couples into an opposite roll rate and hence build up of attitude and aircraft heading. After the rudder is brought back to zero the stable spiral mode slowly brings the wings level, indicated by the angle of bank, ϕ, returning to zero and by a constant heading, ψ, of -12°.

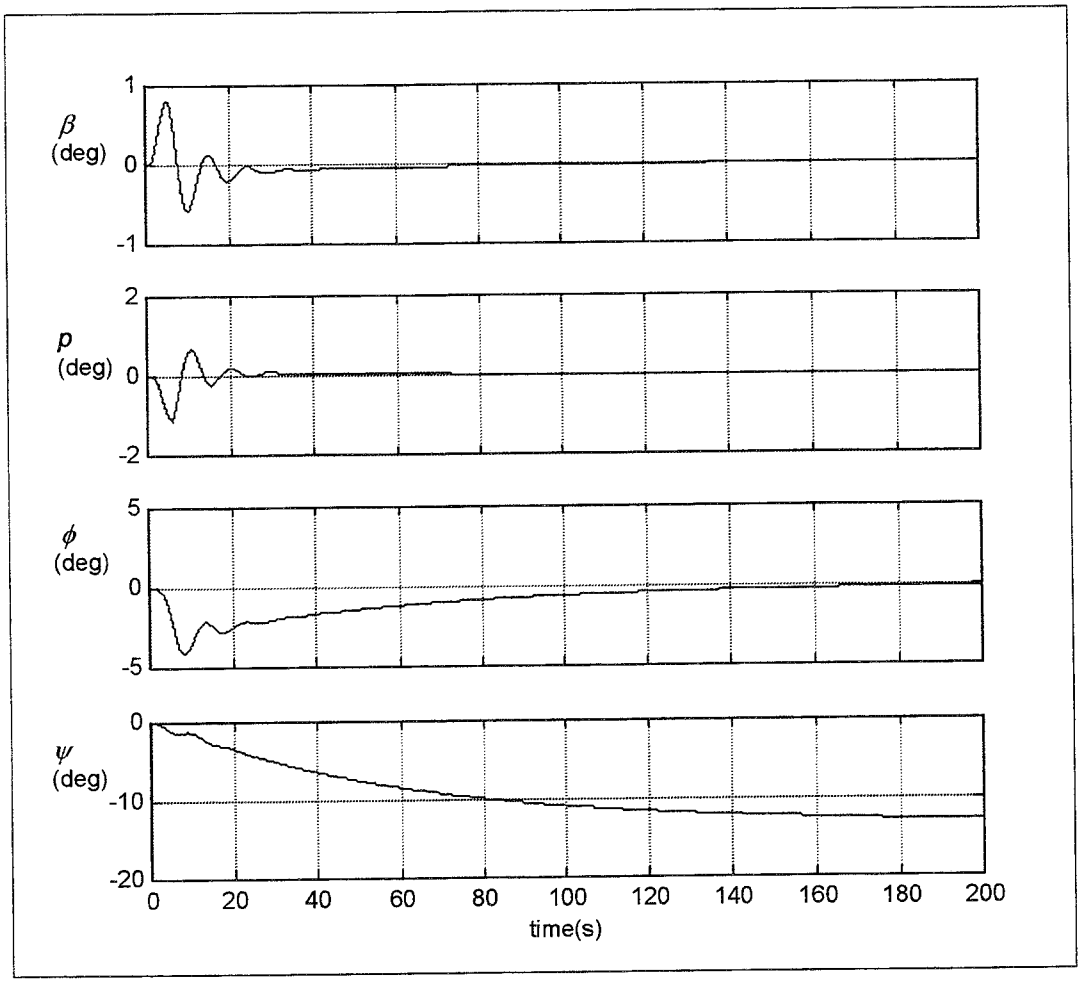

Figure 4.15 Spiral mode response

4.6.3 Dutch roll mode

The dutch roll can be excited by a disturbance in yaw, in this case initiated by an impulse to the rudder, figure 4.16. There is an initial negative yaw rate, N_ζ, together with a

positive roll rate, L_ζ, due to the rudder centre of lift acting above the aircraft's axis of rotation. However, the build up of positive sideslip starts to generate negative rolling moment, L_r, which rolls the wings. Damping in roll, L_p, opposes this but leaves the aircraft in a sideslip. Weathercock stability, N_r, provides a restoring moment, which brings the sideslip back through zero, with the yaw inertia resulting in an overshoot. Thus the cycle starts again in the opposite direction. This motion results in a vertical ellipse being traced at the wing tips.

The responses show that roll rate and sideslip are 180° out of phase but of similar magnitude. In this case the dutch roll mode is stable. The damped natural frequency, ω, is shown to generate oscillatory motion in all three response variables with time periods of approximately 9.8s.

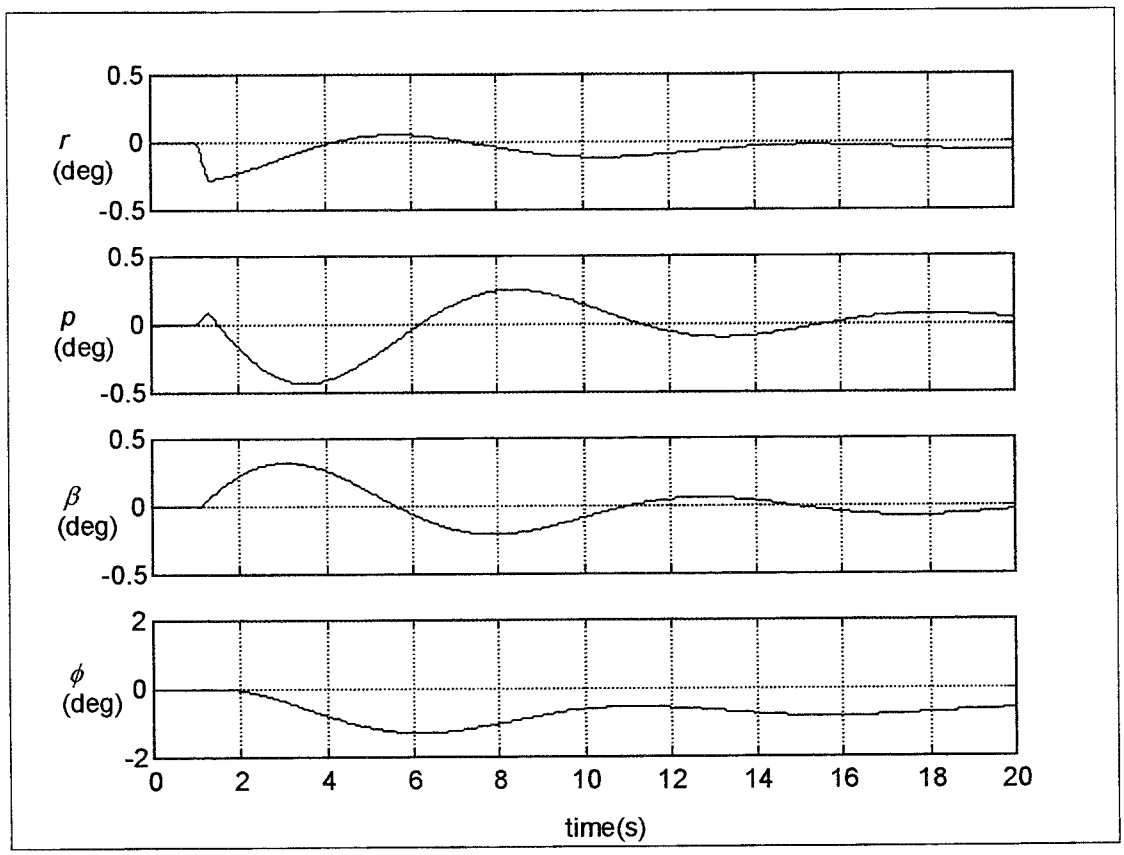

Figure 4.16 Excitation of dutch roll mode

A significant portion of the response is in roll due to the low roll/yaw moment of inertia ratio, in the region of 1/7 or 0.14, for this type of aircraft configuration. The roll/yaw response ratio, ϕ/β, calculated from the parameters of interest shown in figure 4.16 is approximately 4.0, as ϕ = 1.3 and β = 0.32, hence it is an inverse relationship to the moment of inertia ratio.

In addition, according to MIL-STD-1797A, a relatively large value of roll/yaw ratio does not equate to '*classical*' aircraft characteristics.

4.6.4 Flying quality requirements

The time constant of the roll mode, T_r, for a class III aircraft is required to be less than the specified maximum values given in table 4.4. The roll mode time constant of 0.68s is seen to fall easily within level 1 handling qualities limits.

Flight phase category		T_r	
	Level 1	Level 2	Level 3
A, B and C	1.4s	3.0s	10s

Table 4.4 Roll mode time constant specifications

In addition, MIL-STD-1797A states *"for aircraft with a roll rate response that is not easily approximated by a first order equation, an alternative specification such a bandwidth may be in order"*.

The aircraft's roll performance is specified in terms of the change of bank angle achieved in a given time, in response to a step function in roll command. For a class III aircraft the time to achieve a 30° change in bank angle and the corresponding level are specified in table 4.5. The roll performance requirement is also based on a range of airspeeds, however only the values for low speed, $V_{min} \leq V < 1.8\ V_{min}$, are given here.

Flight phase category	Level 1	Level 2	Level 3
B	2.3s	3.9s	5.0s
C	2.5s	4.0s	6.0s

Table 4.5 30° bank angle requirements

Figure 4.17 shows the aircraft roll performance for full-scale aileron input at 1 second. For a 30° step input the bank angle is achieved within approximately 1 second, well within level 1 criteria for flight phase category B, see table 4.5. However, related studies carried out by the author have shown how roll performance can be degraded when control surface actuators are modelled [18]. An example is overlaid on figure 4.17 in dashed red, the time to achieve 30° of bank is now approximately 1.6 seconds, however this is still within the specified performance criteria.

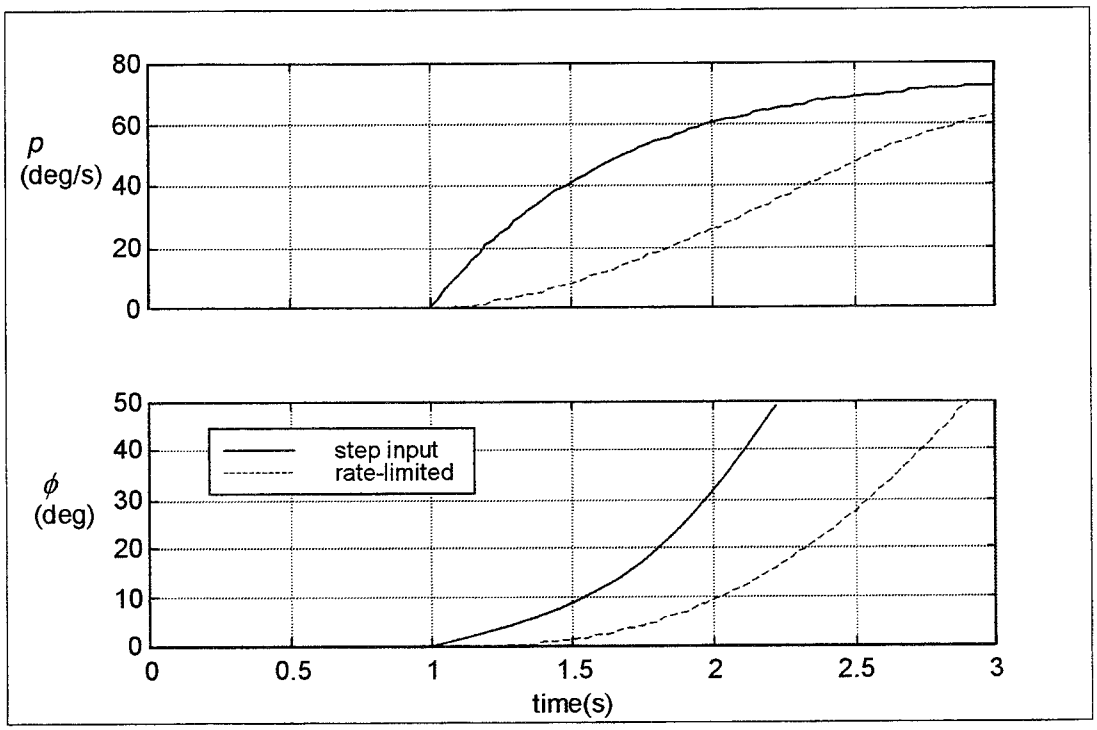

Figure 4.17 Roll performance

A stable spiral mode is acceptable regardless of its time constant, hence a T_s of 56.8s satisfies the requirements.

However, if the mode is unstable then the following specification applies. The time taken for the bank angle to double following an initial disturbance in bank angle of up to 20° must not exceed the values given in table 4.6.

Flight phase category	Level 1	Level 2	Level 3
A and C	12.0s	8.0s	5.0s
B	20.0s	8.0s	5.0s

Table 4.6 Unstable spiral mode stability specification

The values of the important dutch roll parameters are specified in table 4.7 for a class III aircraft. For flight phase category B, the requirements for level 1 handling qualities are a minimum value of damping ratio, ζ_d, of 0.08, a minimum dutch roll frequency, ω_d, of 0.5 and a combination, $\zeta_d\omega_d$, of 0.15. ESCT's respective values are 0.2215, 0.663 and 0.146 showing that the aircraft satisfies level 1 flying qualities for damping and frequency, however, it just drops into level 2 requirements for the damping-ratio product.

In addition, it is stated that it is permissible to use the yaw control to reduce any sideslip, which tends to retard roll rate. However, yaw control is not permitted to induce sideslip, which enhances the roll rate.

Flight phase category	Level 1			Level 2			Level 3		
	ζ_d	$\zeta_d\omega_d$	ω_d	ζ_d	$\zeta_d\omega_d$	ω_d	ζ_d	$\zeta_d\omega_d$	ω_d
B	0.08	0.15	0.5	0.02	0.05	0.5	0.0	-	0.4
C	0.08	0.10	0.5	0.02	0.05	0.5	0.0	-	0.4

Table 4.7 Dutch roll mode requirements

4.7 Lateral/directional transfer function analysis

The stability characteristics have already been established, therefore it is required to analyse the aircraft's lateral/directional response to control inputs.

The response of all variables to an aileron or rudder input is dominated by the denominator parameters, namely the time constants, damping ratio and natural frequency, and is common to all the response transfer functions. Hence, the differences between the individual responses are entirely determined by their respective numerators.

4.7.1 Roll rate to aileron

$$\frac{p}{\xi}(s) = \frac{(s-0.0085)(s+0.1624\pm 0.6343i)}{(s+1.4755)(s+0.0176)(s+0.1468\pm 0.646i)} \text{deg}\, s^{-1}/\text{deg} \qquad (4\text{-}24)$$

where

$$\frac{p}{\xi}(s) = \frac{(s+1/T_\phi)(s^2+2\zeta_\phi\omega_\phi+\omega_\phi^2)}{(s+1/T_r)(s+1/T_s)(s^2+2\zeta_d\omega_d s+\omega_d^2)} \qquad (4\text{-}25)$$

hence $\zeta_\phi = 0.248$, $\omega_\phi = 0.6548$ and $T_\phi = 1/0.0085 = 117.647$s.

The numerator in the transfer function factorises into one very slow unstable root and a complex conjugate pair.

4.7.2 Roll attitude to aileron

$$\frac{\phi}{\xi}(s) = \frac{(s+0.1615\pm 0.6338i)}{(s+1.4755)(s+0.0176)(s+0.1468\pm 0.646i)} \text{deg}/\text{deg} \qquad (4\text{-}26)$$

where

$$\frac{\phi}{\xi}(s) = \frac{(s^2+2\zeta_\phi\omega_\phi+\omega_\phi^2)}{(s+1/T_r)(s+1/T_s)(s^2+2\zeta_d\omega_d s+\omega_d^2)} \qquad (4\text{-}27)$$

and $\zeta_\phi = 0.247$ and $\omega_\phi = 0.654$ rad/s

The numerator consists of a complex conjugate pair.

The s-plane diagram in figure 4.18 shows how the complex pair of roots describing the dutch roll mode are almost exactly cancelled by the complex zeros effectively removing its visibility in the response.

In addition, the frequency response represented by the bode diagram shows that for a constant step input the dcgain of 143.9 deg/deg at low frequencies will result in a continual build up in attitude. As the control input frequency increases past the spiral mode frequency, $1/T_s$, the gain attenuates and phase lag increases. While the gain is greater than 0dB up to the roll subsidence frequency, $1/T_r$, the aircraft will respond positively to an aileron input, however control sensitivity will gradually reduce.

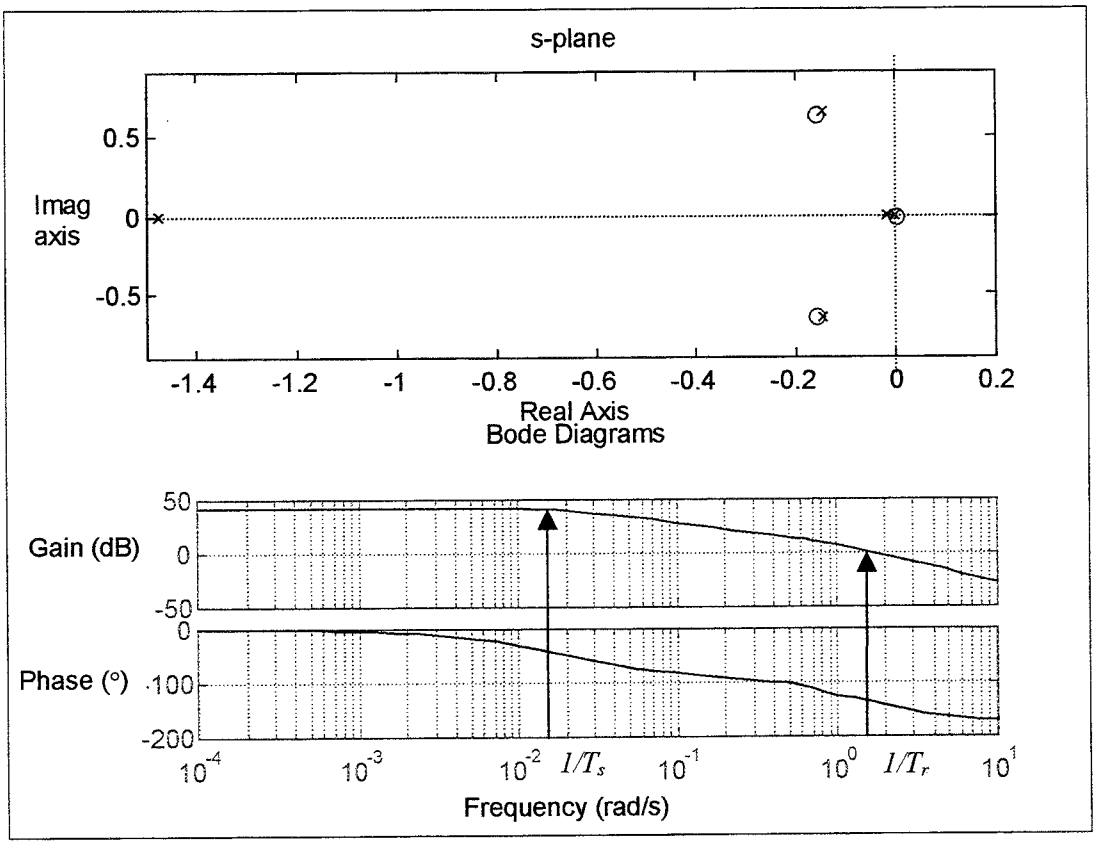

Figure 4.18 Roll attitude response to aileron input

4.7.3 Yaw rate to aileron

$$\frac{r}{\xi}(s) = \frac{(s+0.7353)(s+0.0962\pm 0.6593i)}{(s+1.4755)(s+0.0176)(s+0.1468\pm 0.646i)} \deg s^{-1}/\deg \qquad (4\text{-}28)$$

where

$$\frac{r}{\xi}(s) = \frac{(s+1/T_\psi)(s^2+2\zeta_\psi\omega_\psi+\omega_\psi^2)}{(s+1/T_r)(s+1/T_s)(s^2+2\zeta_d\omega_d s+\omega_d^2)} \qquad (4\text{-}29)$$

and $\zeta_\psi = 0.1443$, $\omega_\psi = 0.6663$ and $T_\psi = 1/0.7353 = 1.36$s.

The numerator has factorised into three roots, one real and stable and a complex conjugate pair.

Figure 4.19 shows the low frequency gain to be 10.3 deg/s for a 1° aileron deflection and for control inputs up to approximately 0.2 rad/s there will be a positive response in yaw rate. At this frequency there is 90° of phase lag continuing to ω_d as expected, describing the roll/yaw coupling of the dutch roll mode.

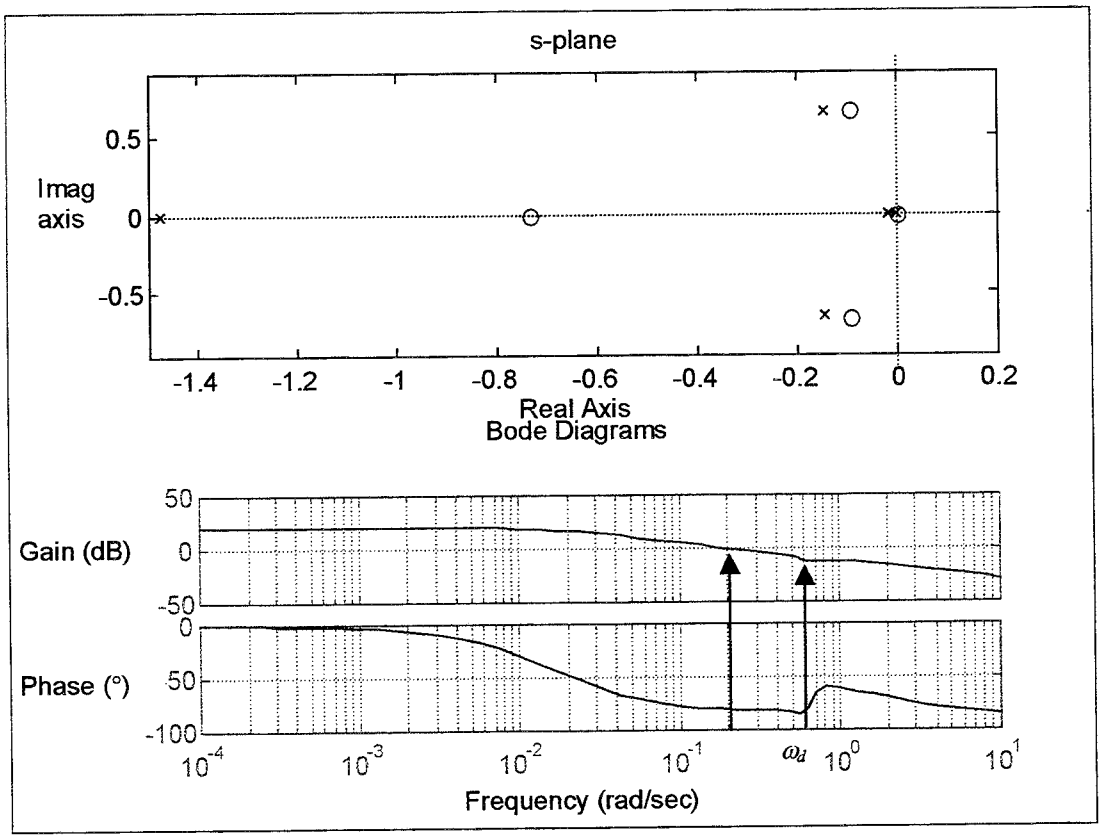

Figure 4.19 Yaw rate response to aileron input

4.7.4 Sideslip to aileron

$$\frac{\beta}{\xi}(s) = \frac{(s-3.799)(s+0.4761\pm 0.6344i)}{(s+1.4755)(s+0.0176)(s+0.1468\pm 0.646i)} \text{deg/deg} \qquad (4\text{-}30)$$

where

$$\frac{\beta}{\xi}(s) = \frac{(s+1/T_\beta)(s^2+2\zeta_\beta\omega_\beta+\omega_\beta^2)}{(s+1/T_r)(s+1/T_s)(s^2+2\zeta_d\omega_d s+\omega_d^2} \qquad (4\text{-}31)$$

where $\zeta_\beta = 0.6003$, $\omega_\beta = 0.7932$ rad/s and $T_\beta = 0.2632$s.

The numerator is fourth order and has factorised into a complex pair and a real root located on the right-hand side of the s-plane, see figure 4.20.

The bode diagram shows that at low frequencies there is a constant dcgain of 5.59 deg/deg. At the dutch roll mode frequency, ω_d, there is a slight peak in gain as expected. The transfer function zero at 3.799 rad/s will result in non-minimum phase behaviour, however, it is so fast acting that its influence on the response will be negligible.

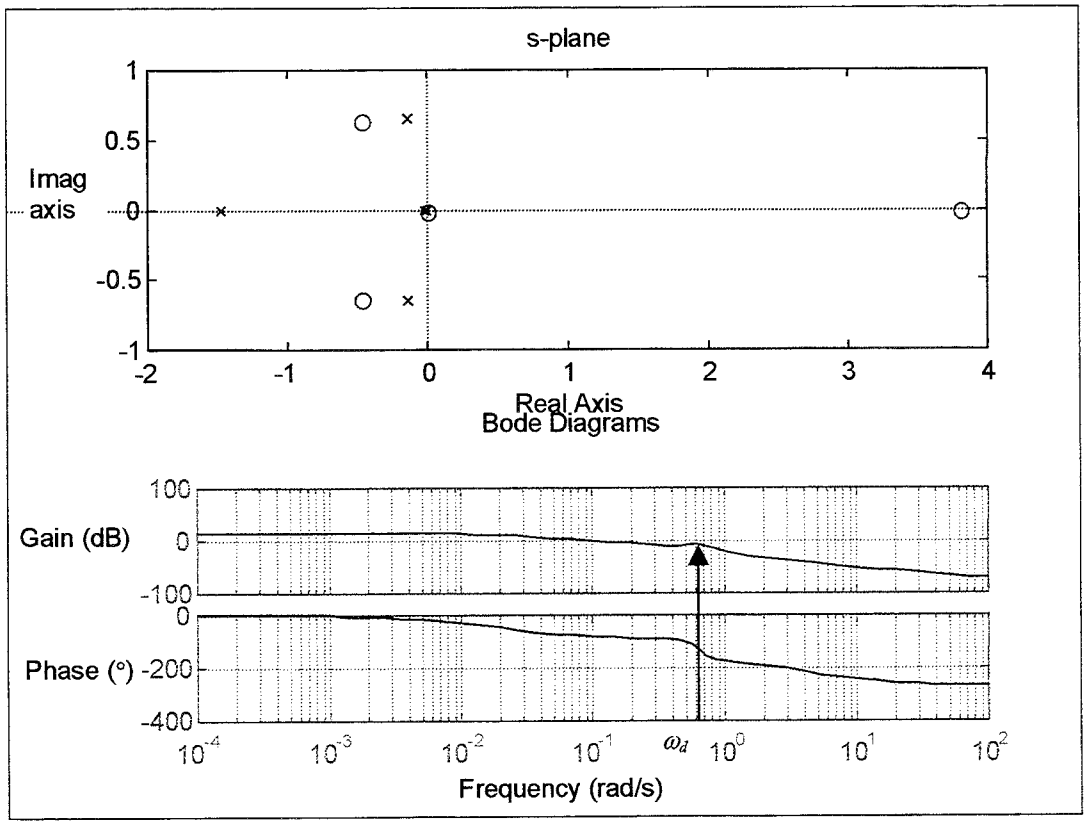

Figure 4.20 Sideslip response to aileron input

4.7.5 Rudder

The response parameters are dominated by the dutch roll mode. A step input was chosen which causes the aircraft to diverge from its equilibrium condition. The positive rudder displacement generates a negative yaw rate, while wing sweepback effects generate a negative rolling moment as seen in the time response, figure 4.13. As the aircraft slowly diverges the angle of bank builds and the heading continues to change resulting in a descending spiral. The initial positive sideslip due to the negative yaw rate is replaced by negative sideslip due to the previous effects. Finally, the change to negative sideslip results in a positive roll rate and the subsequent roll off in bank angle as the aircraft continues to fly in circles.

4.7.6 Roll rate to rudder

$$\frac{p}{\zeta}(s) = \frac{(s+1.4822)(s-0.0087)(s-2.7448)}{(s+1.4755)(s+0.0176)(s+0.1468\pm 0.646i)} \deg s^{-1}/\deg \qquad (4\text{-}32)$$

where

$$\frac{p}{\zeta}(s) = \frac{(s+1/T_{\phi 1})(s+1/T_{\phi 2})(s+1/T_{\phi 3})}{(s+1/T_r)(s+1/T_s)(s^2+2\zeta_d\omega_d s+\omega_d^2)} \tag{4-33}$$

and $T_{\phi 1} = 0.674$s, $T_{\phi 2} = 114.94$s and $T_{\phi 3} = 0.364$s.

The numerator is third order and is composed entirely of real roots, one to the left of the imaginary axis and the remaining two on the right of the s-plane, figure 4.21. The almost exact cancellation of the roll subsidence root by the respective numerator zero can clearly be seen, leaving the dutch roll mode to dominate the response.

The time response shows the initial roll rate response to be opposite to that commanded, this is a characteristic of the non-minimum phase zero in the transfer function, at 2.75, and is known as the adverse roll response to rudder. This is due to the centre of pressure (CP) of the rudder being located above the longitudinal axis of rotation, hence generating a positive roll moment, before wing sweep effects dominate and overcome with negative roll moment.

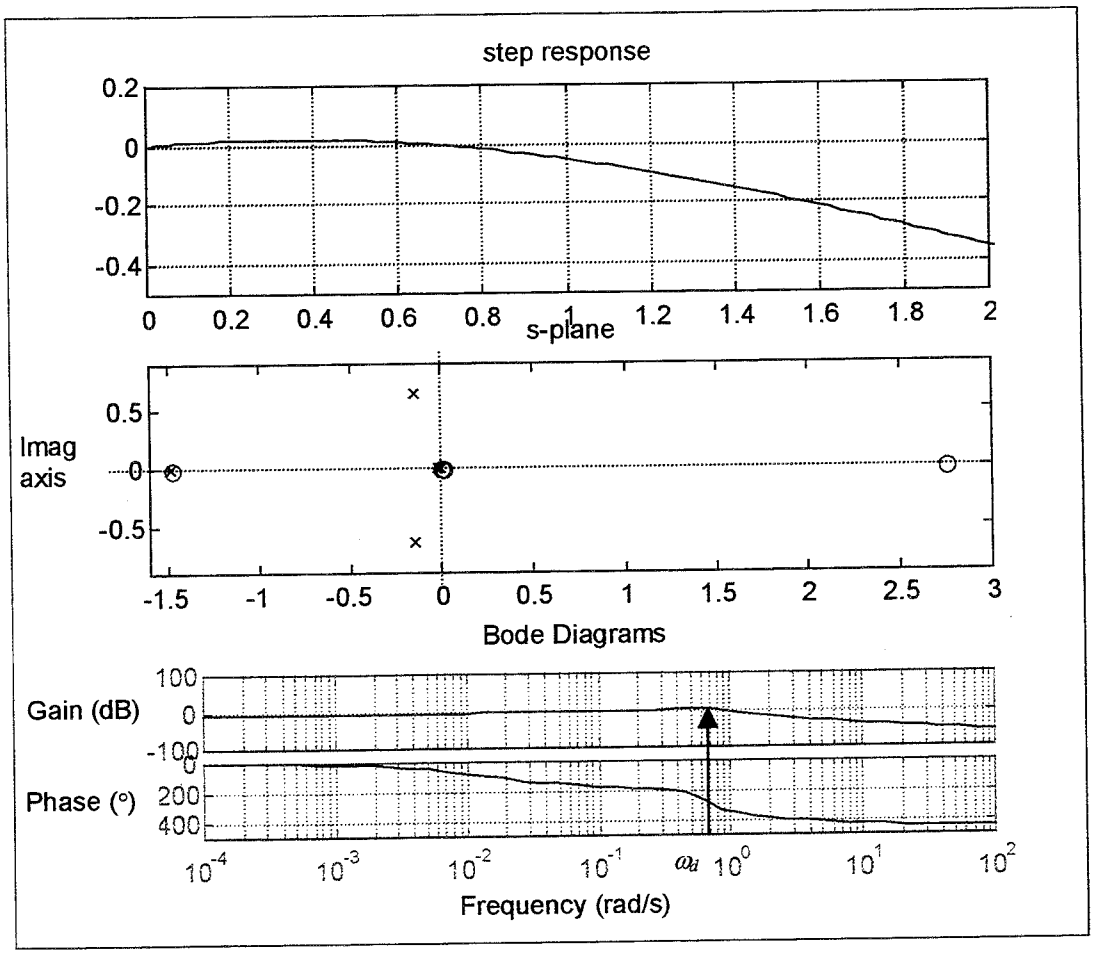

Figure 4.21 Roll rate response to rudder input

The bode diagram shows that at low frequency there is very little roll rate response, 0.387deg/s/deg in response to a rudder input, which is as expected. There is a slight peak

in gain at the dutch roll frequency, ω_d, indicating how a relatively high frequency rudder input will excite the dutch roll mode.

4.7.7 Roll attitude to rudder

$$\frac{\phi}{\zeta}(s) = \frac{(s+1.48)(s-3.66)}{(s+1.4755)(s+0.0176)(s+0.1468\pm 0.646i)} \text{deg/deg} \tag{4-34}$$

where

$$\frac{\phi}{\zeta}(s) = \frac{(s+1/T_{\phi 1})(s+1/T_{\phi 2})}{(s+1/T_r)(s+1/T_s)(s^2+2\zeta_d\omega_d s+\omega_d^2)} \tag{4-35}$$

where $T_{\phi 1} = 0.675$s and $T_{\phi 2} = 0.273$s.

The numerator is second order and has factorised into two real roots, one positive the other negative.

4.7.8 Yaw rate to rudder

$$\frac{r}{\zeta}(s) = \frac{(s+1.475)(s+0.0836\pm 0.306i)}{(s+1.4755)(s+0.0176)(s+0.1468\pm 0.646i)} \text{deg}\,s^{-1}/\text{deg} \tag{4-36}$$

where

$$\frac{r}{\zeta}(s) = \frac{(s+1/T_\psi)(s+2\zeta_\psi\omega_\psi+\omega_\psi^2)}{(s+1/T_r)(s+1/T_s)(s^2+2\zeta_d\omega_d s+\omega_d^2)} \tag{4-37}$$

and $T_\psi = 0.675$, $\zeta_\psi = 0.263$ and $\omega_\psi = 0.317$ rad/s.

The numerator term is composed of one real root with time constant equivalent to the roll subsidence root of 0.67s and a complex conjugate pair.

The exact cancellation of the roll subsidence mode by the respective numerator zero is clearly illustrated on the s-plane, figure 4.22. Hence, the dutch roll and spiral modes will dominate the shape of the yaw response.

The dcgain of 3.3 deg/s/deg will result in a continual heading change for a step rudder input. The bode diagram shows that at low frequencies the aircraft yaw response will be exactly in phase with the input. Phase lag increases with the input frequency, however gain stays almost constant up to the spiral mode frequency. After this point gain rapidly reduces until rising again to peak at the dutch roll frequency resulting in the aircraft yaw response once again following the rudder input. At frequencies greater than ω_d both the gain and phase roll off rapidly.

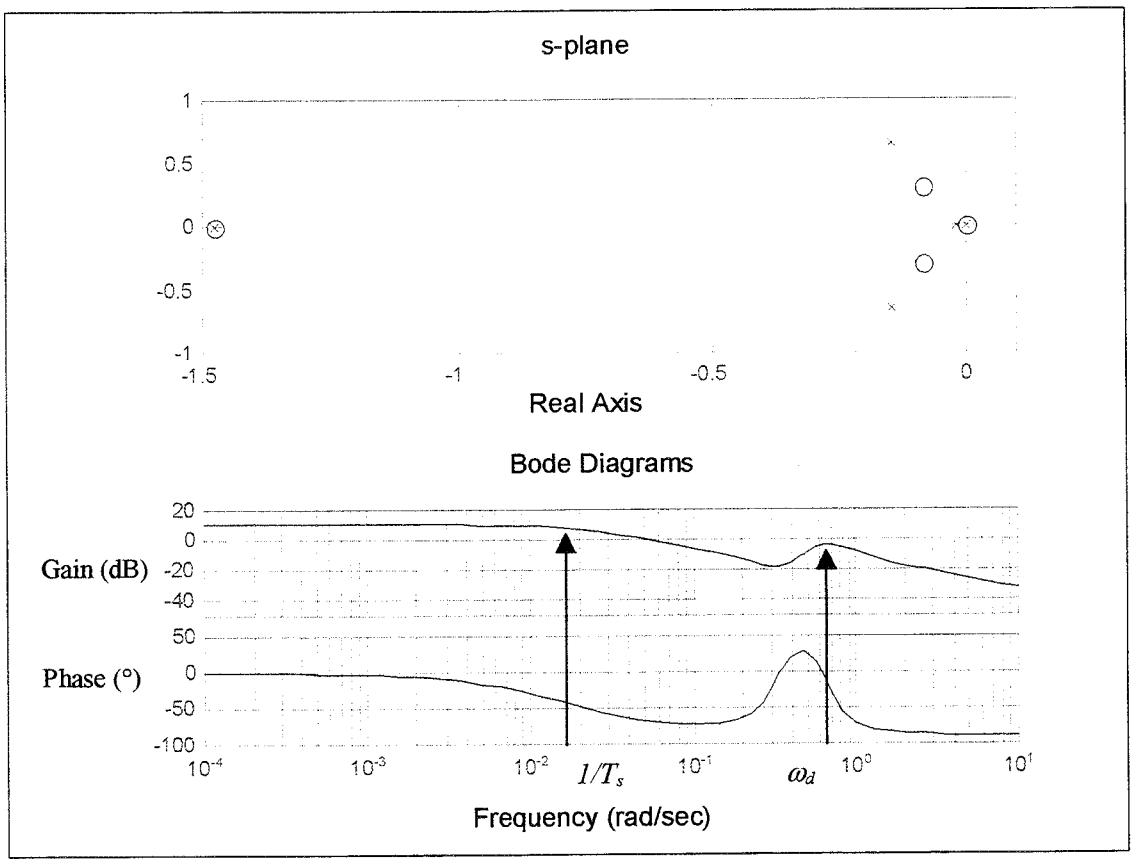

Figure 4.22 Yaw rate response to rudder input

4.7.9 Sideslip response to rudder

$$\frac{\beta}{\zeta}(s) = \frac{(s+1.4757)(s+12.345)(s-0.0323)}{(s+1.4755)(s+0.0176)(s+0.1468\pm 0.646i)} \text{deg/deg} \tag{4-38}$$

where

$$\frac{\beta(s)}{\zeta(s)} = \frac{(s+1/T_{\beta 1})(s+1/T_{\beta 2})(s+1/T_{\beta 3})}{(s+1/T_r)(s+1/T_s)(s^2+2\zeta_d\omega_d s+\omega_d^2)} \tag{4-39}$$

and $T_{\beta 1} = 0.68$s, $T_{\beta 2} = 0.081$s and $T_{\beta 3} = 30.96$s.

The numerator is third order, with one large root and one small of order $1/T_s$ and the other close to $1/T_r$.

The roll subsidence mode is cancelled by the zero at 1.4757, while the non-minimum phase zero at 0.032 rad/s results in an opposite sense initial response in sideslip as witnessed in the time response.

The bode diagram, figure 4.23, shows that at low frequencies there is a gain of 1.34 deg/deg showing a negative steady sideslip for a positive rudder input. The gain stays relatively constant until reaching a slight peak at ω_d, whereupon it begins to roll off, hence equating to the effective control bandwidth.

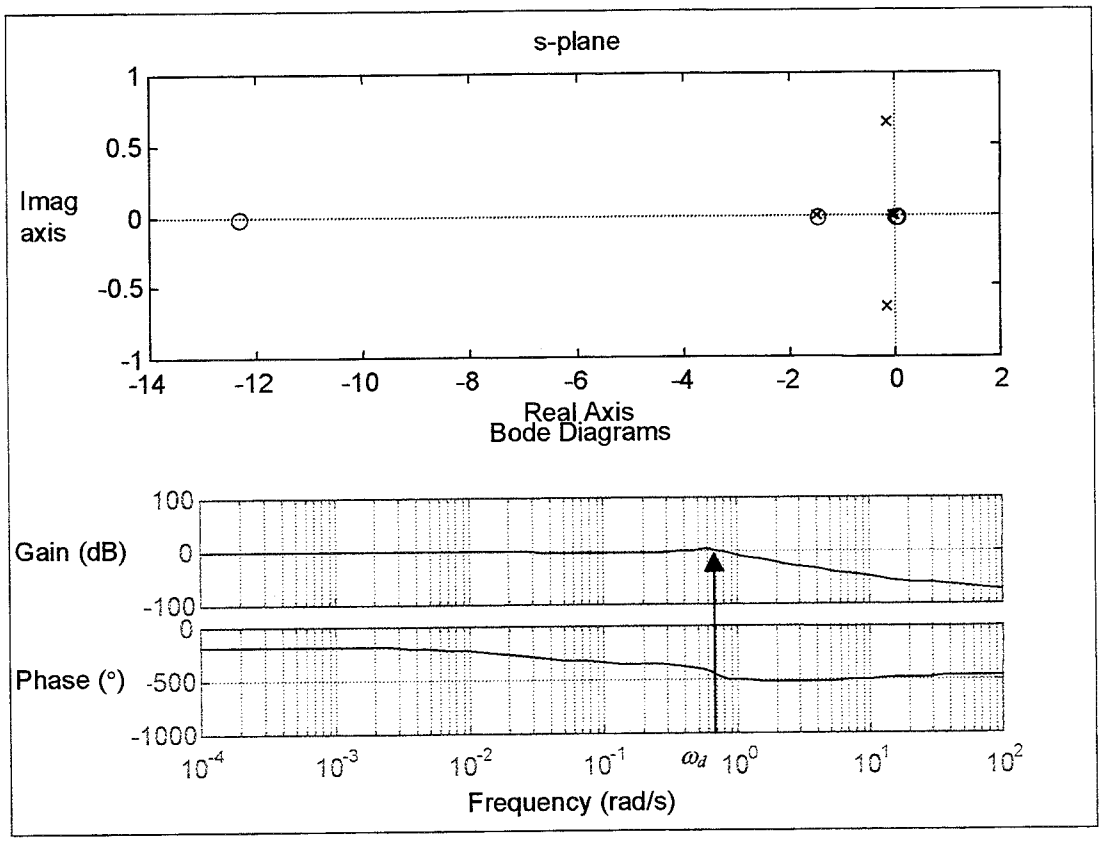

Figure 4.23 Sideslip response to rudder input

4.8 Eigenvector analysis

The mode content in each of the motion variables is given most precisely by the eigenvectors. Therefore, the eigenvector matrix, $\mathbf{V}$,and their magnitudes, $|\mathbf{V}|$, has been generated from the lateral/directional state matrix, equation 4-17.

- The content of row1, equation 4-41, shows that all of the modes are of similar magnitude in lateral velocity and hence sideslip, β.
- The roll subsidence mode dominates in roll rate p and hence roll attitude ϕ.
- The spiral mode has almost zero visibility in any of the 'fast' rates, but can be seen to affect the 'slow' attitudes as expected.
- The dutch roll mode dominates in heading angle due to its inherent yaw motion and also contributes to the roll rate and attitude through roll coupling.

roll subsidence mode dutch roll mode spiral mode

$$\mathbf{V}=\begin{bmatrix} 0.9446 & -0.7114+0.6962i & -0.7114-0.6962i & -1.0000 \\ 0.2709 & 0.0242-0.0440i & 0.0242+0.0440i & 0.0000 \\ 0.0142 & 0.0126+0.0115i & 0.0126-0.0115i & 0.0001 \\ -0.1847 & -0.0713-0.0235i & -0.0713+0.0235i & 0.0019 \\ -0.0097 & 0.0128-0.0225i & 0.0128+0.0225i & -0.0076 \end{bmatrix} \begin{matrix} :v \\ :p \\ :r \\ :\phi \\ :\psi \end{matrix} \quad (4\text{-}40)$$

and

$$|\mathbf{V}|=\begin{bmatrix} 0.9446 & 0.9954 & 0.9954 & 1.0000 \\ 0.2709 & 0.0502 & 0.0502 & 0.0000 \\ 0.0142 & 0.0171 & 0.0171 & 0.0001 \\ 0.1847 & 0.0751 & 0.0751 & 0.0019 \\ 0.0097 & 0.0259 & 0.0259 & 0.0076 \end{bmatrix} \begin{matrix} :v \\ :p \\ :r \\ :\phi \\ :\psi \end{matrix} \quad (4\text{-}41)$$

5 FINAL APPROACH

5.1 Introduction

It has already been shown how the aircraft characteristics, described by the dynamic modes, change with the aircraft trim condition hence requiring independent analysis. In addition, evidence suggests that an SCT's longitudinal handling is of greatest concern due principally to the large pitch inertia coupled with marginal control power located at the wing trailing edge. Therefore, the assessment of the aircraft during the final approach phase will be restricted to longitudinal (pitching) motion.

The aircraft mathematical model has been initialised with the CG located at the NP, the undercarriage down and locked and trimmed in the final approach configuration, see table 5.1, equating to flight phase category C.

Final approach	$\alpha°$	$\theta°$	$\gamma°$	Vt (kts)	Height (ft)	U/C	$\eta°$
	13.75	10.75	-3	155	500	down	-2.12

Table 5.1 Initial conditions

5.2 Linear state model

The state space model describing longitudinal motion has been generated from the 6 DoF non-linear mathematical model. The state equations, 5-1, and output equations, 5-2, in terms of the concise derivatives are shown below.

$$\begin{bmatrix} \dot{u} \\ \dot{w} \\ \dot{q} \\ \dot{\theta} \end{bmatrix} = \begin{bmatrix} -0.0110 & 0.0433 & 1.7295 & -7.1876 \\ -0.0691 & -0.6975 & -7.0678 & -54.8976 \\ 0.00011 & 0.00116 & -0.35407 & 0.0911 \\ 0 & 0 & 1 & 0 \end{bmatrix} \begin{bmatrix} u \\ w \\ q \\ \theta \end{bmatrix} + \begin{bmatrix} -0.0077 \\ -0.2162 \\ -0.01020 \\ 0 \end{bmatrix} [\eta] \quad (5\text{-}1)$$

$$\begin{bmatrix} q \\ \theta \\ \alpha \\ vt \\ n_{zcg} \\ n_{zp} \\ \gamma \end{bmatrix} = \begin{bmatrix} 0 & 0 & 57.2958 & 0 \\ 0 & 0 & 0 & 57.2958 \\ -0.1708 & 0.6979 & 0 & 57.2957 \\ 0.9715 & 0.2372 & 0 & 0 \\ -0.0070 & -0.0711 & -0.7266 & -5.4439 \\ -0.0066 & -0.0763 & 0.8448 & -5.8487 \\ 0.1707 & -0.6979 & 0 & 0 \end{bmatrix} \begin{bmatrix} u \\ w \\ q \\ \theta \end{bmatrix} + \begin{bmatrix} 0 \\ 0 \\ 0 \\ 0 \\ -0.0221 \\ 0.0229 \\ 0 \end{bmatrix} [\eta] \quad (5\text{-}2)$$

The relative magnitudes and signs of the concise pitching moment aerodynamic derivatives, m_u, m_w, m_q and m_θ are important to the stability and dynamic properties of

the aircraft. The speed derivative term, m_u, is seen to be nearly zero (0.00011) indicating that it has almost no effect on stability, equation 5-1. The pitch stiffness derivative, m_w, although small is positive indicating a statically unstable aircraft. The pitch damping derivative, m_q, is negative although small.

The output equation, 5-2, shows the conversion from radians to degrees of the first three variables while the other outputs are composed of elements of the model states. The accelerations, n_{zcg} and n_{zp} have the addition of components in the D matrix indicating direct lift effects from the control, η.

5.3 Longitudinal dynamic modes

For the aircraft configuration, in approach trim conditions, the longitudinal characteristic equation describing the dynamic modes is as shown below, equation 5-3.

$$(s^4 + 1.0626s^3 + 0.1788s^2 + 0.0024s - 0.0016) = 0 \tag{5-3}$$

Equation 5-3 factorises into two real and one complex conjugate pair of roots

$$(s - 0.0746)(s + 0.8607)(s^2 + 0.2765s + 0.0257) \tag{5-4}$$

which equate to

$$(s + 1/T_1)(s + 1/T_2)(s^2 + 2\zeta_{3rd}\omega_{3rd}s + \omega_{3rd}^2) \tag{5-5}$$

One of the real roots is positive, hence unstable and very slow so will dominate the aircraft's dynamic long-term response. The other real root is negative and an order of magnitude faster. The 2nd order term is known as the 3rd oscillatory mode and is characterised by having short period like damping combined with phugoid like frequency and is usually characteristic of a statically unstable aircraft.

The parameters describing the 3rd oscillatory mode are as follows

damping ratio, $\zeta_{3rd} = 0.863$

frequency, $\omega_{3rd} = 0.16$ rad/s

period $T_{3rd} = 2\pi/\omega = 39$ s

These values are in broad agreement with those obtained by a similar study [26], quoted below, achieved with a baseline SST configuration, of similar size and geometry, at an approach speed of 153 kts and with a longitudinal instability margin of 4%MAC.

damping ratio, $\zeta_{3rd} = 0.507$

frequency, $\omega_{3rd} = 0.171$ rad/s

period $T_{3rd} = 2\pi/\omega = 42.72$ s

5.4 Longitudinal transfer functions

The longitudinal transfer function characteristics have been thoroughly analysed for the low-speed cruise. Therefore, for the final approach only the corresponding transfer functions and their defining parameters are shown.

$$\frac{q}{\eta}(s) = \frac{s(s+0.0149)(s+0.7181)}{(s-0.0746)(s+0.8607)(s^2+0.2765s+0.0257)} \deg s^{-1}/\deg \quad (5\text{-}6)$$

$T_{\theta 1}$ = 67 s , $T_{\theta 2}$ = 1.39 s

$$\frac{\theta}{\eta}(s) = \frac{(s+0.0149)(s+0.7181)}{(s-0.0746)(s+0.8607)(s^2+0.2765s+0.0257)} \deg/\deg \quad (5\text{-}7)$$

$T_{\theta 1}$ = 67 s , $T_{\theta 2}$ = 1.39 s

$$\frac{\alpha}{\eta}(s) = \frac{(s+3.8467)(s^2+0.049s+0.0324)}{(s-0.0746)(s+0.8607)(s^2+0.2765s+0.0257)} \deg/\deg \quad (5\text{-}8)$$

T_{α} = 0.26 s , ω_{α} = 0.18 rad/s, ζ_{α} = 0.136 , T = $2\pi/\omega_{\alpha}$ = 34.9 s

$$\frac{\gamma}{\eta}(s) = \frac{(s-0.0313)(s-1.615)(s+1.636)}{(s-0.0746)(s+0.8607)(s^2+0.2765s+0.0257)} \deg/\deg \quad (5\text{-}9)$$

$T_{\gamma 1}$ = 31.95 s, $T_{\gamma 2}$ = 0.619 s, $T_{\gamma 3}$ = 0.611 s

$$\frac{vt}{\eta}(s) = \frac{(s+0.3802)(s-1.7367)(s+1.9622)}{(s-0.0746)(s+0.8607)(s^2+0.2765s+0.0257)} ms^{-1}/\deg \quad (5\text{-}10)$$

T_{vt1} = 2.63 s, T_{vt2} = 0.575 s, T_{vt3} = 0.51 s.

$$\frac{a_{zcg}}{\eta}(s) = \frac{(s-0.0275)(s-1.596)(s+0.0105)(s+1.6396)}{(s-0.0746)(s+0.8607)(s^2+0.2765s+0.0257)} ms^{-2}/\deg \quad (5\text{-}11)$$

T_{a1zcg} = 36.36s, T_{a2zcg} = 0.626s, T_{a3zcg} = 95.24s, T_{a4zcg} = 0.609s.

$$\frac{a_{zp}}{\eta}(s) = \frac{(s-0.0276)(s+0.0106)(s+0.7133\pm 1.435i)}{(s-0.0746)(s+0.8607)(s^2+0.2765s+0.0257)} ms^{-2}/\deg \quad (5\text{-}12)$$

T_{a1p} = 36.23 s, T_{a2p} = 94.34 s, ζ_{azp} = 0.445, ω_{azp} = 1.6 rad/s.

5.5 Time response analysis

In order to excite the longitudinal dynamic modes a unit pulse elevator input was applied at $t = 0$, see figure 5.1.

The fast, stable, real root dominates in pitch resulting in an initial first order rate response after which the oscillatory and slow unstable modes start to dominate resulting in a long term pitch acceleration rather than rate response as demanded.

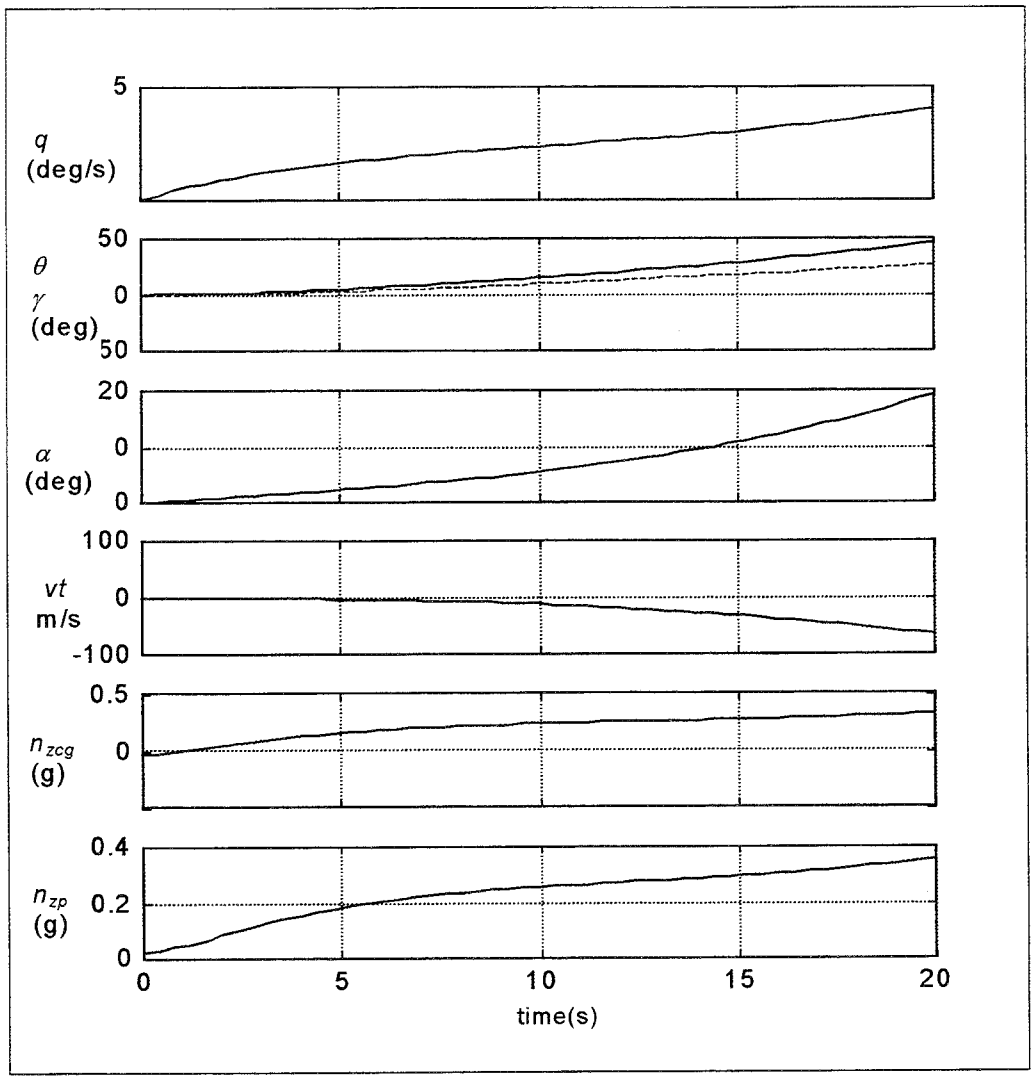

Figure 5.1 Longitudinal response to a step elevator input

The effect of the unstable root can clearly be observed as a slow divergence in all the aircraft response variables. The steadily increasing angle of attack, due to the reduction in speed, results in a divergence between the aircraft attitude and flightpath responses.

The effect of the 3rd oscillatory mode can be best observed in the flightpath response to an impulse input, figure 5.2. The time period, T_{3rd}, of approximately 39 seconds is clearly visible, however the large value of damping, $\zeta_{3rd} = 0.863$, suppresses the oscillation after approximately one cycle.

There is an initial normal acceleration at the CG opposite to that expected due to elevator lift effects, however this is not mirrored at the pilot station.

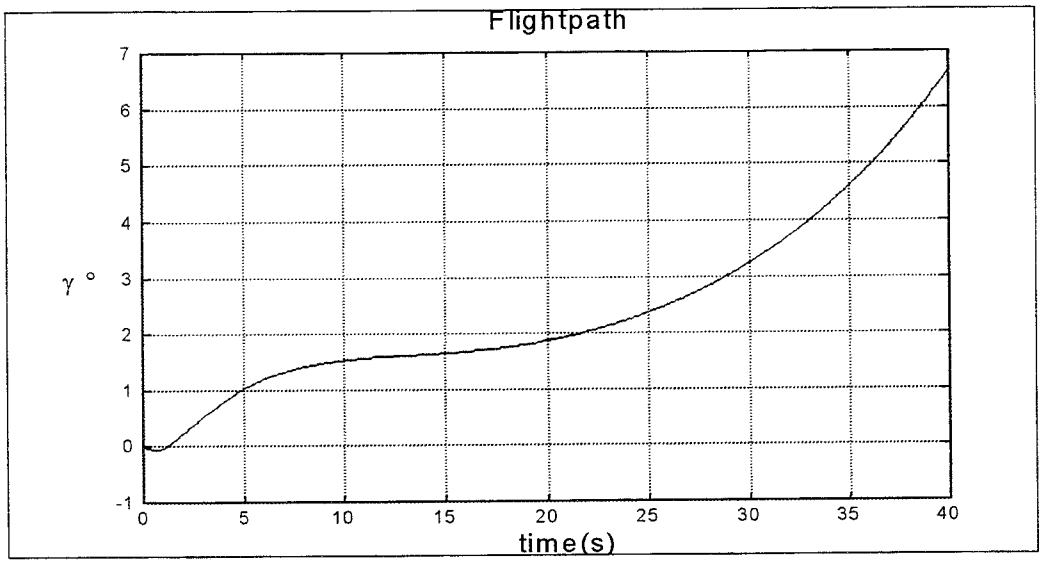

Figure 5.2 3rd oscillatory mode

6 Conclusions

The principal aerodynamic properties that distinguish the low speed stability, control and handling characteristics of an SCT aircraft are:

- The requirement for relaxed longitudinal stability in order to reduce trim drag, both at higher speeds as the aerodynamic centre moves aft and to improve performance at lower speeds through reduced control surface sizing. The relaxed stability, achieved through locating the CG at the NP, results in an unconventional dynamic response on the approach characterised by a 3rd oscillatory mode with short period damping and phugoid like frequency combined with two real modes, one of which is unstable.
- The low static margin when flying at low-speed coupled with the absence of a second control surface results in relatively low pitch damping, M_q, combined with a high pitch inertia, I_y. The aircraft's unaugmented longitudinal response to a control input is thus characterised by a low pitch acceleration, hence sluggish pitch response combined with a slow time to settle. Solutions include feeding back either incidence or pitch rate to restore stability and enhance the manoeuvre response as well as augmenting control power by providing a second pitch control surface.
- The delta wing's low lift curve slope requiring large angles of attack on the approach in order to generate sufficient low-speed lift at the expense of considerable amounts of induced drag. Hence the aircraft flies considerably below the minimum drag speed, known as *'backside'* operation, resulting in speed instability and difficult flightpath control. The effects of speed instability are that at a constant engine thrust on a -3° flightpath, the short term response to an aft stick movement is an increase in height relative to the flightpath. The long-term effect is an increase in drag and consequent steepening of the flightpath. Conversely, a forward stick movement initially steepens the flightpath and in the long term, the increase in speed causes the aircraft to fly above the flightpath. These effects can be overcome by use of an auto-throttle, to control speed through engine thrust. For manual control, the technique is to control the airspeed through pitch attitude and to maintain the glide slope by adjusting engine thrust.
- The pronounced longitudinal non-minimum phase behaviour due to the movement of large trailing edge lift producing surfaces for pitch manoeuvre control. With only wing trailing edge mounted elevons for pitch control, their small moment arm requires a large control deflection to generate the required pitch acceleration. The *'up'* elevon results in negative lift from the control surface and an initial loss in aircraft height until the aircraft incidence is modified and total lift increased. This non-minimum phase behaviour, characterised by a positive zero in the response transfer function, results in an undershoot in flight path response. Resulting in a hesitation in height response which may result in a heavy landing if a correction is made late into the approach.
- Significant delta wing generated ground effect resulting in some cushioning of the landing, hence reduced sink rates. However, the negative pitching moments degrade the rate of nose rotation on take-off and may prove disconcerting to the pilot when the aircraft leaves its effect.

- The pilot's location far ahead of the undercarriage resulting in difficulty in judging mainwheel position during landing at high approach attitudes.
- The capability to generate relatively rapid rates of roll due to the inherently low roll inertia combined with the large and effective elevon control surfaces. However, the low value of the roll damping derivative, L_p, leads to a large roll mode time constant since $\tau_p \approx I_x/L_p$, the roll control power of the elevons is also large resulting in a tendency to over-control in roll. In addition, the rolling moment due to sideslip being a function of sweepback angle and incidence tends to oppose the demanded roll manoeuvre if sideslip is allowed to build hence slowing the initial response.
- A dutch roll mode characterised by a near pure rolling oscillation due to the large value of L_v combined with a low roll inertia. In addition, it has a relatively high frequency and hence short period, requiring the mode to be adequately damped to ensure acceptable handling characteristics.
- A large yaw/roll inertia ratio resulting in a tendency for the unaugmented aircraft to roll about the longitudinal body axis and not the velocity vector, hence degrading heading response.

7 References

1. Orlebar C, *The Concorde story*, The Hamlyn Publishing Group Limited, London, 1995.
2. Gautrey J, *FCS architecture analysis and design for a FBW generic regional aircraft*, CoA Report 9604, Cranfield University, 1996.
3. Tobie et al, *A new longitudinal handling qualities criterion*, The Boeing Company, Commercial Airplane Division, 1966.
4. Hanke D, *Handling Quality Analysis of Flightpath Rate Command Systems*, Institut fur Flugmechanik, Braunschweig, 1993.
5. Anon, *Flying Qualities of Piloted Aircraft, MIL-STD-1797A*, Department of Defence Interface Standard, 1990.
6. Brockhaus R, *Handling Qualities of Hypersonic Aircraft and Related Control Requirements*, Institute for Flight Guidance, Technical University of Braunschweig, 1991.
7. Kehrer W T, *Longitudinal stability and control of large supersonic aircraft at low speed*, Paper No 64-586, ICAS conference, Paris, France, 24-28 Aug, 1964.
8. Pinsker W J G, *The landing flare of large transport aircraft*, RAE TR 67297, 1967.
9. Grantham W D, Nguyen L T, Deal P L, Neubauer Jr M J, Smith P M, Gregory F D, *Ground-Based and In-Flight Simulator Studies of Low-Speed Handling Characteristics of Two Supersonic Cruise Transport Concepts*, NASA Technical Paper 1240, Jul 1978.
10. Sudderth R W, Bohn J G, Caniff M A, Bennett G R, *Development of longitudinal handling qualities criteria for large advanced supersonic aircraft*, NASA CR-137635, Mar 1975.
11. Noot N A L, *Low speed performance aspects of foreplanes and tailplanes*, Aerodynamics office, Commercial Aircraft Division, BAC Ltd, AERO/TN/NALN/PS/496, 1977.
12. Brailsford E N, *Some General Considerations of Foreplanes and Tailplanes*, Aerodynamics office, Commercial Aircraft Division, BAC Ltd, SST/B59-N-03.140/11434, 1976.
13. Scotland R L, *Proposal to Employ a Canard Control to Improve the Handling Characteristics* , Aerodynamics office, BAC Ltd, SST/59-N-04.141/11495, 1976.
14. Scotland R L, *Proposal to Employ a Canard Control to Improve the Handling Characteristics* , Aerodynamics office, BAC Ltd, SST/59-N-04.141/11495, 1976.
15. Steer A J, Reed A D S, *Preliminary studies into the low speed control requirements for the European Supersonic Commercial Transport*, DERA/AS/FDS/CR97091/1, Mar 1997.
16. Steer A J, *Further studies into the European Supersonic Commercial Transport low speed control requirements*, DERA/AS/FMC/CR97390/1.0, Sep 1997.

17. Steer A J, *A piloted simulation study of longitudinally unstable ESCT configurations following failure of the primary FCS*, DERA/AS/FMC/CR980518/1.0, Dec 1998.

18. Steer A J, *An evaluation of the lateral/directional control power requirements for ESCT*, DERA/AS/FMC/CR980518/1.0, Dec 1998.

19. Smith P R, Burnell J J, *Non-linear Dynamic Inversion (NDI): A top down approach to control law design*, DRA/FDS/CR94081/1.0, Mar 1994.

20. Smith P R, *A simplified approach to Non-linear Dynamic Inversion based flight control*, DRA/FDS/CR96140/1.0, Mar 1996.

21. Smith P R, *A theoretical analysis of the simplified Non-linear Dynamic Inversion approach to flight control*, DERA/AS/FDS/CR97109/1.0, Mar 1997.

22. Patel Y, *A comparison of inverse based multivariable control methods*, DERA/AS/FMC/CR980451/1.0, Oct 1998.

23. Gibson J C, *The definition, understanding and design of aircraft handling qualities*, Report LR-756, T U Delft, Faculty of Aerospace Engineering, 1995.

24. Tomlinson B N, *SESAME – A Systems of Equations for the Simulation of Aircraft in a Modular Environment*, RAE TR79008, 1979.

25. Cook M V, *Flight Dynamics Principles*, Arnold Press, 1997.

26. McCarty C A, Feather J B, Dykman J R, Page M A, *Design and analysis issues of integrated control systems for High Speed Civil Transports*, NASA CR-186022, 1992.